LIVER FIBROSIS ASSESSMENT USING A PALM-SIZED TRANSIENT ELASTOGRAPHY SYSTEM: PERFORMANCE EVALUATION AND EXAMINATION STANDARDS

HUANG ZIHAO

PhD

The Hong Kong Polytechnic University

2025

The Hong Kong Polytechnic University

Department of Biomedical Engineering

LIVER FIBROSIS ASSESSMENT USING A PALM-SIZED TRANSIENT ELASTOGRAPHY SYSTEM: PERFORMANCE EVALUATION AND EXAMINATION STANDARDS

HUANG ZIHAO

A thesis submitted in partial fulfilment of the

requirements for the degree of Doctor of Philosophy

July 2024

CERTIFICATE OF ORIGINALITY

I hereby declare that this thesis is my own work and that, to the best of my knowledge and belief, it reproduces no material previously published or written, nor material that has been accepted for the award of any other degree or diploma, except where due acknowledgment has been made in the text.

Signature: _____

Name of Student: HUANG ZIHAO

Abstract

Background: Chronic liver disease (CLD) is a major public health issue worldwide. Liver fibrosis is the common pathway for CLD of various etiologies, culminating in cirrhosis and liver cancer. Transient elastography (TE), endorsed by the WHO, is an established method for assessing liver fibrosis via liver stiffness measurement (LSM). However, technical barriers remain toward an efficient examination and point-of-care application, as conventional TE relies on wired connections, possesses a bulky size, has high unreliable and failure rates, and necessitates extensive training. Chapter 1 provides a systematic review to consolidate existing evidence on these TE-specific limitations, attributing them to the (1) absence of a standardized measurement protocol and (2) inadequacy of visual guidance during the TE procedure.

Objectives: This thesis comprises a series of three integrated studies, aiming to bridge the above-mentioned gaps from technical and clinical perspectives.

Methods and Findings: Chapter 2 aims to offer a technical remedy by incorporating point-of-care ultrasound (POCUS) and anatomical imaging guidance into TE. Specifically, we introduced a palm-sized wireless TE system with real-time B-mode imaging guidance. A methodological study was conducted to evaluate the performance of this newly developed system in eight reference phantoms and 121 adult patients with various CLDs. Results demonstrated the feasibility of employing a fully integrated phased array probe to provide accurate, reliable, and valid LSM. Its small footprint, along with B-mode guidance capability, can greatly facilitate the uptake of liver fibrosis screening.

Chapter 3 aims to offer a practical guideline via establishing a standardized TE

measurement protocol for clinical implementation. Specifically, we sought to identify an ideal site and respiratory condition for TE probe placement by investigating the morphological and biomechanical characteristics of different intercostal spaces (ICSs) overlying the liver. This observational study involving 89 participants employed a combination of ultrasound techniques, including 2D B-mode, 2D elasticity, and 3D ultrasound imaging. Results suggested the 8th ICS on the mid-axillary line as the preferred measurement site, owing to its greater width, smaller width-change, greater angle, lower stiffness, and smaller abdominal wall thickness. Additionally, performing TE at end-inspiration is recommended to minimize interferences from ribs and subcutaneous fat. These recommendations can serve as a guide for novices to shorten learning curve and improve examination efficiency.

Chapter 4 presents an observational study (n=62) to further scrutinize into the effects of supine, seated, and standing postures on liver stiffness, as well as on the feasibility and reliability of TE. Results showed the postural dependency of liver stiffness, which was exhibited differently in healthy controls and patients with varying fibrosis stages. Different postures did not influence the success rate and reliability metrics of TE. Consequently, body positioning should be standardized and cautiously considered when interpreting LSM results.

Conclusions: This thesis advocates for technical improvements and clinical procedural standardization in TE, which can provide actionable insights into addressing challenging cases and scaling up liver fibrosis assessment. Specifically, the key findings may advance TE technique in the long run, ultimately eliminating the failure and unreliable results, alleviating the training burden of TE practitioners, and streamlining the examination procedure in clinical settings. **(500 words)**

Publications Arising from the Thesis

Peer-reviewed Journal Papers:

1. **Huang, Z.-H.**, Lam, S.-K., Cheng, L.-K., Lin, Y.-M., & Zheng, Y.-P. (2024). Determining the Ideal Measurement Site and Respiratory Condition for Liver Transient Elastography: Toward Clinical Practice Standardization. *Insights into Imaging*, 15(1), 114. https://doi.org/10.1186/s13244-024-01692-x (Q1, 2023 JCR IF=4.1, Rank 30/204 in Radiology, Nuclear Medicine & Medical Imaging)

2. **Huang, Z.-H.**, Wang, L.-K., Cai, S.-Y., Chen, H.-X., Zhou, Y., Cheng, L.-K., Lin, Y.-W., Zheng, M.-H., & Zheng, Y.-P. (2024). Palm-Sized Wireless Transient Elastography System with Real-Time B-Mode Ultrasound Imaging Guidance: Toward Point-of-Care Liver Fibrosis Assessment. *Diagnostics (Basel)*, 14(2), 189. https://doi.org/10.3390/diagnostics14020189 (Q1, 2023 JCR IF=3.0, Rank 59/329 in Medicine, General & Internal)

3. **Huang, Z.-H.**, Deng, M.-H., Lin, Y.-M., Ye, C.-H., Zheng, M.-H., and Zheng, Y.-P. (2024). Body Posture Can Modulate Liver Stiffness Measured by Transient Elastography: A Prospective Observational Study. *BMC Gastroenterology*, 24(1), 386. https://doi.org/10.1186/s12876-024-03473-8 (Q3, 2023 JCR IF=2.5, Rank 72/143 in Gastroenterology & Hepatology)

4. Wang, X.-Y., Liu, B., Wu, C.-L., **Huang, Z.-H.**, Zhou, Y., Wu, X.-M., & Zheng, Y.-P. (2024). Shear Wave Trajectory Detection in Ultra-fast M-mode Images for Liver Fibrosis Assessment: A Deep Learning Based Line Detection Approach. *Ultrasonics*, 142, 107358.

https://doi.org/https://doi.org/10.1016/j.ultras.2024.107358 (Q1, 2023 JCR IF=3.8, Rank 5/40 in Acoustics)

Granted Patents:

5. **Huang, Z.-H.**, Wang, L.-K., Zheng, Y.-P. Method, Detection System, and Storage Medium for Biological Tissue Elasticity Measurement in Multi-Dimension (具有维度的生物组织弹性检测方法，检测系统和存储介质), Chinese Invention Patent, Publication No.: CN111772677B, Patent No.: ZL202010644961.1, Grant Date: 2023-06-13.

6. **Huang, Z.-H.**, Wang, L.-K., Cheng, L.-K., Zheng, Y.-P. Method and Apparatus for Evaluating Contact State of Ultrasound Probe Based on Soft Tissue Morphology (基于软组织形态评估超声探头接触状态的方法及装置), Chinese Invention Patent, Publication No.: CN113208646B, Patent No.: ZL202110184305.2, Grant Date: 2024-02-06.

7. **Huang, Z.-H.**, Deng, M.-Q., Wang, L.-K., Zheng, Y.-P. Method and Apparatus for Quality Control Evaluation of Tissue Elasticity Measurement (用于组织弹性测量的可靠性评估方法及系统), Chinese Invention Patent, Publication No.: CN118975822B.

8. Zheng, Y.-P., **Huang, Z.-H.**, Cheng, L.-K., Wang, L.-K. Method and Apparatus for Expanding Functions of Ultrasound Imaging System (拓展超声成像设备的功能的方法和系统), Chinese Invention Patent, Publication No.: CN114533119B.

9. Wang, L.-K., **Huang, Z.-H.**, Jiang, T.-Y., Chen, H.-Z., Li, G.-Y., Zheng, Y.-P.

Method and Apparatus for Performance Testing of Ultrasound Shear Wave Elastography Probe (用于超声剪切波探头的性能检测装置和方法), Chinese Invention Patent, Publication No.: CN118203353B, Patent No.: ZL202410631506.6, Grant Date: 2024-07-16.

10. Wu, C.-L., Deng, M.-Q., **Huang, Z.-H.**, Wang, L.-K., Zheng, Y.-P. Method and Apparatus for Liver Steatosis Quantification Based on Ultrasonic Radiofrequency Signals (基于超声射频信号的肝脏脂肪变性定量检测方法及装置), Chinese Invention Patent, Publication No.: CN118512209B.

11. **Huang, Z.-H.**, Wang, L.-K., Cheng, L.-K., Chung K.-L., Zhou, Y.-J., Zheng, Y.-P. Handheld Ultrasound Device (手持式超声设备), Chinese Design Patent, Publication No.: CN307385892S, Patent No.: ZL202230073761.5, Grant Date: 2022-06-03.

Conference Proceedings:

12. **Huang, Z.-H.**, & Zheng, Y.-P. Liver Stiffness is Subject to Postural Changes. *The 10th International Conference on Biomedical Engineering and Systems*, 3-5 August 2023, London, United Kingdom. DOI: 10.11159/icbes23.151

13. **Huang, Z.-H.**, & Zheng, Y.-P. Refining Liver Fibrosis Assessment: Palm-sized Transient Elastography Guided with B-mode Imaging. *The 33rd Annual Meeting of the Asian Pacific Association for the Study of the Liver (APASL)*, 27-31 March 2024, Kyoto, Japan.

Other Publications Authored During the PhD Study

Peer-reviewed Journal Papers:

1. **Huang, Z.-H.**, Ma, C. Z.-H., Wang, L.-K., Wang, X.-Y., Fu, S.-N., & Zheng, Y.-P. (2022). Real-Time Visual Biofeedback via Wearable Ultrasound Imaging Can Enhance the Muscle Contraction Training Outcome of Young Adults. *Journal of Strength and Conditioning Research*, 36(4), 941-947. https://doi.org/10.1519/JSC.0000000000004230 (Q2, 2023 JCR IF=2.5, Rank 33/127 in Sport Sciences)

2. Cai, S.-Y., Lin, Y.-S., Chen, H.-X., **Huang, Z.-H.**, Zhou, Y. & Zheng, Y.-P. (2024). Automated analysis of pectoralis major thickness in pec-fly exercises: evolving from manual measurement to deep learning techniques. *Visual Computing for Industry, Biomedicine and Art*, 7(1), 8. https://doi.org/10.1186/s42492-024-00159-6 (Q2, 2023 JCR IF=3.2, Rank 130/353 in Engineering, Electrical & Electronic)

Granted Patents:

1. **Huang, Z.-H.**, Wang, L.-K., Zheng, Y.-P. Muscle Training Method and System for Providing Visual Feedback by Using Ultrasonic Imaging (利用超声成像提供视觉反馈的肌肉训练方法及系统), Chinese Invention Patent, Publication No.: CN112089442B, Patent No.: ZL202010854798.1, Grant Date: 2023-10-13.

2. Ma, Z.-H., Zheng, Y.-P., **Huang, Z.-H.** Method, System, and Terminal for Balance and Gait Training (一种平衡和步态的训练方法、系统及终端), Chinese Invention Patent, Publication No.: CN109147904B, Patent No.: ZL201811005548.X,

Grant Date: 2022-05-03.

Award

2024 Champion of Three Minute Thesis (3MT®) Competition

2024 BME Research Student Annual Conference

Department of BME, The Hong Kong Polytechnic University

Acknowledgments

Pursuing a Ph.D. is literally a tough and special journey, especially when it began at the epicentre of the COVID-19 pandemic in 2021. Completing this thesis is a celebration of those who have supported and inspired me along the way.

First and foremost, my deepest gratitude must go to my supervisor, Professor Zheng Yong-Ping. I sincerely appreciate the autonomy, flexibility, and opportunities he has granted me throughout the years, without which I could not have come this far and completed the thesis. I still remember every long conversation we had, despite his tight schedule, to set the tone for my Ph.D. direction and career growth. He has exemplified what it means to be an innovative researcher, a dedicated educator, a successful leader, and an honest person. I consider myself incredibly lucky to have an inspiring role model and mentor in my early career. I also wish to acknowledge the insightful opinions and constructive advice from Dr. Lam Sai-Kit, Dr. Wong Wai-Chi and Prof. Zheng Ming-Hua during my study period.

Developing the Liverscan Project is a team effort, no doubt. I extend my appreciation to those talented engineers and colleagues who dedicate themselves to moving this project forward: Mr. Wang Li-Ke, Dr. Zhou Yong-Jin, Ms. Cheng Connie, Dr. Chung Alan, Mr. Jia Xiao-Jia, Ms. Lau Yoyo, Dr. Lin Yang-Min, Mr. Shi Xiao-Dong, Ms. Jiang Tian-Yu, and Ms. Deng Miao-Qin. With a full sense of gratitude, I think this has been a great team to work with.

Speaking of support, I am truly grateful to my family. To my dearest parents and my beloved wife-to-be Duo, thank you for being my greatest pillars of strength. Your unconditional love and care have shaped who I am today. Another source of support

along this long journey is the sea off Hoi Sham Park and the sky above the rooftop of 11 Sheung Heung Road in To Kwa Wan. These two places cultivate my inner peace, especially during the struggles with my academic endeavour. Visiting there always helps me find my way out physically, mentally, emotionally, and spiritually.

Last but not least, I would like to acknowledge myself. As I near the conclusion of this remarkable Ph.D. journey, I have come to realize that accomplishment hinges not on being the smartest, but on being the most persistent and the most resilient.

Table of Contents

List of Figures

List of Tables

List of Abbreviations

1D	One dimensional
2D	Two dimensional
3D	Three dimensional
ALD	Alcoholic liver disease
ARFI	Acoustic radiation force impulse
AUC	Area under the curve
AUROC	The area under the receiver operating characteristic curve
BMI	Body mass index
CHB	Chronic hepatitis B
CHC	Chronic hepatitis C
CI	Confidence interval
CLD	Chronic liver disease
CV_{ME}	Coefficient of variation of measurement error
ECM	Extracellular matrix
FOV	Field of view
fs	Fibroscan®
ft	Fibrotouch®
HBV	Hepatitis B virus
HCV	Hepatitis C virus
HSC	Hepatic stellate cell
ICC	Intraclass correlation coefficient
ICS	Intercostal space
IQR	Interquartile range
IVC	Inferior vena cava
kPa	Kilopascals

LS	Liver stiffness
LSM	Liver stiffness measurement
MASH	Metabolic dysfunction-associated steatohepatitis
MASLD	Metabolic dysfunction-associated steatotic liver disease
MRE	Magnetic resonance elastography
MRI	Magnetic resonance imaging
NAFLD	Non-alcoholic fatty liver disease
PBC	Primary biliary cirrhosis
pSWE	Point shear wave elastography
POCUS	Point-of-care ultrasound
ROI	Region of interest
SCD	Skin–liver capsule distance
SEM	Standard error of measurement
SPH	Sinusoidal pressure hypothesis
SWE	Shear wave elastography
TE	Transient elastography
US	Ultrasound

Chapter 1. Introduction

1.1 Epidemiology of Chronic Liver Disease

Chronic liver disease (CLD) represents a significant global public health challenge. CLD is characterized by the progressive impairment of liver functions persisting for over six months. This condition manifests through various histopathological changes including the infiltration of hepatic tissue by inflammatory cells, changes in the hepatocyte such as ballooning, necrosis, or apoptosis, myofibroblast proliferation, and fibrotic accumulation. The spectrum of etiologies is broad for CLD, encompassing exposure to toxins, prolonged alcohol misuse, viral infections caused by hepatitis B virus or hepatitis C virus (HBV or HCV), autoimmune diseases, genetic and metabolic-associated disorders, or a mix of these components [1]. Because these factors are common, CLDs are highly prevalent worldwide. In 2017, approximately 1.5 billion individuals were affected by CLD; the majority of cases were attributed to metabolic dysfunction-associated steatotic liver disease (MASLD, previously known as non-alcoholic fatty liver disease [NAFLD]), which accounts for 60%, followed by 29% from HBV, 9% from HCV, and 2% related to alcohol-associated liver disease (ALD) [2].

The multiple causes of CLD, including chronic hepatitis B (CHB), ALD, MASLD, and chronic hepatitis C (CHC), follow a common pathway toward liver fibrosis and ultimately cirrhosis **(Figure 1-1)**. This progression significantly increases the risk of developing portal hypertension, hepatic insufficiency, and hepatocellular carcinoma (HCC) [3]. CLD accounted for 1.6% and 1.7% of mortality in the America in 2021 and 2022, respectively, making it the tenth most common cause of death [4] **(Table 1-1 and Figure 1-2)**. Major complications such as cirrhosis (1,200,000 deaths) and HCC (790 thousand deaths) contribute to 3.5% of global mortality [5].

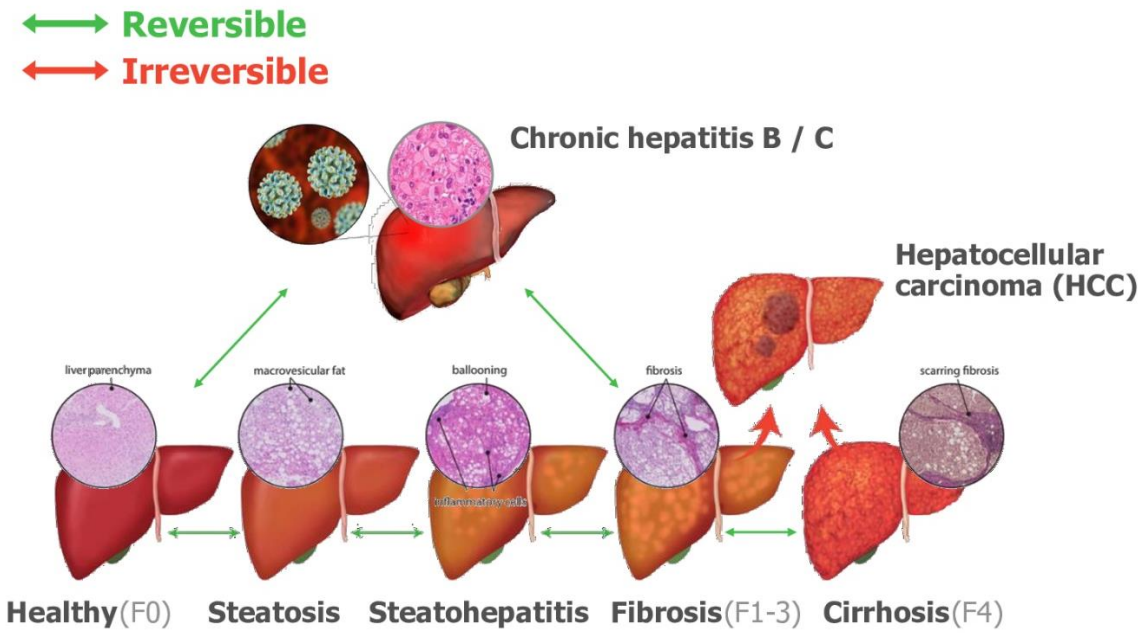

Figure 1-1. Progression of liver damage.

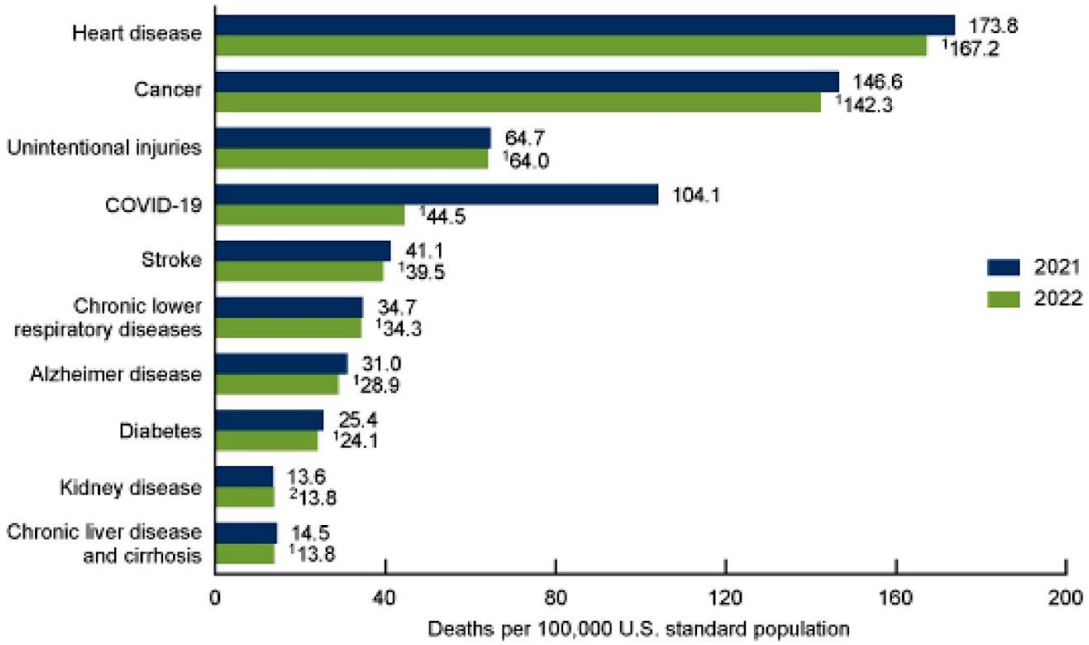

Figure 1-2. Mortality rate for the 10 leading causes of death adjusted by age in United States for 2021 and 2022 (adapted from https://www.cdc.gov/nchs/products/databriefs/db492.htm).

Table 1-1. Number of deaths, percentage of total deaths, and age-adjusted mortality rate for the 10 leading causes of death adjusted by age in United States for 2021 and 2022 (adapted from https://www.cdc.gov/nchs/fastats/leading-causes-of-death.htm).

Rank[1]	Cause of death (based on *International Classification of Diseases, 10th Revision*)	2021			2022		
		Number	Percent	Rate[2]	Number	Percent	Rate[2]
...	All causes	3,464,231	100.0	879.7	3,279,857	100.0	798.8
1	Diseases of heart (I00–I09,I11,I13,I20–I51)	695,547	20.1	173.8	702,880	21.4	167.2
2	Malignant neoplasms (cancer) (C00–C97)	605,213	17.5	146.6	608,371	18.5	142.3
3	Accidents (unintentional injuries) (V01–X59,Y85–Y86)	224,935	6.5	64.7	227,039	6.9	64.0
4	COVID-19 (U07.1)	416,893	12.0	104.1	186,552	5.7	44.5
5	Cerebrovascular diseases (stroke) (I60–I69)	162,890	4.7	41.1	165,393	5.0	39.5
6	Chronic lower respiratory diseases (J40–J47)	142,342	4.1	34.7	147,382	4.5	34.3
7	Alzheimer disease (G30)	119,399	3.4	31.0	120,122	3.7	28.9
8	Diabetes mellitus (E10–E14)	103,294	3.0	25.4	101,209	3.1	24.1
9	Nephritis, nephrotic syndrome and nephrosis (kidney disease) (N00–N07,N17–N19,N25–N27)	54,358	1.6	13.6	57,937	1.8	13.8
10	Chronic liver disease and cirrhosis (K70,K73–K74)	56,585	1.6	14.5	54,803	1.7	13.8
...	All other causes (residual)	882,775	25.5	...	908,169	27.7	...

... Category not applicable.
[1]Based on number of deaths.
[2]Deaths per 100,000 U.S. standard population.

NOTES: Numbers showing percentage by cause are rounded, so these numbers may not add to 100.0%. The 10 leading causes of death accounted for 72.3% of all U.S deaths in 2022. Causes of deaths are ranked according to number of deaths. Rankings for 2021 data are not shown.

SOURCE: National Center for Health Statistics, National Vital Statistics System, mortality data file.

According to the WHO, Global Burden of Disease Study reported that 1.75 million deaths were attributed to liver disease in 2010, including 0.752 million from HCC and 1.03 million from cirrhosis [6]. Of them, cirrhosis of the liver ranked within the top 10 leading causes of death in both low-income and low-middle-income in 2019 **(Figure 1-3)**. Liver cancer was among the top 10 leading causes of death in upper-middle-income countries In 2012 [5] **(Figure 1-4)**. Cirrhotic patients are classified as either compensated (stage F=4 with or without esophageal varices) or decompensated (clinical manifestations of portal hypertension such as variceal bleeding, hepatic encephalopathy, ascites, spontaneous bacterial peritonitis, and/or hepatorenal syndrome) [7]. While CHB and CHC remain a primary driving force for cirrhosis-related deaths in Asia, the incidence and mortality are decreasing due to increased HBV vaccination and effective antiviral treatments [8]. However, other causes of CLD are

expected to remain steady or increase. Epidemiological research indicates that MASLD incidence is rising globally, particularly due to the obesity and diabetes epidemics. Additionally, global alcohol consumption increased from 2005 to 2010 and is projected to continue rising [9]. Consequently, ALD accounts for the majority of cirrhosis-related deaths in Europe, with mortality rates on the rise in nations such as Finland and the United Kingdom [10]. It is worth noting that cirrhosis also elevates the risk of developing liver cancer [2]. Given these facts, the overall prevalence of cirrhosis is unlikely to decline without significant epidemiological interventions. Early detection of CLD patients at increased risk for developing decompensation or HCC is vital for implementing optimal management strategies to improve patient outcomes.

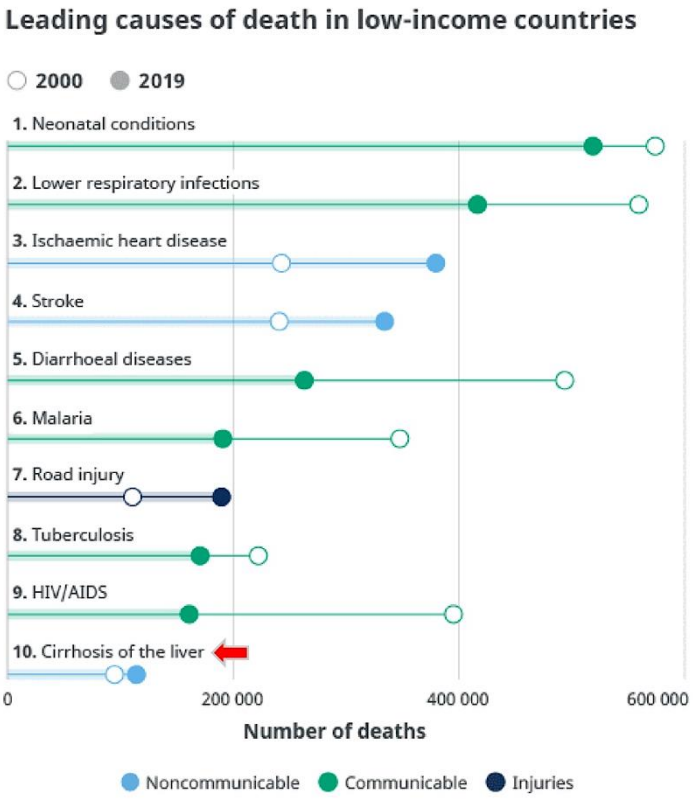

(A)

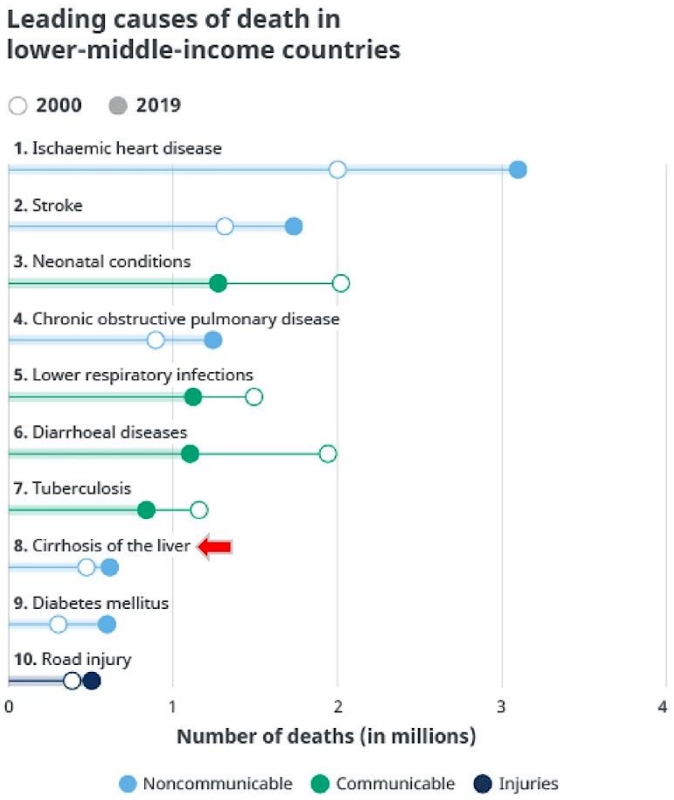

(B)

Figure 1-3. Leading causes of death in 2019 for (A) low-income and (B) low-middle-income countries (adapted from https://www.who.int/news-room/fact-sheets/detail/the-top-10-causes-of-death).

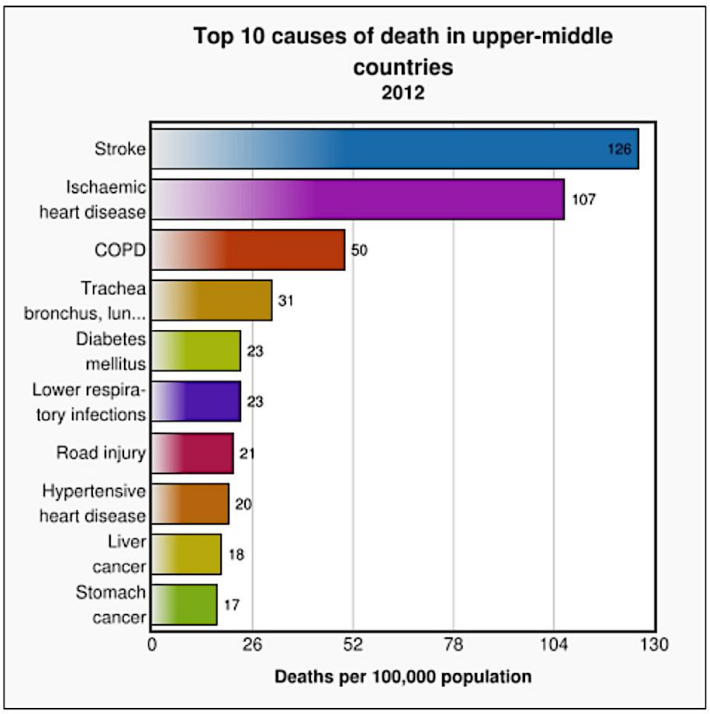

Figure 1-4. Leading causes of death in 2012: upper-middle-income countries (adapted from https://www.who.int/news-room/fact-sheets/detail/the-top-10-causes-of-death).

1.2 Natural History of Liver Fibrosis

Historically, hepatic fibrogenesis was thought to be a model of the wound-healing response to long-term liver injury [11]. Hepatic fibrosis is characterized by an excessive deposition of collagen and other components of the extracellular matrix in response to long-term damage [12]. It is considered the most important histological change in CLD, as liver fibrosis can determine disease progression to cirrhosis and other clinically relevant events, such as liver-associated complications and deaths. Therefore, the management of a patient with CLD requires close assessment of fibrosis. The diagnosis, however, is rarely established in the early stages, because mild-to-moderate fibrosis often presents no overt symptoms and can easily go unnoticed. At the other end of the spectrum, cirrhosis is a diffuse process that transforms normal liver architecture into structurally abnormal nodules [12]. As a final stage of fibrosis progression, cirrhosis disrupts liver architecture, forms widespread nodules, reorganizes vascular structures, and promotes neo-angiogenesis [11].

Both genetic and environment-related risk factors affect the natural progression of fibrosis [11]. Clinically, fibrosis may rapidly advance to cirrhosis under conditions such as repeated episodes of acute alcohol-related hepatitis, cholestasis, sub-fulminant liver failure, and post-transplantation HCV reinfection [13]. Cirrhosis with the following manifestations of extensive fibrotic nodules, advanced portal hypertension, and markedly impaired synthetic function is typically deem as an irreversible condition [14]. Nonetheless, clinical evidence [11, 14-16] indicates that liver fibrosis can be reversed, stabilized, or prevented in case of addressing potential underlying cause. Furthermore, patients may experience fibrotic regression when they are under the treatment with novel adjunctive anti-fibrotic medications, such as anti-oxidants and angiotensin

inhibitors, or with immunosuppressive, anti-inflammatory, or anti-viral agents [17].

Only few studies have reported the prevalence of liver fibrosis. Large-scale screening studies [9, 18-22] reveal that the detection rates of clinically significant fibrosis among the general adult population is substantial, ranging from 5.6% to 7.5%. Furthermore, the prevalence increases dramatically in cohorts at risk for CLD, varying between 18% and 27%. For example, Poynard et al. [22] observed a presumed prevalence of 2.8% for advanced fibrosis and 0.3% for cirrhosis in a sample of 7,463 healthy individuals over 40 years old. Another French study at a primary care center [18] found that 7.5% of 1,190 patients aged above 45 years, who had not previously been diagnosed with liver disease and were receiving medical check-ups, exhibited moderate-to-severe fibrosis. Cirrhosis has also been detected in 0.7% of these cases. Other research [21, 23, 24] targeting patients with the common risk factors of CLD, such as excessive alcohol consumption or type 2 diabetes, reported even higher prevalence of advanced fibrosis (up to 27.9%) and cirrhosis (from 2.4 to 4%). In these studies, MASLD was the leading cause of liver fibrosis [18, 21-24].

1.3 Pathophysiology of Fibrogenesis

Acute liver injury, such as those caused by HBV or HCV infections, prompt the generation of hepatic parenchymal cells to replace those necrotic or apoptotic cells. This mechanism involves an inflammatory response and restricted accumulation of the extracellular matrix (ECM), particularly in the form of fibrillar collagen. However, if liver damage becomes chronic, the liver regeneration fails, leading to the replacement of hepatocytes with excessive ECM. Liver fibrogenesis is a complex process primarily driven by activating and transforming hepatic stellate cells (HSCs) into myofibroblasts [16, 25]. Activated HSCs are the main ECM-producing cells. When migration and accumulation occur at sites of tissue repair,, activated HSCs secret substantial amounts of ECM and regulate its degradation [25]. The fibrotic distribution in CLD varies depending on its aetiology [26]. In patients with chronic viral hepatitis and cholestatic liver diseases, the fibrotic tissues surround portal tracts, whereas in alcohol-induced cases, fibrosis predominantly affects pericentral and perisinusoidal areas.

The transformation of HSCs into myofibroblasts is generally regulated by their interaction with various cell types and the activation of specific pathways [27]. Certain types of cells, such as injured hepatocytes, Kupffer cells, endothelial cells, and lymphocytes all contribute to the activation of HSCs [28]. Hepatocyte injury results in releasing reactive oxygen species as well as cellular contents , which in turn cause the activation of Kupffer cells to secrete pro-inflammatory and pro-fibrogenic factors [27, 29]. These factors promote HSC activation and the onset of fibrogenesis. For example, several platelet-derived growth factors, primarily produced by Kupffer cells, serve as a predominant mitogen in this process [11]. Furthermore, Kupffer cells play

a dual role in fibrogenesis. In cases of chronic injury, they advance fibrosis progression by releasing chemokines that recruit immature monocyte-derived Ly6C^{hi} macrophages. On the other hand, Ly6C^{hi} macrophages can differentiate into pro-resolution restorative macrophages, which secrete fibrolytic matrix and the anti-inflammatory cytokine interleukin-10 [11]. These elements are involved in resolving fibrosis.

Oxidative stress is another important factor involved in liver fibrosis. Reactive oxygen species generated during chronic tissue damage can lead to the overexpression of genes associated with ECM remodelling, inflammation, and fibrogenesis [11, 30]. Conditions such as ALD and metabolic dysfunction-associated steatohepatitis (MASH) are particularly linked to oxidative stress-induced fibrogenesis [30]. Other factors include intestinal microbiota, tissue hypoxia, epigenetic modifications, and the mechanical characteristics of the underlying ECM [31]. Furthermore, various hepatic cell types, apart from HSCs, can exhibit fibrogenic potential. Specifically, myofibroblasts originating from small portal vessels proliferate adjacent to biliary tracts in cholestasis-induced fibrosis to initiate the accumulation of collagen [32, 33]. Overall, the pathogenesis of hepatic fibrosis involves a complex interplay among hepatocytes, inflammatory cells, HSCs, and various molecular pathways, driving the fibrosis deposition and remodelling [11, 16].

1.4 Conventional Assessment for Liver Fibrosis

The conventional assessment modalities for liver fibrosis include liver biopsy and serological testing.

1.4.1 Liver Biopsy

Histologic analysis of liver specimens obtained via biopsy has long been regarded as the reference standard for evaluating the severity of liver fibrosis **(Figure 1-5)**. Histopathologists routinely apply several staging systems, including Ishak, METAVIR, and Batts-Ludwig [34]. These common scoring systems assess the location and extent of portal and periportal fibrosis, bridging fibrosis, and nodularity to determine the fibrosis stage. The METAVIR system, the most widely used, categorizes fibrosis severity as follows: F0 = normal liver, F1 = minimal fibrosis, F2 = significant fibrosis, F3 = advanced fibrosis, and F4 = cirrhosis. Studies have shown that fibrosis severity as determined by these scoring systems correlates well with clinical outcomes in liver disease. Specifically, cirrhosis, (equivalent to stage F4 in METAVIR, stage 4 in Batts-Ludwig, or stages 5–6 in Ishak) is directly linked to increased liver-related morbidity and mortality. Consequently, the detection of cirrhosis in those at-risk patients with CLD carries significant clinical implications [35].

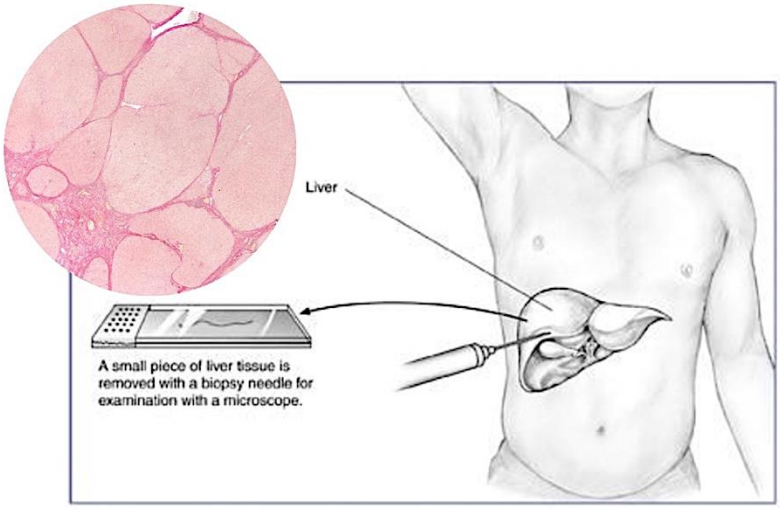

Figure 1-5. Percutaneous liver biopsy (adapted from https://www.niddk.nih.gov/health-information/diagnostic-tests/liver-biopsy).

However, percutaneous biopsy procedure for the liver is subject several limitations [34, 36-38]. It is inherently invasive and can cause minor but not negligible complications such as temporary pain in roughly 20% of patients [36]. More severe complications, such as bleeding, hemobilia, bile peritonitis, bacteremia, sepsis, pneumothorax, hemothorax, and even death, arise in roughly 1.1% of procedures [36]. Sampling error also limits liver biopsy, with a standard biopsy core representing only 1/50,000 of the entire volume of the liver [38, 39]. Some degree of sampling variability is inevitable. This is particularly problematic in the context of the heterogeneous distribution of fibrosis, although obtaining high-quality, adequately sized biopsy samples can partially mitigate this pitfall. Research indicates that specimens containing eleven or more portal tracts yield equally accurate results compared to larger tissue samples, whereas those with fewer possibly cause understaging [40]. Inter-observer agreement among pathologists is also imperfect, with the kappa statistic varying between 0.5 to 0.9, depending on pathologists' experience and expertise [34]. Another drawback is its semiquantitative nature [34]. Fibrosis

represents a continuous spectrum rather than a set of discrete categories. Yet, current staging systems employ an ordinal semi-quantitative scale with only a limited number of stages, which proves particularly inadequate for patients nearing end-stage liver disease. Specifically, those four-stage systems, such as Batts-Ludwig and METAVIR, tend not discriminate between early and advanced or established cirrhosis, each associated with different prognoses and incidences of clinical events [34]. In light of those obstacles, there exists a need to develop quantitative evaluation methods that provide a continuous and wide range of values to depict the fibrosis continuum.

Over the past decades, significant advancements and growing interest have emerged in developing non-invasive and quantitative biomarkers to assess fibrosis through biological and physical properties. These biomarkers fall into two main categories: (1) serum biomarkers to represent the pathophysiology of liver fibrosis (refer to **Chapter 1.4.2**) and (2) imaging biomarkers which utilize the principle of elastography to indirectly measure tissue stiffness (refer to **Chapter 1.5**).

1.4.2 Serum Biomarker Analysis

Serum biomarkers can be categorized into two primary types: indirect or direct biomarkers. Indirect markers encompass a wide variety of blood tests, including platelets, bilirubin, and aminotransferase in serum samples. They serve as a surrogate for liver dysfunction caused by fibrosis but do not directly link with fibrotic deposition. direct markers are explicitly associated with ECM metabolism and include elements of matrix degradation as well as cytokines and chemokines related to fibrinogenesis. Both individual markers and their combinations have been proposed for diagnosing fibrosis. These diagnostic tools include patented proprietary panels such as enhanced liver fibrosis (ELF) test and composite scores integrating clinical features with serum

markers, such as the FibroTest, Fibrosis-4 (FIB-4), AST to Platelet Ratio Index (APRI), and NAFLD fibrosis score. Those tests are among the most widely used, validated, and encompass both proprietary and non-patented varieties.

For example, the FIB-4 score, which is typically derived from age, platelet counts, AST, and ALT levels, has shown an area under the receiver operating characteristic (AUROC) between 0.74 to 0.87 in detecting advanced fibrosis (F≥3) [41, 42]. Another test, the NAFLD fibrosis score, specifically developed for MASLD, was effective in excluding clinically advanced fibrosis and cirrhosis, with negative predictive values (NPVs) exceeding 90% [43]. Several practical superiorities of using serum biomarkers to evaluate liver fibrosis [44, 45] include their ease of use, high utility to large populations, good inter-laboratory reproducibility, and relatively low costs. However, they are not yet widely available and are non-specific, insensitive for early-stage fibrosis, unable to accurately to discriminate between intermediate stages of fibrosis. Additionally, their accuracy may be compromised by renal or liver failure [46].

1.5 Elastography-Based Assessment for Liver Fibrosis

1.5.1 Technology Overview and Clinical Indications

In recent years, several novel imaging biomarkers have been developed and proposed for the quantitative evaluation of liver fibrosis. These include ultrasound or MRE-derived liver parenchymal stiffness, proton nuclear magnetic resonance (^{1}H NMR) spectroscopy [47], diffusion weighted MR imaging [48], CT or MR-derived liver surface nodularity score [49, 50], MR-derived T1 relaxometry [51], and macromolecular proton fraction mapping [52]. Among these, liver stiffness measurement (LSM) with elastography has emerged as the most promising and clinically valuable tool for assessing liver fibrosis [39, 53-56]. Elastography, which can be performed using either ultrasound or MR, quantifies the Young's modulus of the liver by measuring its response to applied mechanical stress (i.e., manual compression or shear wave). In general, liver elastography is classified according to the type of excitation method **(Figure 1-6)**: (1) strain imaging, which uses quasi-static mechanically-induced displacement through active external compression or passively-induced physiologic motion such as heart beat, or (2) shear wave imaging, which uses dynamic mechanically-induced vibration or ultrasound-generated propagating shear wave stimuli.

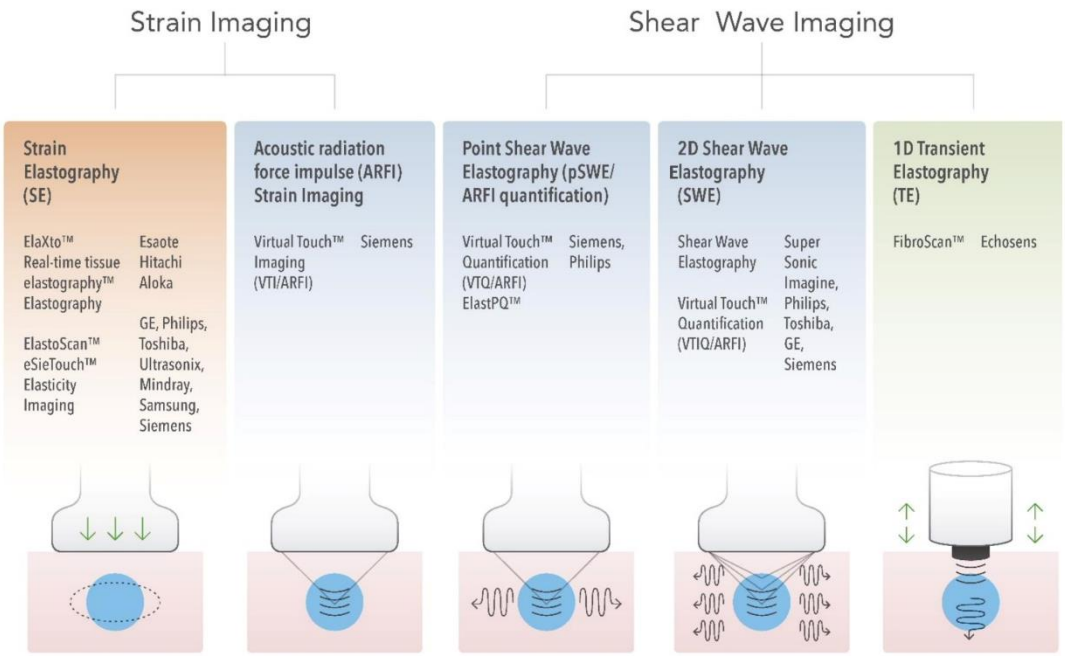

Figure 1-6. Technical overview of ultrasound elastography techniques (adapted from [39]).

Despite existing reports on strain elastography in the application of diagnosing liver fibrosis [57, 58], its clinical use remains limited. This thesis does not delve into the technical and application details of strain elastography, due to the scant literature available. Conversely, shear wave-based elastography has attracted more attention within the hepatology community and is now commonly implemented in clinical settings. This category of techniques works in the way of monitoring the propagation of shear waves through liver tissues to estimate liver stiffness. Different methods are employed to allow the generation of shear waves, including: (1) acoustic radiation force impulse (ARFI) excitation in point shear wave elastography (pSWE) and two-dimensional shear wave elastography (2D-SWE, see **Chapter 1.5.3**); or (2) controlled external vibration at the liver surface in one-dimensional transient elastography (1D-TE, see **Chapter 1.5.4**) and magnetic resonance elastography (MRE, see **Chapter 1.5.2**). Among these liver elastography techniques, TE is considered the most

commonly used and the best-validated worldwide [53-56, 59], making it the primary focus of this thesis.

Liver elastography is clinically indicated for patients requiring fibrosis staging for CLD. The primary objective is to determine the presence or absence of advanced fibrosis, as outlined in **Chapters 1.1 and 1.2**, since advanced fibrosis necessitates frequent monitoring and prioritizes therapy prescription. Additional indications include screening apparently asymptomatic individuals, following up on previously diagnosed fibrosis, confirming suspected cirrhosis, and investigating unexplained portal hypertension. With the advent of new antiviral treatments that effectively manage viral hepatitis and halt fibrosis progression, another key indication is to assess treatment response and potentially tailor follow-up interventions [53-56, 59].

1.5.2 Magnetic Resonance Elastography

The development of MRE took place at the Mayo Clinic in 1995 [60]. MRE can be integrated as an add-on sequence in an examination of abdominal MRI or independently conducted as a stand-alone liver elastography examination. The commercially available MRE system operates via an active driver attached to the liver surface to generate continuous mechanical vibration at a typical frequency 60 Hz, a modified phase-contrast sequence to image the propagating shear waves, and a processing algorithm to reconstruct color-coded MRE-specific elastograms using an inversion algorithm [59, 61]. The basic principle and representative elastograms are depicted in **Figure 1-7**. MRE allows sampling of a large area of the liver (≥250 cm^3), exceeding the sampling size of liver biopsy by over 5,000 times and that of TE by 250 times [62]. Results are generally reported as the magnitude of the complex shear modulus in kilopascals (kPa), equivalent to one-third of the Young's modulus

commonly applied in TE. Liver stiffness measured by MRE generally ranges between 0 and 8 kPa.

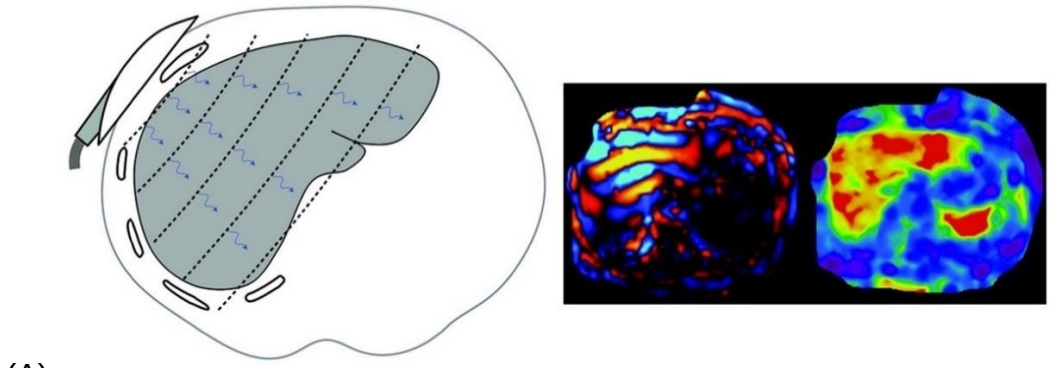

(A)

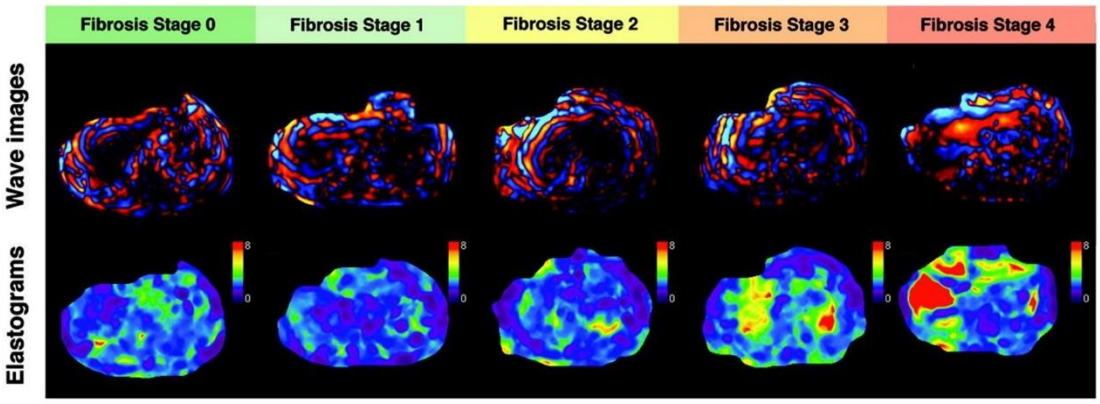

(B)

Figure 1-7. MRE for liver fibrosis assessment. (A) Illustration of the technical principle; (B) Companion elastograms produced by MRE from representative cases with fibrosis stages 0, 1, 2, 3, and 4, respectively (adapted from [59]).

Numerous studies have established a clinically significant correlation between MRE-derived liver stiffness and the histologic stage of fibrosis in biopsy-proven cohorts [61]. A systematic review and pooled individual MASLD data analysis by Singh and colleages [63] identified the optimal MRE cut-off values for diagnosing fibrosis stages 1, 2, 3, and 4 as 2.88, 3.54, 3.77, and 4.09 kPa, respectively. Another meta-analysis of twelve studies involving nearly 700 patients determined that the sensitivity, specificity, as well as AUROC for the detection of advanced fibrosis (F3–F4) were 85%,

85%, and 0.93, respectively [64]. Comparative studies have also evaluated the diagnostic accuracy between MRE and TE [65, 66]. One study reported the comparable AUROC values for detecting clinically significant fibrosis (F≥2) in 111 obese individuals with CLD (TE vs. MRE: 0.91 and 0.93; p = 0.551), with technical failure rates below 15% for both techniques [65].

MRE offers the technical advantages of 3D stiffness analysis of the entire liver volume and its utility in obese patients or patients with ascites. Additional benefits include its compatibility with contrast-enhanced MRI for detecting HCC. However, the high cost, limited availability, and time-consuming nature of MRE hinder its routine use in clinical settings. Another limitation is its reduced reliability or inability to scan the livers with iron overload due to MR signal loss [59, 61].

1.5.3 Ultrasound Elastography: 2D Shear Wave Elastography (2D-SWE)

Instead of a single focal location as in pSWE **(Figure 1-8, A)**, 2D-SWE is based on the combination of utilizing acoustic radiation force induced within liver tissues by focused ultrasound beams at multiple focal zones **(Figure 1-8, B)** and an ultra-fast ultrasound sequence with over 10,000 frames per second. This technology is capable of monitoring of a cone-shaped, quasi-planar shear wave front in real-time [67]. A quantitative parametric map is generated to display the Young's modulus of the liver, facilitating the visualization of fibrosis distribution in two dimensions.

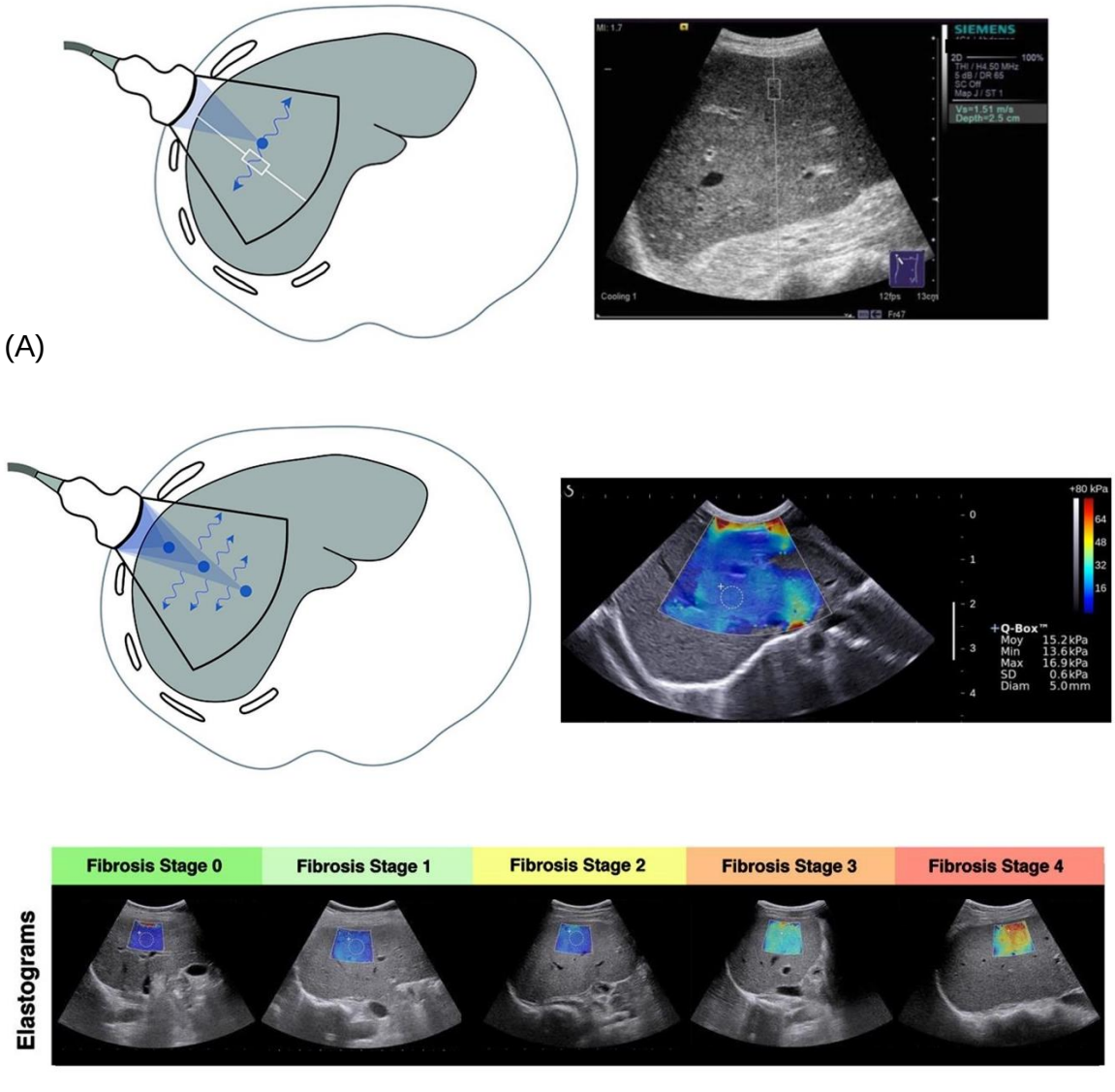

Figure 1-8. ARFI-based SWE for liver fibrosis assessment. Illustration of the technical principle of (A) pSWE and (B) 2D-SWE; (B) Companion elastograms produced by 2D-SWE from representative patients with fibrosis stages 0, 1, 2, 3, and 4, respectively (adapted from [59, 68]).

Strong correlation of liver stiffness measured by 2D-SWE and histology-determined fibrosis severity has been well-documented across multiple studies [39, 59, 68]. Additionally, the diagnostic performance has been thoroughly validated and is comparable to that of TE across various etiologies of CLD. For instance, the very first study comparing 2D-SWE against 1D-TE involved 121 biopsy-proven CHC patients,

achieving an AUROC of 0.92 and establishing a cut-off value of 7.1 kPa for clinically significant fibrosis (F≥2) [69]. More recently, Wang and colleagues [70] introduced a novel technique based on convolutional neural network (CNN), termed deep learning radiomics of elastography (DLRE). Its combination was shown to supplement the diagnostic performance of 2D-SWE, increasing the AUROC to over 0.97 for both advanced fibrosis and cirrhosis. Additionally, 2D-SWE has shown prognostic value in cirrhosis. Some studies demonstrated its feasibility in predicting esophageal varices, portal hypertension, and survival in cirrhotic patients [71].

Unlike TE, 2D-SWE provides more robust LSM in presence of ascites and obesity. This is because the shear waves generated in 2D-SWE originate locally inside the liver, whereas liquid fluid and subcutaneous fat can impede shear wave propagation in TE. Another strength is the simultaneous visualization of a color-coded map superimposed on a B-mode ultrasound image allowing operators to be guided by both anatomical and stiffness information. This real-time guidance helps to effectively avoid including non-liver parenchymal tissues and identifying artifacts, thereby enhancing the accuracy. The larger and multiple regions of interest (ROIs) enable averaging of LSM, reducing sampling variability and better assessing fibrosis heterogeneity. However, its drawbacks include restricted availability, inapplicability in points of service, and fewer large-scale diagnostic test studies compared to TE [59]. Additionally, greater technical expertise and training resources are required. Thus, 2D-SWE generally necessitates the involvement of a radiologist or sonographer.

1.5.4 Ultrasound Elastography: Transient Elastography (TE)

The initial development of 1D-TE dates back to the late 1990s [72, 73]. TE was not only the first elastography technique commercially available for clinical use, but also

the first diagnostic imaging system specifically designed for liver applications. To date, TE has become the most widely used and validated elastography method for assessing hepatic fibrosis [53-56, 59]. **Figure 1-9** presents its technical principle and representative elastograms characterizing the varying stages of liver fibrosis.

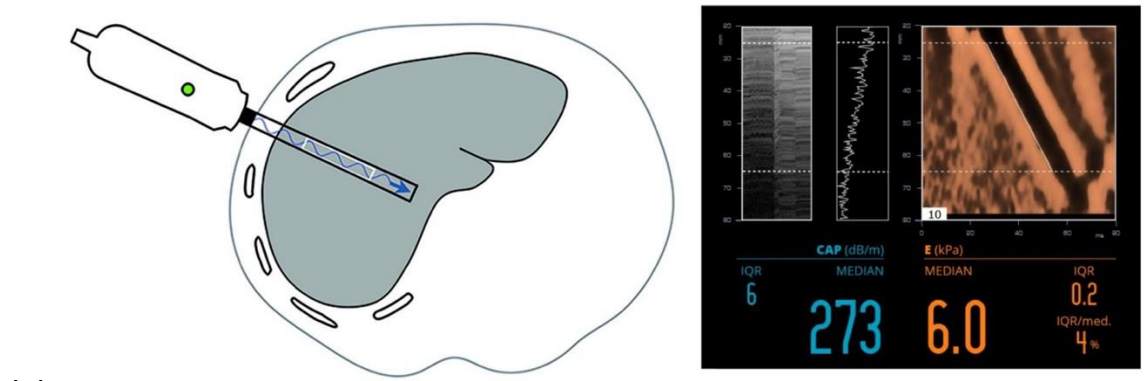

(A)

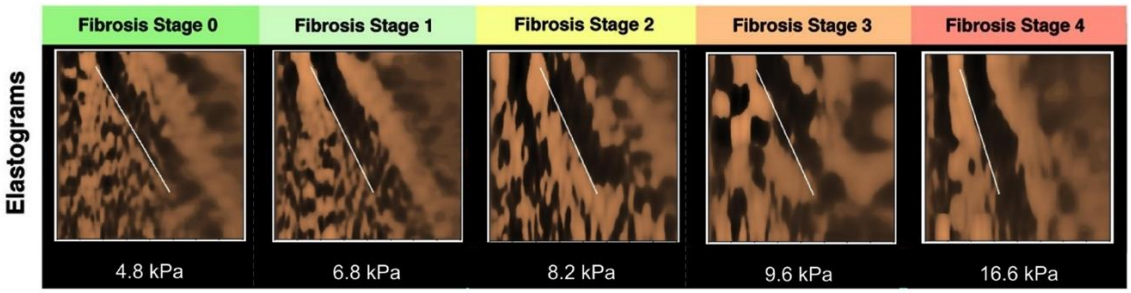

(B)

Figure 1-9. 1D-TE for liver fibrosis assessment. (A) Illustration of the technical principle; (B) Companion elastograms produced by 1D-TE from representative patients with fibrosis stages 0, 1, 2, 3, and 4, respectively (adapted from [59, 66]).

TE probe typically consists of both an ultra-fast single-element transducer and a mechanical vibrator [74]. Validated probes include a 3.5-MHz M probe with a measurement depth range of 25–65 mm for patients with a standard morphotype, a 2.5-MHz XL probe with a measurement depth range of 35–75 mm for obese patients, and a 5.0-MHz S probe with a measurement depth range of 20–50 mm for patients with a narrow intercostal space, such as children. TE measures the velocity of 50-Hz

shear waves, which are generated externally by transient vibration and propagating through the liver. The typical procedure is outlined as follows [53-56]: TE is generally a stand-alone system without anatomic imaging capability for procedural guidance. Instead, baseline imaging is on basis of M-mode images with multiple RF signal lines sampled in real-time. Operators select and sample a portion of the liver parenchyma at a specific measurement depth below the skin, avoiding major vascular structures. The mechanical vibrator then exerts a vibrating external source controlled at a fixed frequency of 50 Hz on the body surface to generate shear waves, which propagate symmetrically relative to the axis of the transducer tip. The same transducer uses ultrasound with an ultra-high frame rate (~5000 frame/s) to track the displacements induced by the propagating shear wave through the liver tissue. The Young's modulus can be inferred accordingly by measuring the speed of the wave. The sampling volume has dimensions of approximately 1 cm in width and 4 cm in length, making it more than 100 times larger than a biopsy sample.

TE results are reported as the Young's modulus of the liver in kPa, with values typically spanning from 2.5 kPa to 75.0 kPa. To ensure the intended performance and accuracy, the following quality criteria for reliable TE have been established: (1) ≥ 10 valid acquisitions; (2) a ratio of valid acquisitions to the total number of attempts of ≥ 60%; and (3) an interquartile range (IQR) / median value of LSM of ≤ 30%. TE results with an IQR/median ratio greater than 30% are considered particularly unreliable [75, 76]. The favourable utility of TE lies in its relatively low cost, short procedure time, and potential as a point-of-care test in a hepatologist’s office or bedside setting. Remarkably, TE possesses a liver application-oriented nature and standardizes wave frequency at 50 Hz, which ensure measurement comparison. For a detailed discussion on the technical limitations of TE, refer to **Chapter 1.6**.

Extensive studies have evaluated TE against histology across various causes of CLD, including CHB, CHC, HIV coinfection, MASLD, ALD, autoimmune hepatitis (AIH), as well as in primary biliary cirrhosis (PBC) and primary sclerosing cholangitis (PSC) [53, 54, 74, 77, 78]. For example, a meta-analysis involving forty biopsy-proven cohort studies by Tsochatzis et al. [79] reported a sensitivity of 79% and a specificity of 78% for F≥2 fibrosis, and a sensitivity of 83% and a specificity of 89% for F=4 cirrhosis. Due to its excellent inter- and intra-observer agreement (ICC of 0.98) [79, 80] and favourable diagnostic performance [79], TE is recommended as a way to monitor treatment response to antiviral drugs, implement post-transplant care, and prioritize therapy for patients at high risk of progression, such as HIV-HCV co-infection [54]. TE also has prognostic values and has demonstrated a correlation with the hepatic venous pressure gradient (HVPG) for identifying portal hypertension [81]. Other prospective longitudinal follow-up studies have further shown that LS can predict the future development of decompensated cirrhosis, HCC, and mortality in those earlier diagnosed with CHC, CHB, and cholestatic liver disease [82, 83]. Specifically, in an analysis of 103 patients with PBC, a 2.1 kPa/year increase in TE-measured LS corresponded to an 8.4 times higher risk of progressing to liver decompensation and death [84]. More recently, a novel diagnostic algorithm specifically for MASH, known as the FibroScan-aspartate aminotransferase (FAST) score, was developed with the aim of identifying MASH patients at risk of clinically significant fibrosis [77]. This algorithm has showed outstanding performance, with AUROCs being 83% in the training cohort and being 92% in the validation cohorts.

1.6 Limitations of TE

According to the existing body of literature, several factors are known to compromise the accuracy and clinical implementation of TE [39, 59, 85, 86]. Some confounding factors are technique- and instrument-specific, while others are biological and patient-related confounders. Details about these existing challenges of TE are elaborated in the following sub-sections.

1.6.1 Difficulty in Liver Localization

One commonly reported limitation of TE is the insufficient visual guidance to locate the liver and further determine where the measurement is being obtained within a specific parenchymal region [54, 55, 59, 87-89]. Although TE is an ultrasound-based technique, it is performed without direct B-mode image guidance which can provide detailed anatomic information. Instead, the ROI is identified using a combination of A- and M-mode imaging to form low-quality guidance. Consequently, TE operators face challenges in determining an adequate acoustic window free of rib shadowing, vessel distortion, and other artifacts that interfere with LSM. This anatomic imaging incapability can cause examination inefficiency, as well as failures and unreliable TE results [39, 75]. Furthermore, because no grayscale images are provided, the exact anatomic location or landmark in the liver from which the LSM is made is not documented. This deficiency may complicate procedural standardization and introduce sampling variability in longitudinal monitoring applications. Detailed discussions are presented in **Chapter 2**.

1.6.2 Inherent Technical Inability in Special Populations

Several limitations relate to the specific, inherent characteristics of TE. From a methodological standpoint, mechanical stimuli via external vibration are applied at the

skin surface; therefore, ascitic fluid, ribs, and subcutaneous fat inevitably interfere with the propagation of ultrasound and shear waves. TE failure and unreliability frequently occur in these patient populations and with operators who have limited experience [75, 90]. In a study involving 276 overweight or obese patients, the failure and unreliable rates of TE were remarkably high at 16% and 50%, respectively [91]. In this regard, TE is particularly limited in the settings of obesity [74, 75, 88, 90], narrow intercostal spaces [74, 88, 92] and, when inexperienced operators position the transducer tip over a sub-optimal acoustic window [39, 75]. Additionally, performing TE is nearly impossible in the presence of perihepatic ascites [86].

Some patient-related confounders, such as obesity or narrow intercostal space-related TE failures, can be partly overcome with the use of the XL or S probe. Myers et al. demonstrated that TE failure was significantly less frequent with the XL probe than with the M probe (1.1% vs. 16%; $p < 0.001$) [91]. However, the literature regarding the technical feasibility of the XL probe in overweight populations is inconsistent, with some studies reporting the unreliable and failure rates still as high as 23% [93, 94]. Furthermore, the S probe did not improve TE in small adults, who generally have an inadequate acoustic window. Its unreliable rate was shown to be statistically similar to that of the M probe ($p = 0.2$) [92].

From a clinical application standpoint, TE samples a smaller portion of the hepatic parenchyma compared to MRE and 2D-SWE. Hence, similar to liver biopsy, TE provides a single-value measurement, which cannot assess the heterogeneity of fibrosis distribution in the liver [55]. Another inherent limitation includes the limited ability to discriminate between adjacent fibrosis stages, particularly for intermediate stages (F≥2 or F≥3) [86, 95], due to a substantial overlap of liver stiffness values in

the continuum. Additionally, TE exhibits a relatively lower diagnostic performance for intermediate stages compared to cirrhosis [86].

1.6.3 Heavy Training Cost

TE requires substantial operator experience and training to meet its established quality criteria [86]. In a large-cohort study involving over 13,000 TE examinations [75], the failure rate was 8.3% when the operators had only performed fewer than 500 examinations and 3.5% when the operators had rich experience of beyond that threshold ($p < 0.001$). Operator inexperience (<500 vs. ≥500 examinations) may also influence the reliability of TE. The rate of unreliable results dropped dramatically from 30.5% to 15.6% of cases when an experienced operator participated [75]. This finding suggested a long learning curve for TE, contradicting earlier claims that a novice can achieve reliable results after a short training period of only 50 examinations. Instead, this proves that TE tends not to be learned in a short time and requires extensive practice. This pitfall further highlighted the need for adequate operator training and professional expertise; however, it may present an extra heavy burden to novice or non-specialist operators. Although another study [96] demonstrated a shorter learning curve of 100 examinations, such a training requirement is still considered rigorous and imposes a heavy training cost in a real-world clinical context. Further discussion on this topic is included in **Chapter 3**, where a cost-effective solution is also presented accordingly.

1.6.4 Confounders of Liver Stiffness

Various confounding factors, independent of the actual fibrosis stages, can influence liver stiffness, [56, 85, 97, 98]. Besides physiologic conditions such as the Valsalva maneuver [99], deep inspiration [85] and postprandial state [100, 101],

certain disease processes, including acute hepatitis [102, 103], cardiac insufficiency [104, 105], cholestasis [106], and hepatic arterial or portal hypertension [107, 108], have been reported to impair the diagnostic performance of TE. Body mass index (BMI) has also been reported as an important confounder [109]. False positive results of TE have also been observed in cases of excessive alcohol intake [110]. The influence of hepatic steatosis is still a matter of debate, since inconsistent results have been reported in the literature. Some studies [111-113] indicate that steatosis may falsely elevated LS, resulting in a false positive rate of 23.6% for diagnosing Stage 2 fibrosis [111], whereas others do not [114, 115]. **Chapter 4** provides a detailed review of how these factors confound TE, and includes an exploratory study on body posture as another potential confounder.

1.7 Research Gaps

With a growing clinical interest in developing new TE techniques or refining existing practices for liver fibrosis assessment, it is essential to understand the current confounders hindering an effective TE assessment. According to the literature review conducted in **Chapter 1.6**, several research gaps exist. Generally, both the (1) technical or instrument-related factors and (2) patient- or procedure-related factors can influence the accuracy and clinical utility of liver TE. The common reasons behind those limitations appear to be interconnected. Specifically, the high unreliable and failure rates, along with the substantial learning burden of TE, can be attributed to the lack of (1) a standardized measurement protocol and (2) a visual imaging guidance technique to assist the TE examination.

1.7.1 Technical Perspective: No Adequate Imaging Guidance

Traditionally, TE was developed as a measurement tool without direct 2D image guidance of anatomic information, which has been a significant technical limitation [54, 55, 59, 87-89]. This can cause TE failure, an unreliable result, and lower examination efficiency. In the literature, previous studies have identified a significantly higher technical success rate for 2D-SWE than for TE, likely due to the real-time B-mode guidance capability of 2D-SWE [116, 117]. Additionally, two other studies have demonstrated that using B-mode imaging beforehand to select an optimal site prior to TE reduces the failure and unreliable rates [118], and presents no learning curve [119]. Therefore, we speculate that real-time B-mode imaging as procedural guidance is equally or even more beneficial compared to pre-TE B-mode imaging.

Given these added values together with the lack of existing works in the literature, there is a pressing demand for incorporating real-time B-mode imaging into TE, and

evaluating its effectiveness in terms of LSM. This technical improvement would allow for simultaneous anatomic visualization and stiffness measurement of the liver in a fully integrated probe setting. As a new form of TE, it is necessary to systematically evaluate the performance of a real-time B-mode guided TE system before its widespread clinical adoption for liver fibrosis assessment.

1.7.2 Clinical Perspective: No Standardization of TE Measurement Protocol

One of the practical challenges of liver elastography is the lack of standardization in using TE devices [120]. To address this issue, efforts by Quantitative Imaging Biomarkers Alliance (QIBA) are being undertaken to quantify biases between different systems, vendors, and operators using calibrated phantoms [121, 122]. The QIBA initiative strives to improve the consistency of measurement results, allowing for meaningful comparisons in clinical practices and research trials. These QIBA efforts will hopefully define standardized technical parameters and settings for LSM as a biomarker for liver fibrosis staging. However, in addition to technical standardization, procedural standardization is equally crucial for obtaining reliable and accurate results [39]. Despite this, the standardization of TE measurement protocols has received very little attention in the liver community.

Current major hepatology organisations (e.g., American Association for the Study of Liver Diseases [AASLD], European Association for the Study of the Liver [EASL], and Asian Pacific Association for the Study of the Liver [APASL]) provide little guidance on standardization of the TE examination procedure, because of the paucity of data. Specifically, there are no clear guidelines on selecting measurement sites for a standard practice in this regard [123]. Under this circumstance, the choice of where to measure varies among patients and is operator-dependent. Operators often rely on

their own experience or a trial-and-error method during the procedure, which may introduce measurement variability and largely reduce examination efficiency as well as patient comfort. On top of that, there is no standardization of a respiratory technique for the TE examination procedure. Although the supine posture is generally regarded as the standard of care for TE, alternative patient positioning is sometimes used in real-world practices due to special circumstances. For instance, patients with orthopnea, ankylosing spondylitis or mobility constraints may find it challenging to assume a supine posture. Yet, research on the effect of common daily postures (e.g., non-supine seated or standing positions) on TE is lacking. It is imperative to develop specific examination standards for TE, while no relevant research has been reported.

1.8 Objectives of the Study

The overarching goals of the thesis are to

1) Evaluate the performance of a palm-sized wireless TE system with real-time B-mode imaging guidance.
2) Establish a standardized measurement protocol for TE.

The outcomes of the thesis contribute to reduce failure and unreliable rates, improve examination efficiency, and ease the training burden associated with TE.

The specific aims of the thesis are listed as follows:

1) **Specific Aim-1:** To introduce and evaluate a palm-sized wireless TE system with real-time B-mode imaging guidance for liver fibrosis assessment in both laboratory phantom and clinical settings **(Chapter 2)**.
2) **Specific Aim-2:** To identify an ideal measurement site and respiratory condition for the TE examination via an observational study by leveraging 2D and 3D ultrasound imaging techniques for characterization of the morphological and biomechanical properties of different ICSs, with comprehensive analyses in aspects of the feasibility, reliability, and validity of intercostal ultrasound measurements **(Chapter 3)**.
3) **Specific Aim-3:** To further scrutinize into the effects of body posture (supine, seated, and standing) on liver stiffness, and on the success rate and reliability of TE, via an observational study of healthy subjects and patients with varying degrees of fibrosis severity **(Chapter 4)**.

The objectives for each individual chapter of the thesis are specified below:

Chapter 2: To address the research gap stated in **Chapter 1.7.1**, a methodological

study was conducted for the technical performance analysis of a novel B-mode guided TE system in both laboratory phantom and clinical settings. The objectives of this study were to

1) Introduce a newly developed palm-sized real-time B-mode imaging guided TE system for the assessment of liver fibrosis.
2) Evaluate the accuracy of this new TE system in quantifying the Young's modulus of tissue-mimicking elasticity phantoms across a spectrum of reference values (2 kPa to 75 kPa).
3) Evaluate the reliability and validity of this new TE system for LSM in adult patients with confirmed CLD of various etiologies.
4) Examine the effect of vibration amplitude on TE-derived liver stiffness.

Chapter 3: To address the research gap stated in **Chapter 1.7.2**, an observational study was conducted in an attempt to standardize the measurement site and respiratory condition used for the TE examination procedure. The objectives of this study were to

1) Explore the feasibility of applying 2D and 3D ultrasound imaging to characterize the morphological and biomechanical properties of the ICSs on the right inferior rib cage.
2) Establish the reliability and validity of 2D and 3D ultrasound-based intercostal measurements.
3) Investigate the differences in the morphological and biomechanical properties among different ICSs.
4) Examine the effect of respiration on the morphological and biomechanical properties of the ICSs.
5) Assess the relationship between the distribution of the ICSs and the presence

of the liver.

6) Analyse the factors influencing the morphological and biomechanical properties of the ICSs.

Chapter 4: To address the research gap stated in **Chapter 1.7.2**, another observational study was conducted in an attempt to standardize the patient positioning technique used for the TE examination procedure. The objectives of this study were to

1) Explore the feasibility of performing TE in a non-lying posture for liver fibrosis assessment.
2) Examine the effect of body posture on liver stiffness using TE in healthy subjects and patients with known CLD.
3) Examine the effect of body posture on the success rate and reliability criteria of LSM using TE.

1.9 Outline of the Thesis

This thesis comprises five main chapters. **Chapter 1** outlines the background, motivation, objectives, and overall structure of the thesis. Specifically, it includes a comprehensive literature review on the epidemiology, natural history, pathogenesis, and diagnosis of liver fibrosis. In view of the invasiveness of biopsy, the rapid development of non-invasive methods has received significant attention in the hepatology community. Herein, it is pertinent to discuss two different but complementary approaches: a biological approach based on surrogate markers and a physical approach based on LSM with elastography. In this thesis, the focus is particularly on TE, a state-of-the-art liver elastography technique. Although considered the non-invasive standard for liver fibrosis assessment, TE has some pitfalls. A systematic review is thus conducted to consolidate the existing evidence on TE-specific limitations, paving the way for the research gaps and objectives of this thesis. Consequently, two main research gaps that hinder the advancement of TE were identified.

Chapters 2 through 4 cover the essence of this thesis to address these gaps. Technical and procedural improvements for TE are proposed with the hope of reducing the failure and unreliable rates, as well as easing the training burden. **Chapter 2** introduces a newly developed, palm-sized TE system incorporating real-time B-mode imaging guidance for liver anatomy, and reports a comprehensive performance analysis in both laboratory phantom and clinical settings (Specific Aim-1). **Chapter 3 and Chapter 4** set out to establish clinical practice standards for TE, minimizing potential confounding effects arising from the examination procedure. **Chapter 3** presents an observational study encompassing a series of analyses through

combining 2D-SWE, 2D B-mode, and 3D ultrasound imaging techniques to identify an ideal site and respiratory condition for TE probe placement (Specific Aim-2). **Chapter 4** delivers an observational study of healthy subjects and CLD patients to investigate how various body postures influence liver stiffness, and the feasibility and reliability of TE (Specific Aim-3). This exploratory research adopted a novel TE system, which has been fully validated in **Chapter 2**. The results from **Chapter 3 and Chapter 4** provide valuable references for designing a straightforward and evidence-based protocol for TE practitioners. Finally, **Chapter 5** draws conclusions from the studies presented in **Chapters 2 to 4**. Recommendations for future works are also elaborated.

Chapter 2. Evaluation of Palm-Sized Wireless TE System Guided by Real-Time B-Mode Ultrasound Imaging

This chapter has been published as:

Palm-Sized Wireless Transient Elastography System with Real-Time B-Mode Ultrasound Imaging Guidance: Toward Point-of-Care Liver Fibrosis Assessment.

Huang, Z.-H., Wang, L.-K., Cai, S.-Y., Chen, H.-X., Zhou, Y., Cheng, L.-K., Lin, Y.-W., Zheng, M.-H., & Zheng, Y.-P.

Diagnostics, vol. 14, no. 2, p. 189, 2024, doi: 10.3390/diagnostics14020189.

2.1 Background

Chronic liver disease (CLD) represents a major and rising public healthcare issue, affecting an estimated 844 million individuals worldwide [124]. It can be caused by viral infections, such as hepatitis B or C virus, by excessive alcohol consumption, or by dietary habits leading to metabolic dysfunction-associated steatotic liver disease (MASLD), which was formerly called non-alcoholic fatty liver disease (NAFLD). Liver fibrosis is the common pathway for CLDs of various etiologies, culminating in cirrhosis. Cirrhosis alone causes 1.16 million deaths globally, ranking as the 11th leading causes of death in 2015 [5]. Although early fibrosis has been shown to be partly reversible [125], cirrhosis is, by definition, deemed an irreversible condition. Hence, the goal of CLD management is to monitor liver fibrosis severity and prevent progression to cirrhosis.

Biopsy is historically the reference standard for diagnosing liver fibrosis. However, its invasive nature impedes long-term CLD monitoring. Histologic analysis of liver specimens is also subject to inter-pathologist variability and sampling error [37]. The

serum biomarker method is minimally invasive, but its specificity and accuracy have been questioned [46]. These limitations have led to the rapid development of elastography modalities for assessing liver fibrosis in hepatology [56].

Shear wave-based elastography methods rely on shear wave propagation speed to quantify the mechanical properties of hepatic tissues, serving as a surrogate biomarker for liver fibrosis [53]. Although magnetic resonance elastography (MRE) has shown promising diagnostic accuracy against histology, its limited availability, high cost, and lengthy examination time have hindered its widespread clinical adoption. In contrast, the technological advantages of ultrasound elastography for characterizing the degree of liver fibrosis are being non-invasive, low-cost, rapid, of high patient acceptance, and having proven, excellent histopathological correlation. Two-dimensional shear wave elastography (2D-SWE) is one such technique that employs ultrasonically induced acoustic radiation force impulses to generate shear waves within the liver for liver stiffness measurement (LSM). 2D-SWE allows the simultaneous acquisition of anatomic B-mode images and stiffness mapping of the liver [67]. Another noteworthy technique is transient elastography (TE). TE by means of mechanical vibration excitation measures the speed of a 50 Hz shear wave propagating through the skin surface into the liver parenchyma [74]. Recommended by the World Health Organization (WHO) [126, 127] and major clinical guidelines [53-56, 128, 129], TE stands as an established and best-validated approach for the first-line assessment of CLD. Numerous studies have validated LSM with TE for diagnosing liver fibrosis across various etiologies, and demonstrated its role in treatment follow-up and prognosis prediction [53, 54].

Despite its success in hepatology, a commonly reported limitation of TE is the lack

of sufficient visual guidance for sampling the liver of interest [54, 55, 59, 87-89]. Conventional TE has primarily focused on the design of a single-element transducer, providing LSM alongside M-mode. Because no anatomic B-mode images are provided, TE practitioners have difficulty in targeting a liver parenchymal region devoid of blood vessels or focal lesions for analysis. This limitation contributes to the increasing frequency of TE failure or unreliable results and significantly reduces examination efficiency. Additionally, conventional TE systems have limited clinical acceptance due to their bulky, immobile, and wired natures [117]. The existing setup confines TE assessment to an examination room, potentially limiting its utility beyond a hospital setting. For example, due to the rising prevalence of CLDs and associated risk factors such as obesity, Pere et al. [130] advocated for programs of screening for liver fibrosis. Equipment size is a practical consideration for implementing large-scale liver examinations in the community [131]. This becomes another room for improving TE techniques and expanding its clinical applications. In light of these obstacles, there is a need for incorporating the capability of B-mode imaging and point-of-care ultrasound (POCUS) into the TE examination procedure to make TE suitable for point-of-care applications. Moreover, although the 50-Hz vibration source is commonly chosen in TE research [74], literature specifically investigating other vibration settings for LSM is limited and the ideal vibration amplitude has not yet been determined.

2.2 Study Aims

In this work, we introduce a newly developed TE system (named ‘Liverscan’) which is palm-sized in dimension and enables LSM guided by real-time B-mode imaging of liver morphology. Despite its potential utility beyond routine clinical practice, the Liverscan system has yet to undergo clinical scrutiny. Hence, the primary objectives of this methodological cross-sectional study were to assess the accuracy of LSM using Liverscan on tissue-mimicking phantoms, and the reliability and validity of LSM in adult patients with confirmed CLD of various etiologies. Another objective was to investigate the effect of the vibration amplitude on liver stiffness.

2.3 Methods

2.3.1 Introduction to the Liverscan System

The novel Liverscan® system (Eieling Technology Limited, Hong Kong, China) comprises an all-in-one probe and a paired software installed in a terminal device **(Figure 2-1)**. The battery-driven probe wirelessly connects to a Windows-based notebook computer or tablet via Wi-Fi communication, and houses a voice-coil motor mounted on the axis of a 3.5 MHz phased array ultrasonic transducer. This engineering design allows simultaneous B-mode imaging and stiffness measurement of the liver with a single integrated probe. The cylinder-like probe measures 21.1 cm in length, 5.1 cm in width, and 6.4 cm in height. Its tip serves as both a low-frequency vibrator to generate shear waves and an ultrasonic transmitter–receiver to trace wave propagation. Specifically, the vibrator induces shear waves through external mechanical vibration with low frequency (50 Hz) and mild amplitude. The phased array transducer, configured with 32 elements operating at 20 frames/s, produces real-time B-mode images in a sector field of view (FOV). A single beam centred at the array acquires RF signals at an ultra-fast rate of 6400 frames/s and within a short time span of 80 ms to image the axial component of the shear wave along the beam direction. RF data acquisition from this single scan line synchronizes with the start of mechanical excitation. The system allows for the adjustment of the region of interest (ROI) location axially and radially, aiding in the avoidance of reverberation artifacts beneath Glisson's capsule [55, 69]. In this study, the ROI is set at a depth range of 25–65 mm, consistent with other clinically available TE systems.

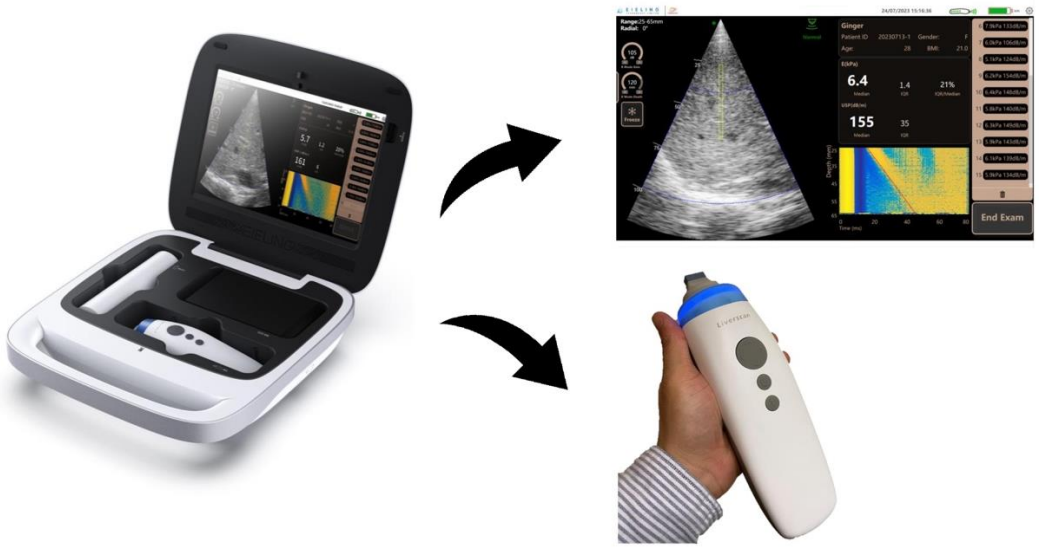

Figure 2-1. Schematic representation of the Liverscan probe and paired software interface. Working principle of the Liverscan system: LSM procedure including shear wave generation and ultrasound acquisition is guided by real-time B-mode imaging. The displacements of the elastic liver tissue caused by the passage of the shear wave are documented via ultra-fast RF acquisitions, resulting in the formation of an elastogram. The elastogram, which estimates the Young's modulus of the liver, is visualized as a strain image as a function of time and depth.

To construct an elastogram (a shear wave propagation map), axial displacements are estimated from the sequences of RF signals using a texture disturbance detection approach. The elastogram appears as a 2D color-coded image representing the spatial–temporal information of the propagating shear wave. A MobileNet-based regression algorithm detects and computes the shear wave trajectory, reflecting liver tissue deformation associated with the passage of the shear wave. Shear wave speed is deduced from the slope of the trajectory pattern and converted into the Young's modulus using the equation:

$$E = 3\rho Vs^2$$

where E is the Young's modulus, V_S is the shear wave speed, and ρ is the assumed tissue density (1000 kg/m^3, equivalent to water density).

A computer terminal is used to display B-mode images in real-time alongside the algorithmic calculation of the Young's modulus and corresponding elastogram. This stand-alone processing unit contributes to the downsizing of the probe.

2.3.2 Study Design

The framework of the system evaluation on LSM is summarized in **Figure 2-2**. To evaluate the accuracy of Liverscan in quantifying the Young's modulus, a series of phantoms with established reference values were used **(Figure 2-3)**. Between May 2022 and June 2023, a large clinical trial was conducted, and adult subjects were recruited from two participating institutions: The Hong Kong Polytechnic University and The First Affiliated Hospital of Wenzhou Medical University. To evaluate the feasibility and validity of Liverscan in a clinical setting, we performed head-to-head comparisons of its LSM with other clinically available ultrasound elastography systems: Fibroscan® (fs, Echosens, Paris, France) and Fibrotouch® (ft, Hisky, Wuxi, China), which are based on conventional TE, and Aixplorer® (SuperSonic Imagine, Aix-en-Provence, France), based on 2D-SWE **(Figure 2-3)**. We employed different statistical analyses and compared the results to investigate the variability among the elastography modalities. Additionally, the intra- and inter-operator reliability of LSM using Liverscan were established.

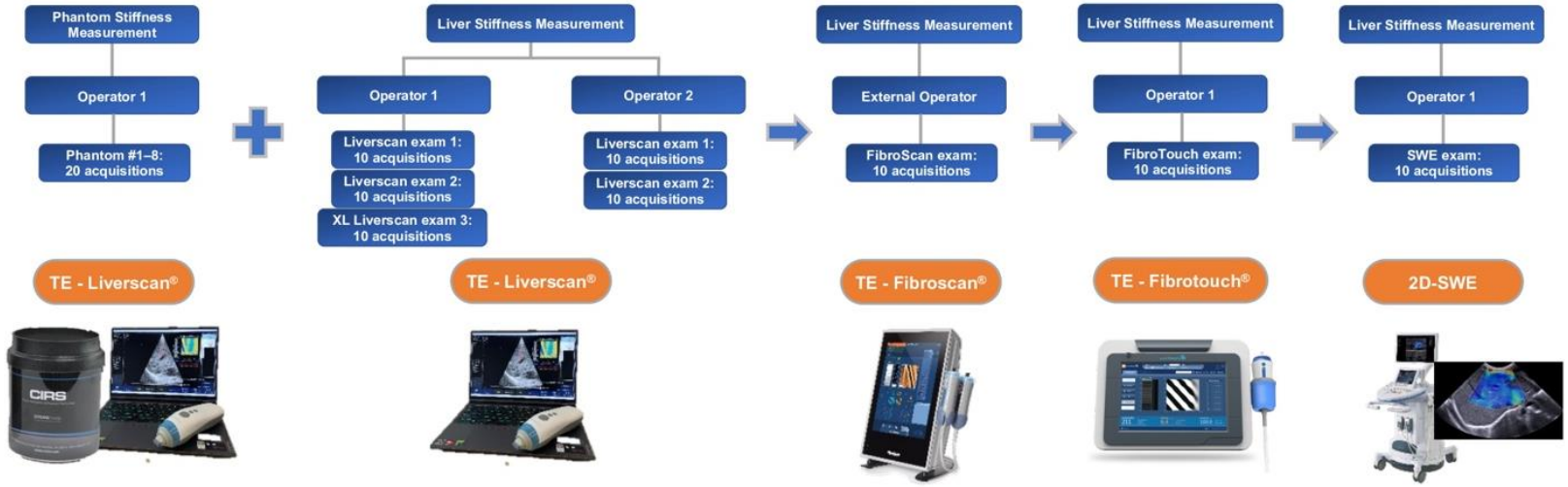

Figure 2-2. A framework for the methodological research to evaluate the palm-sized TE system with real-time B-mode guided LSM.

(A)

(B)

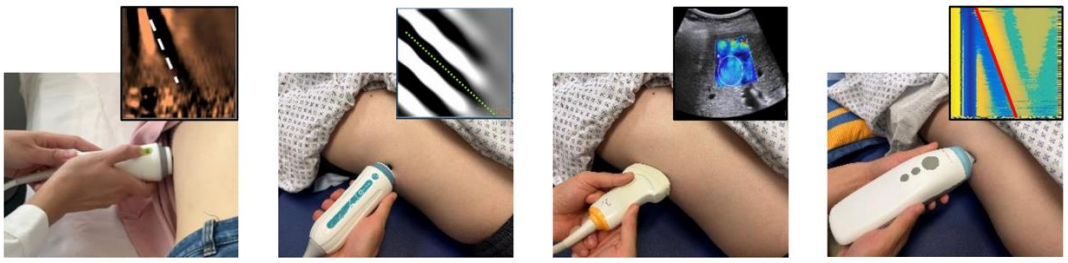

Figure 2-3. Experimental setup for Liverscan validation. (A) Phantom experiment setup: the probe was placed over the phantom using a custom testing platform; (B) Human experiment setup for the comparative study: four liver elastography techniques in a randomized order were administrated to each subject on the same day.

In the Hong Kong cohort, the examinations of Liverscan, conventional TE-ft, and 2D-SWE were conducted on the same day of the examination of conventional TE-fs. While subjects received conventional TE-fs at an external health check clinic (Virtus Medical Centre, Hong Kong, China) where a Fibroscan system is installed, other

elastography examinations were conducted at the Clinical Ultrasound Lab of The Hong Kong Polytechnic University. The examination order among different liver elastography techniques was randomized for each subject. In the Wenzhou cohort, patients underwent the conventional TE-fs and Liverscan examinations on the same day. Demographic, anthropometric, and clinical data were recorded by research coordinators using standard protocols. All operators participating in this study were blinded to the patients' clinical and other liver elastography data. Ethical approval was obtained from the Institutional Review Board of The Hong Kong Polytechnic University (HSEARS20210809002). This prospective, cross-sectional, dual-center imaging study complies with the Declarations of Helsinki and the STROBE reporting criteria.

2.3.3 Phantoms

In order to quantitatively study the accuracy of Liverscan in estimating the Young's modulus, experiments were carried out on multiple commercial elasticity phantoms. As part of Model 039 (Computerized Imaging Reference Systems (CIRS), Inc., Virginia, USA) and KS215 T-3 (Institute of Acoustics, Chinese Academy of Science, Beijing, China), these phantoms were specifically designed for quality control and performance testing of clinical ultrasound-based elastography systems. Prior to assembly, they underwent a process of standard shear wave speed characterization using mechanical vibration excitation. To eliminate the possible impact of viscosity and ease direct comparison among elastography techniques, each phantom contains homogeneous, isotropic, and nearly completely elastic materials. In this study, eight phantoms with respective Young's modulus values of 1.45 kPa, 2.22 kPa, 4.66 kPa, 7.0 kPa, 12.8 kPa, 16.2 kPa, 32.1 kPa and 76.9 kPa were tested. These nominal values encompass the elastic properties spanning healthy through cirrhotic livers and serve as the ground-truth for assessing measurement accuracy.

To obtain measurements, the Liverscan probe was mounted on top of the phantoms and fixed using a probe holder. Ultrasound gel was applied to the phantom surface to ensure acoustic coupling. Twenty valid measurements were carried out in the different locations of each phantom, with the tip of the probe in contact with the phantom surface to maintain mechanical coupling. A static applied force between the transducer and phantom surface was monitored and standardized at 5 newtons across the phantoms. A single operator, blinded to the phantom being tested and its LSM result, was involved. The order of data acquisition was randomized for phantoms. Each stiffness value represents the Young's modulus of the tested phantom, and the mean and median of the twenty phantom measurements were calculated for subsequent statistical analyses.

2.3.4 Subjects

A *priori* analysis using the G*Power software (Heinrich-Heine-Universität Düsseldorf, Düsseldorf, Germany) projected a sample size of 84 subjects for the Pearson correlation, with a medium Cohen's effect size $r = 0.3$, statistical power of 0.8, and a two-sided significance level of 0.05 under a bivariate correlation design. The final target sample size was set at 121 to allow for 30% dropout [78]. Adult subjects were enrolled if they had been diagnosed with CLD caused by hepatitis B virus (HBV), hepatitis C virus (HCV), MASLD, alcoholic liver disease (ALD), or autoimmune hepatitis (AIH) and clinically indicated for follow-up of CLD. Subjects were excluded in the case of ascites, pregnancy, active implantable cardiac device, liver transplantation, and refusal to receive contemporaneous liver elastography examinations. All subjects gave written informed consent and fasted for a minimum of 3 h before an examination procedure.

A total of 121 patients were divided into three subgroups used for different statistical analyses. Specifically, LSM by Liverscan was validated against that by conventional TE-fs in the complete cohort of 121 subjects, in a dual-center setting. We further evaluated the association of Liverscan, conventional TE-ft, and 2D-SWE, in comparison with conventional TE-fs, in the subgroup of 90 subjects. In addition to the comparative studies on the validity of Liverscan, subjects were randomly invited to participate in a sub-analysis assessing operator reliability. Given the expected success rate with Liverscan set at 95%, a projected sample size of 60 was deemed necessary to estimate an excellent intraclass correlation coefficient (ICC) of 0.9 ± 0.05 and a dropout rate of 5% under a two-repetition design [132]. The reliability analysis involved two operators with different levels of experience and expertise; Operator 1 with a background in radiology had six years of experience in TE development and operation, while Operator 2 was a novice trained as an engineer.

As part of the study regarding the vibration amplitude effect, this subgroup of 60 subjects was further used to examine whether liver stiffness measured by Liverscan differs between the two vibration conditions: (a) 2-mm vibration amplitude and (b) 3-mm vibration amplitude. The amplitude level was quantified by the peak-to-peak displacement of a vibrating transducer tip. Of note, specific differences between these two vibration conditions of the Liverscan probe and the Fibroscan M probe include their vibration amplitude (2 or 3 mm vs. 2 mm), shape of their transducer tip (rectangle vs. circle), and size of their transducer tip (16*8 mm vs. 7 mm in diameter).

2.3.5 TE Examination

Based on the technical principle, TE examinations performed in this study fall into two categories: (a) conventional TE without B-mode guidance and (b) B-mode guided

TE.

In the conventional TE session, the Fibroscan (fs) and Fibrotouch (ft) systems were used. According to the procedure described previously [53-56, 74], subjects were asked to lie down in the dorsal decubitus position with the right arm in maximal abduction and placed behind their heads. The transducer tip of the probe was placed onto the skin surface between the ribs at the level of the right lobe of the liver. The Fibroscan XL probe was administrated to obese patients as recommended by an automatic probe selection tool [91]. Subjects who received the examination of conventional TE-fs using either the standard M or XL probe were included in this study. The examination of conventional TE-ft was performed with one universal probe designed for varying patient morphotypes. A minimum of 10 valid acquisitions with conventional TE-fs and TE-ft were performed on each subject, respectively.

In the B-mode guided TE session using Liverscan, the same examination procedure, including patient positioning and measurement protocol, were applied as outlined above. Assisted by real-time B-mode, a sufficiently thick portion of the liver parenchyma free of large vascular structures was identified and consecutively measured ten times. In the intra- and inter-operator reliability study, subjects were assessed twice by each of two operators, generating four experimental conditions per subject:

- First examination of Operator 1;
- Second examination of Operator 1;
- First examination of Operator 2;
- Second examination of Operator 2.

To avoid bias by a learning effect, Operator 1 and 2 independently performed the

Liverscan examinations in a randomized order, each operator being blinded to the LSM results of the other. During the 2nd examination procedure, the operator was blinded to the previously obtained LSM result of the 1st examination. The Liverscan probe was removed from the patient and repositioned between conditions, with the interval no less than 10 min.

In the vibration amplitude study, an attempt was made to collect at least 10 valid acquisitions with each of the 1-mm and 3-mm vibration amplitudes. To control for other possible confounders that might affect liver stiffness value, the measurement site and respiratory phase remained the same across the vibration conditions.

Overall, the same statistical procedure was applied to derive liver stiffness from the three TE examinations with conventional TE-fs, conventional TE-ft, and B-mode guided TE. The median stiffness value (in kPa) of the 10 valid acquisitions was considered representative of the Young's modulus of the liver and was calculated for each of the three TE examinations, respectively. As an indicator of variability between LSMs, the ratio of the interquartile range to the median value (IQR/median) was calculated. TE results were included in the final analysis if at least 10 valid acquisitions were made with an IQR/median ≤30% and a success rate ≥60%.

2.3.6 2D-SWE Examination

2D-SWE was performed using a convex probe (XC6–1, central frequency: 3.5 MHz) of the Aixplorer® system (SuperSonic Imagine, Aix-en-Provence, France) via the right intercostal approach [67, 69, 133]. Subjects were in the supine position with the right arm in maximal abduction. During the stiffness acquisition process, a rectangular SWE box was placed in the right liver parenchyma free of blood vessels, portal tracts, and focal lesions, at least 1 cm in depth from Glisson's capsule and between 2 and 7 cm

from the skin surface. Ten frames of SWE images were obtained from the right hepatic lobe during repeated inspiratory breath-holds. In the subsequent data analysis, a 1 cm diameter circular ROI was placed retrospectively over a region of a relatively homogeneous portion at a depth of 3–6 cm of the SWE box for LSM. To average the possible effect of heterogenous fibrosis, a third-party rater placed five individual ROIs in different sub-regions of each SWE box. The average of five SWE values derived from the circular ROIs and expressed in kPa was kept as the representative result for that SWE image. In this fashion, each SWE image was measured five times producing a total of 50 SWE value acquisitions for each subject. The median of the 50 SWE values obtained from the right-lobe segments was calculated and used in this study as the per-patient Young's modulus of the liver.

2.3.7 Statistical Analyses

All statistical analyses were performed using Statistical Package for Social Sciences (SPSS, IBM corporation, Armonk, NY, USA). The level of significance was set at 0.05.

Descriptive statistics. Cohort characteristics were descriptively summarized, expressing continuous variables as a median (interquartile range [IQR]) and categorical variables as absolute figures with percentages. Confidence intervals (CIs) were reported at the 95% level. A Friedman two-way ANOVA with post-hoc Dunn's test was conducted to compare the liver stiffness (kPa) and its corresponding IQR/median of LSM (%) across four liver elastography techniques, respectively.

Accuracy statistics. Comparisons were made between the Young's modulus of the phantoms measured by Liverscan and that reported by the manufacturers. According to the Radiological Society of North America Quantitative Imaging

Biomarker Alliance (QIBA) [134], three technical performance metrics of linearity, bias, and precision were used for the performance assessment of phantom Young's modulus quantification. Linearity and bias together assess the degree to which LSM provides an estimate of the true value. Linearity was analyzed using a first-order polynomial regression model of the average of measured values against reference values. Bias, defined as the percentage error between the two groups of values, was calculated for each phantom using the formula:

$$Bias\ (\%) = \frac{|Liverscan\ value\ (kPa)\ -\ Reference\ value\ (kPa)|}{Reference\ value\ (kPa)} \times 100\%$$

Precision assesses the relative variability between twenty repeated measurements, and was analyzed using the coefficient of variation (CV).

Validity statistics. Correlation relationships were examined among liver stiffness values measured by conventional TE-fs, conventional TE-ft, Liverscan, and 2D-SWE, respectively. A correlation matrix was constructed to visualize the pairwise comparison of Pearson correlation coefficients, whereby 0.1 <|*r*| <0.3 was considered weak correlation, 0.3 <|*r*|<0.5 moderate correlation, and |*r*|> 0.5 strong correlation. Using convectional TE-fs as the benchmark technique, Bland–Altman plots were constructed to examine the agreement of each pair. The linear relationship of convectional TE-fs against the other three elastography techniques was evaluated pairwise using the simple linear regression model. The Pearson correlation coefficient (*r*) as the strength metric of association, coefficient of determination (R^2) as the strength metric of linearity, and mean difference between techniques as the strength metric of agreement were reported for each pair.

Reliability statistics. We used intraclass correlation coefficient (ICC), standard

error of measurement (SEM), and coefficient of variation method error (CV_{ME}) to assess the inter-operator and intra-operator agreement for stiffness values derived from Liverscan. ICC was interpreted as follows: 0.90–1.00 = excellent, 0.75–0.90 = good, 0.5–0.75 = fair, and <0.5 = poor, according to Koo & Li's conventional criteria [135].

Vibration amplitude comparison. A Wilcoxon matched-pairs signed rank test compared liver stiffness under the 1-mm and 3-mm vibration amplitude levels of TE. Additionally, Pearson correlation of each paired vibration condition of convectional TE-fs and Liverscan were further analyzed.

2.4 Results

2.4.1 Phantom Measurement Accuracy

As presented in **Table 2-1**, the phantom results demonstrated that the measured values (both mean and median) for all phantoms were very close to or within the allowed error range provided by the phantom manufacturers. The linearity across eight reference phantoms is plotted in **Figure 2-4**, with a first-order linear model indicating very strong linear fit ($R^2 = 1$). The precision, as assessed by the CVs of twenty repeated measurements, ranged from 1.0–15.5%, and bias was less than 10% for all phantoms.

Table 2-1. Accuracy analysis of phantom Young's modulus measurement across eight phantoms.

	Ground-truth (kPa)	Mean ± SD / median [IQR] (kPa)*	Bias (%)	CV (%)
Phantom #1	1.45 ± 0.1	1.6 ± 0.2 / 1.5 [0.3]	8.6	15.5
Phantom #2	2.22 ± 0.2	2.2 ± 0.0 / 2.2 [0.0]	1.1	1.0
Phantom #3	4.66 ± 0.5	4.7 ± 0.2 / 4.7 [0.2]	1.4	3.6
Phantom #4	7.0 ± 0.2	6.9 ± 0.3 / 7.0 [0.2]	1.9	4.7
Phantom #5	12.8 ± 1.3	13.1 ± 0.5 / 13.1 [0.6]	2.6	3.7
Phantom #6	16.2 ± 0.6	16.6 ± 0.5 / 16.6 [0.3]	2.2	2.8
Phantom #7	32.1 ± 0.4	32.9 ± 1.9 / 33.0 [2.7]	2.5	5.8
Phantom #8	76.9 ± 7.7	78.8 ± 4.5 / 77.9 [6.3]	2.5	5.7

IQR = interquartile range; SD = standard deviation; CV = coefficient of variation.
*The Young's modulus of phantoms was expressed as mean ± SD or median [IQR] for twenty repeated measurements.

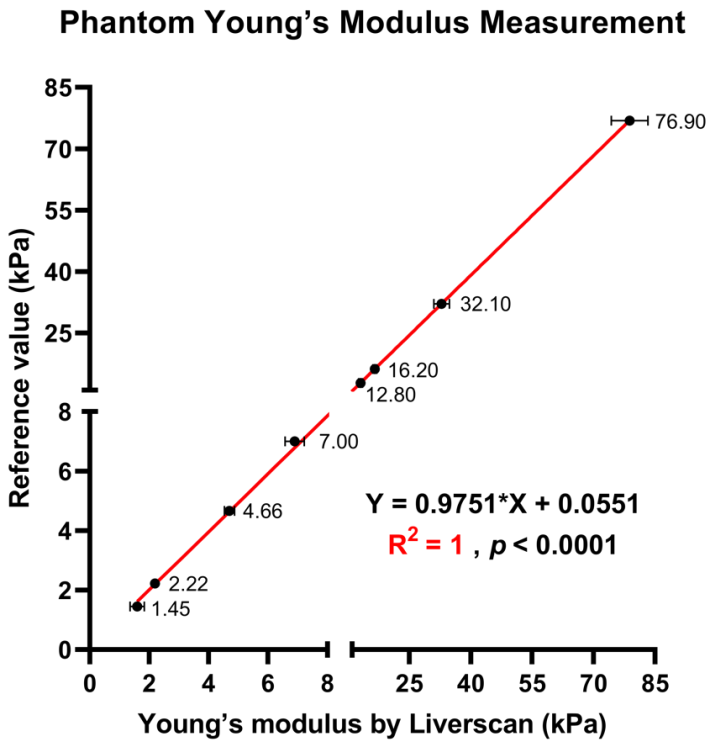

Figure 2-4. Measurement of Young's modulus across eight phantoms with known reference values: scatterplot showing the linear relationship of the Young's modulus of the phantoms derived by Liverscan against the truth values.

2.4.2 Subject Demographics

Between May 2022 and June 2023, a convenience sampling approach was adopted to recruit 121 eligible subjects with a history of known CLD for this study. The characteristics of the 121 patients are outlined in **Table 2-2**. Ninety patients were recruited at The Hong Kong Polytechnic University and thirty-one at The First Affiliated Hospital of Wenzhou Medical University. Fifty-four were women (45%) and the median

age was 54 years (range: 22–73 with an IQR of 18). The majority (41%) of patients were experiencing CHB (additional 21% with coexistent steatosis) or CHC, and 35% had MASLD. The median BMI was 24 kg/m^2 (range: 16–41 with an IQR of 5). In this cohort, the proportion of Fibroscan XL probe use is 10.7%. Over one-third of the patients (35%) were overweight or obese, and more than half (57%) were classified as having central obesity. The median skin–capsular distance was 13 mm (range: 5–26 with an IQR of 7).

Table 2-2. Characteristics of the study cohort (n = 121).

Characteristics	Median [IQR] or Proportion % (n)
• Demographics	
Male	55% (67)
Age, years	54 [18; range 22–73]
Overweight & obese	35% (42)
Central obesity	57% (69)
Metabolic syndrome	15% (18)
• Anthropometrics	
Weight, kg	65 [16; range 43–119]
BMI, kg/m^2	24 [5; range 16–41]
Waist circumference, cm	84 [17; range 65–131]
Skin-to-liver capsule distance, mm	13 [7, range 5–26]
• Liver disease aetiology	
Viral (CHB, CHC)	41% (50)
MASLD	35% (42)
ALD	3% (4)
Coexistence of HBV and MASLD	21% (25)
• Liver stiffness, kPa	
Conventional TE (Fibroscan)	5.4 [4.5; range 2.4–39.9]
B-mode guided TE (Liverscan)	5.9 [5.4; range 2.7–38.2]
• IQR/Median of LSM, %	
Conventional TE (Fibroscan)	12 [8; range 3–27]
B-mode guided TE (Liverscan)	23 [13; range 8–45]

IQR = interquartile range; BMI = body mass index; LSM = liver stiffness measurement; MASLD = metabolic dysfunction-associated steatotic liver disease; CHB = chronic hepatitis B; CHC = chronic hepatitis C; ALD = alcoholic liver disease.

2.4.3 Inter-Technique Difference Comparison

Figure 2-5 summarizes the aggregated LSMs and IQR/median results from the four-technique comparisons in the subgroup of 90 patients. A Friedman ANOVA identified differences in median LSMs among conventional TE-fs (4.6 kPa, IQR: 3.7–5.8), conventional TE-ft (5.8 kPa, IQR: 4.6–6.9), Liverscan (5.3 kPa, IQR: 4.5–6.4), and 2D-SWE (5.8 kPa, IQR: 4.7–6.7), $\chi^2(3) = 64.366$, $p < 0.001$. Post-hoc Dunn's test revealed that Liverscan and 2D-SWE produced the similar stiffness values ($p = 0.364$), which were significantly greater than those by conventional TE-fs (all $p < 0.001$). The aggregated variability of LSMs, as assessed by the ratio of IQR/median, significantly differed across the four techniques, except for conventional TE-fs and 2D-SWE ($p = 1.000$). Notably, Liverscan exhibited the significantly highest median IQR/median value (23% with an IQR of 18–31%, $p < 0.001$), compared with conventional TE-fs (12% with an IQR of 7–15%), conventional TE-ft (8% with an IQR of 4–11%), and 2D-SWE (12% with an IQR of 8–18%).

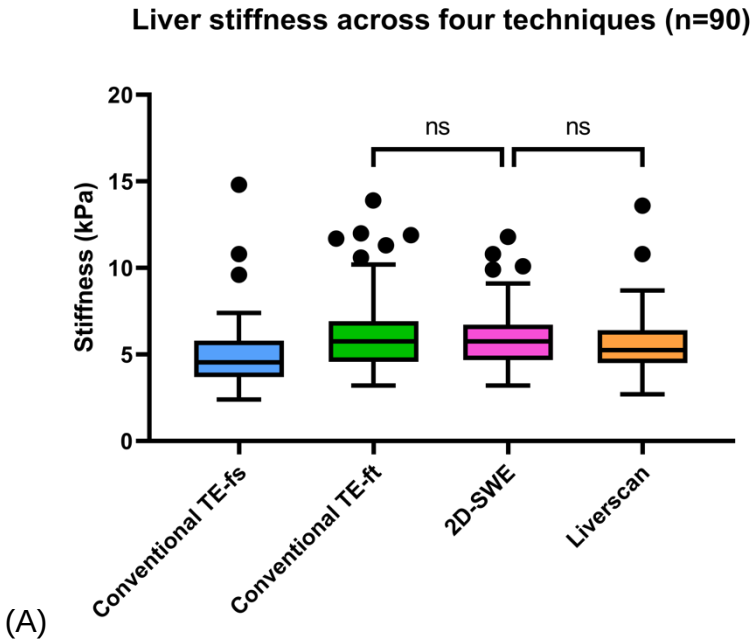

(A)

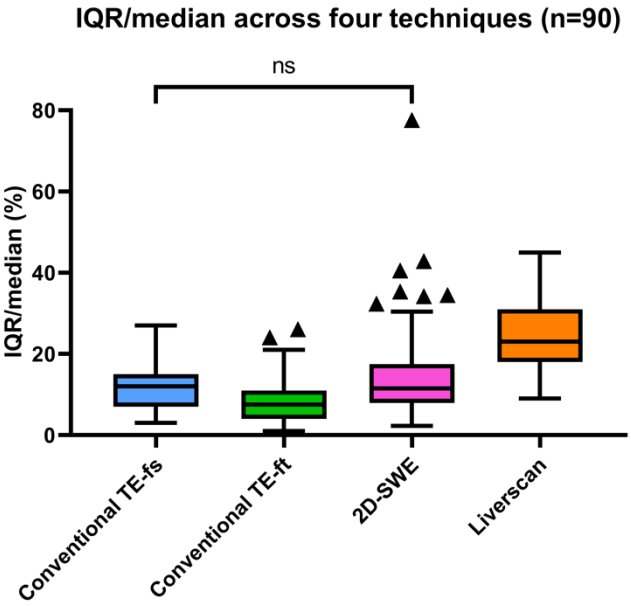

(B)

Figure 2-5. Aggregated results of (A) liver stiffness (kPa) and (B) IQR/median of LSMs (%) among four elastography techniques (ns: $p > 0.05$; $p \leq 0.05$ otherwise).

2.4.4 Operator Reliability

The intra-operator and inter-operator reproducibility of LSM using Liverscan was analyzed in a subgroup of 60 patients **(Table 2-3)**. For intra-operator reliability, $ICC_{(3,1)}$ was 0.913 (95% CI: 0.859 to 0.947) for Operator 1 and 0.890 (95% CI: 0.822 to 0.933)

for Operator 2. To examine whether inter-operator reliability varied with operation experience, we grouped two operators for each of the first and second examination sessions and calculated two independent sets of inter-operator ICCs for comparison. Results showed that the inter-operator $ICC_{(2,1)}$ for the second examination (0.856, 95% CI: 0.770 to 0.911) was marginally larger than that for the first examination (0.824, 95% Cl: 0.721 to 0.891). The SEM and CV_{ME} of all measurements ranged from 0.6 to 0.8 kPa and from 9.6 to 14.0%, respectively.

Table 2-3. Intra- and inter-operator reliability results for liver stiffness measurement (n = 60).

Liver stiffness (kPa)	**$ICC_{(3,1)}$[a]/$_{(2,1)}$[b] (95% CI)**	**SEM (kPa)**	**CV_{ME} (%)**
Intra-operator reliability			
Operator 1	0.913 (0.859–0.947)[a]	0.558	9.605
Operator 2	0.890 (0.822–0.933)[a]	0.679	11.727
Inter-operator reliability			
Exam 1 by Operator 1 vs. 2	0.824 (0.721–0.891)[b]	0.814	14.011
Exam 2 by Operator 1 vs. 2	0.856 (0.770–0.911)[b]	0.761	13.143

ICC = intraclass correlation coefficient; CI = confidence interval; SEM = standard error of measurement; CV_{ME} = coefficient of variation and method error;

Intra-operator ICC: tests between two repeated exams conducted by Operator 1 and 2, respectively;

Inter-operator ICC of Exam 1: tests between the 1st examination conducted by Operator 1 vs. the 1st examination conducted by Operator 2;

Inter-operator ICC of Exam 2: tests between the 2nd examination conducted by Operator 1 vs. the 2nd examination conducted by Operator 2;

[a]ICC computed using two-way mixed model and consistency; [b]ICC computed using two-way random model and consistency.

2.4.5 Pairwise Validity Comparison

Of the 121 patients, liver stiffness as assessed by conventional TE-fs and Liverscan was highly correlated (r = 0.975, 95% CI: 0.964 to 0.982, p < 0.001). The relationship between liver stiffness for each subject was fitted to a linear regression model (Y = 0.9544 × X + 1.107) and the linearity was strong (R^2 = 0.950). A Bland–Altman plot showed a small mean difference of −0.77 kPa (95% limit of agreement: −3.44 to 1.90) between techniques, indicating minimal overestimation by using Liverscan **(Figure 2-6)**.

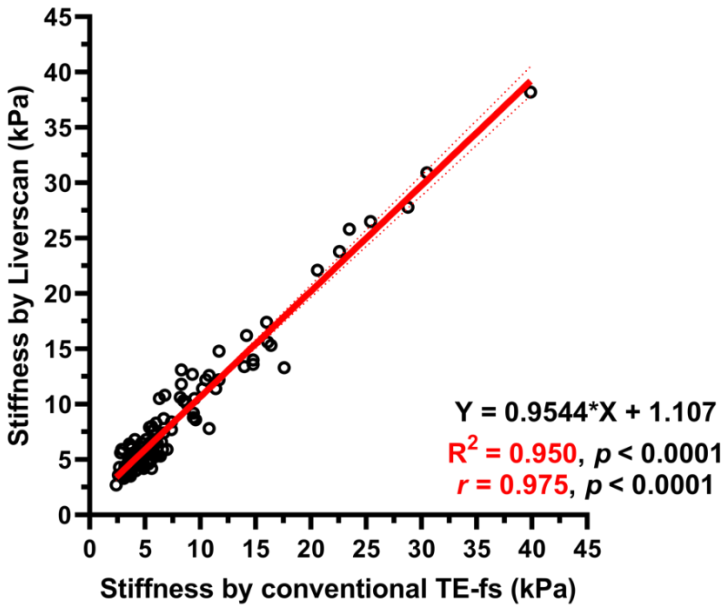

(A)

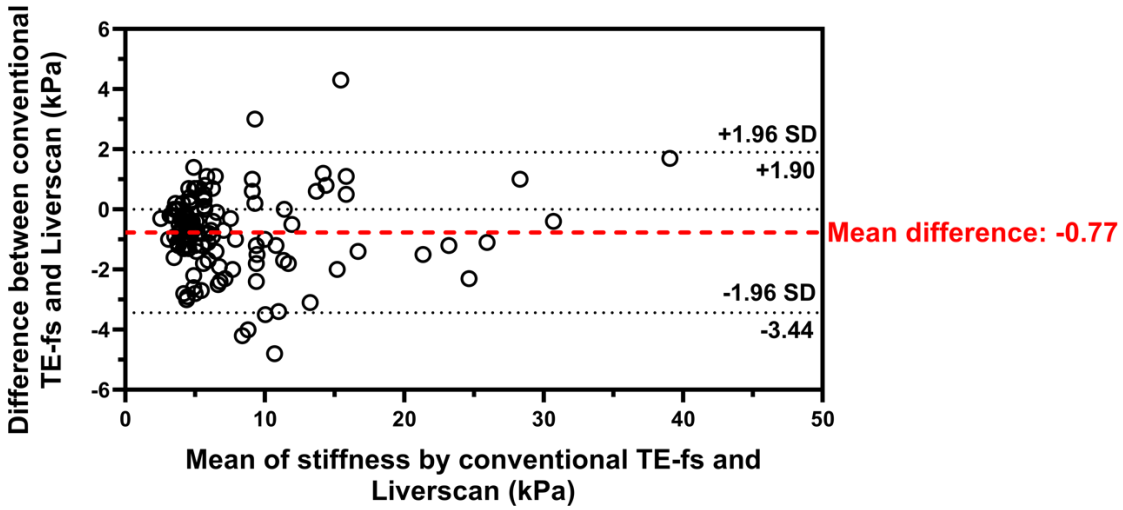

(B)

Figure 2-6. Liver stiffness measured by conventional TE-fs vs. Liverscan. (A) Scatterplot with Pearson correlation and simple linear regression analysis; (B) Bland–Altman analysis.

The correlation matrix results of 90 patients showed positive and statistically significant Pearson correlation coefficients of all pairs (*r* ranging from 0.55 to 0.79, $p < 0.001$), indicating that liver stiffness measured by the four techniques were inter-correlated **(Figure 2-7)**. As the only technique allowing the mapping of fibrotic distribution, 2D-SWE exhibited a similar correlation with conventional TE-fs ($r = 0.62$, 95% CI: 0.471 to 0.731, $p < 0.001$) and Liverscan ($r = 0.66$, 95% CI: 0.524 to 0.762, $p < 0.001$). The strongest correlation was observed in the pair of conventional TE-fs vs. Liverscan, with a Pearson correlation coefficient of 0.79 (95% CI: 0.691 to 0.854, $p < 0.001$). Conventional TE-fs correlated nominally more with Liverscan ($r = 0.79$) than with conventional TE-ft ($r = 0.65$, 95% CI: 0.507 to 0.752, $p < 0.001$) and with 2D-SWE ($r = 0.62$, 95% CI: 0.471 to 0.731, $p < 0.001$). This relationship was confirmed by linear regression and Bland–Altman analyses, where conventional TE-fs and Liverscan demonstrated the lower mean difference of −0.69 kPa (95% limit of agreement: −2.91

to 1.54) and stronger linearity (R^2 = 0.617, p < 0.001) than other pairs **(Figure 2-8)**. Specifically, conventional TE-fs and Liverscan demonstrated the lowest mean difference of −0.69 kPa (95% limit of agreement: −2.91 to 1.54) among all paired comparisons. Most difference scores between the techniques were within the limits of agreement and symmetrically distributed around the mean difference. Greater differences in LSMs were observed at the higher mean values which coincided with the result of the 121-patient cohort. Liverscan-derived measurements exceeded conventional TE-derived measurements, with the mean difference of −0.69 kPa indicating minimal overestimation by using Liverscan. This trend was also observed in conventional TE-ft and 2D-SWE with respect to the reference technique of conventional TE-fs. As assessed by 'goodness-of-fit' in a linear regression model, the linearity of conventional TE-fs against Liverscan (R^2 = 0.617, p < 0.001) was nominally higher than that of conventional TE-fs against conventional TE-ft (R^2 = 0.417, p < 0.001) and 2D-SWE (R^2= 0.381, p < 0.001) **(Figure 2-9)**.

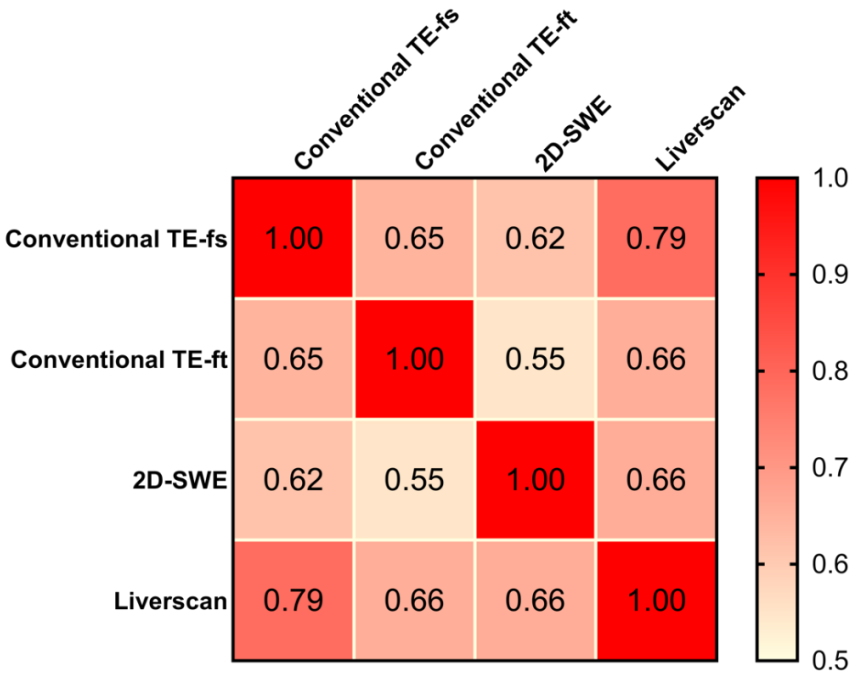

Figure 2-7. Pearson correlation matrix: comparison among four elastography techniques.

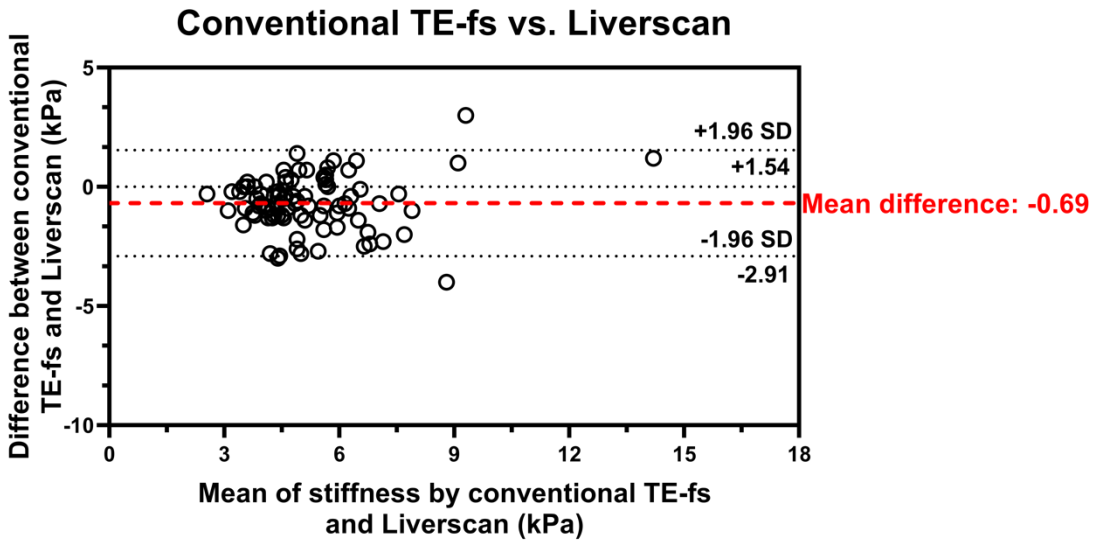

(A)

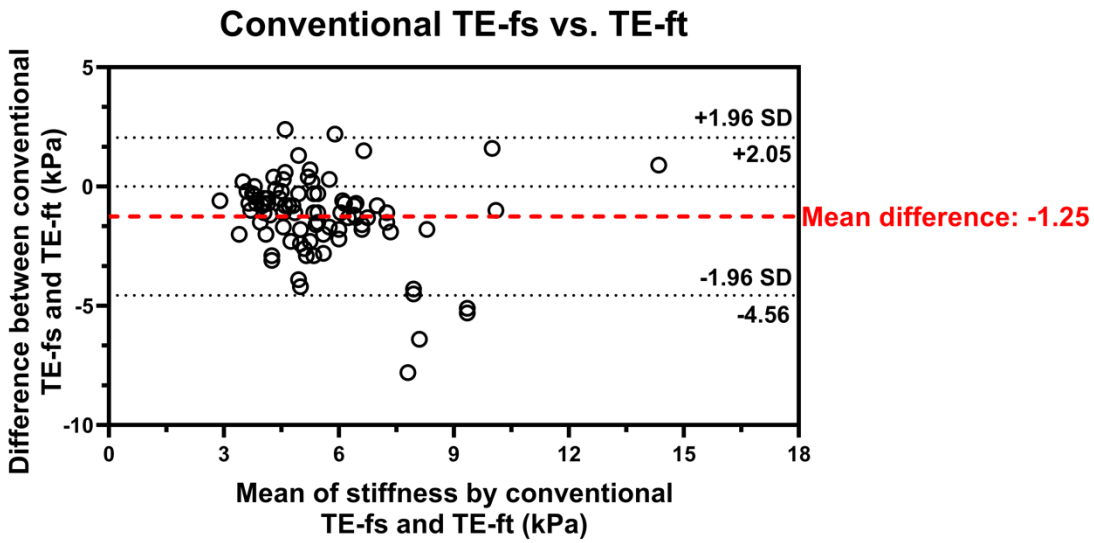

(B)

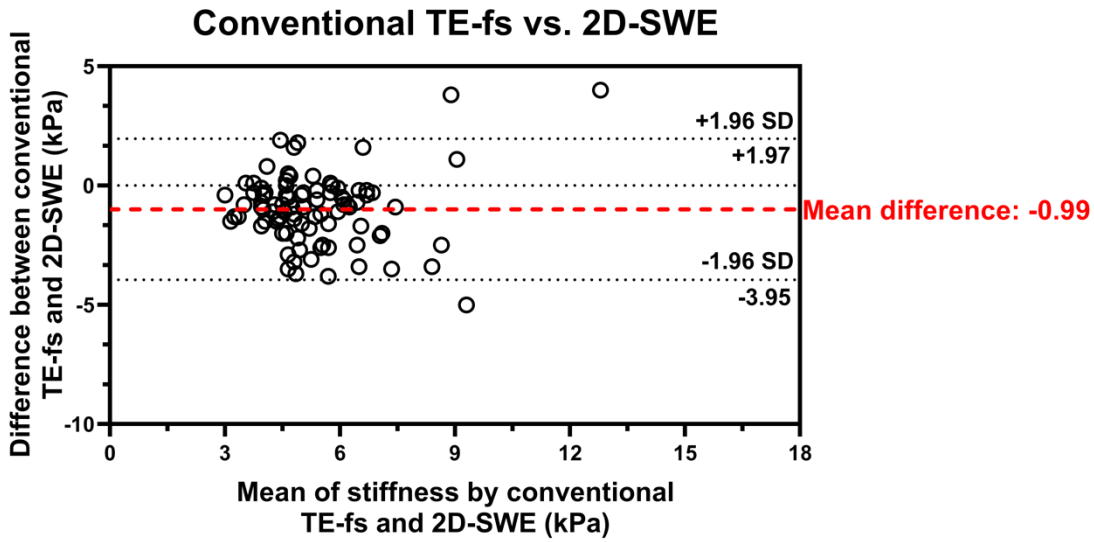

(C)

Figure 2-8. Bland-Altman plots illustrating agreement of liver stiffness between (A) conventional TE-fs vs. Liverscan; (B) conventional-fs vs. conventional TE-ft; (C) conventional TE-fs vs. 2D-SWE.

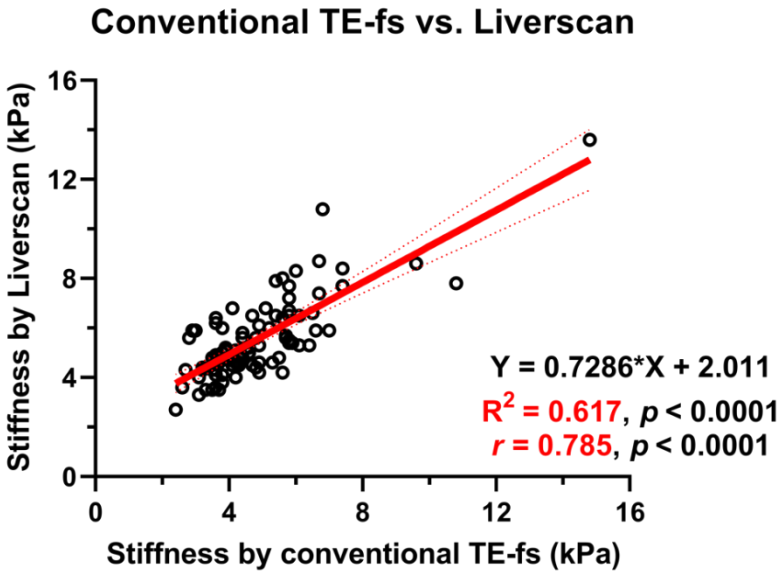

(A)

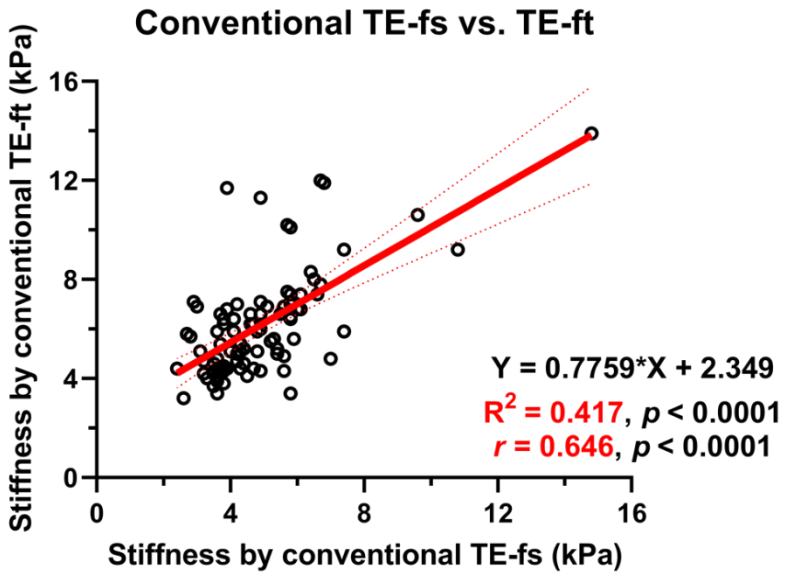

(B)

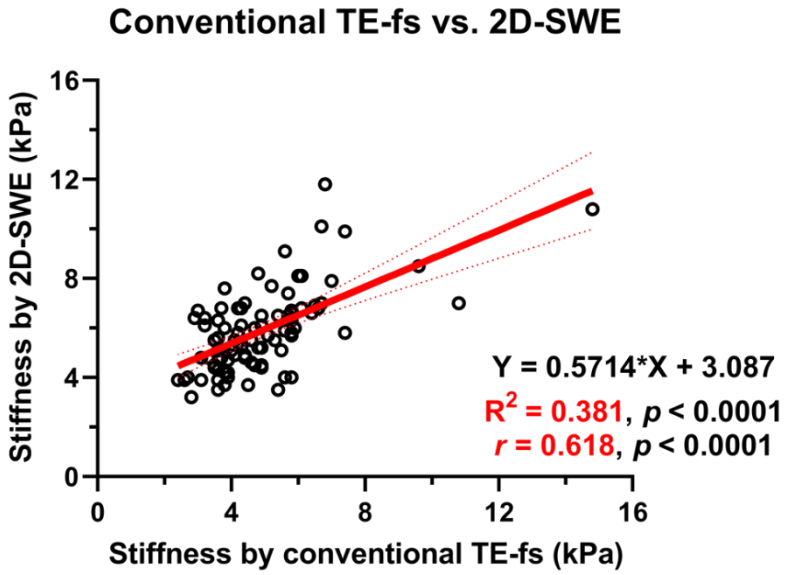

(C)

Figure 2-9. Scatterplots illustrating linearity and correlation of liver stiffness between (A) conventional TE-fs vs. Liverscan; (B) conventional-fs vs. conventional TE-ft; (C) conventional TE-fs vs. 2D-SWE.

2.4.6 Vibration Amplitude Comparison

No significant difference in liver stiffness was found between the 1-mm (5.4 kPa, IQR: 4.7–6.7) and 3-mm (5.3 kPa, IQR: 4.5–6.5) vibration amplitudes exerted by TE,

a median difference of −0.2 kPa, p = 0.121 **(Figure 2-10, A)**. The correlation matrix of Pearson correlation coefficients further visualized pairwise comparisons between liver stiffness measured by the 2-mm vibration amplitude of conventional TE-fs vs. the 1-mm and 3-mm vibration amplitudes of Liverscan **(Figure 2-10, B)**. Inter-correlations were seen among the three different combinations of the amplitude levels. The correlation between the two different vibration conditions of Liverscan was the strongest (r = 0.915, p < 0.001). The correlation of the 2-mm vibration amplitude of conventional TE-fs with the 1-mm vibration condition of Liverscan was comparable to that with the 3-mm vibration condition (r = 0.802 vs. 0.832).

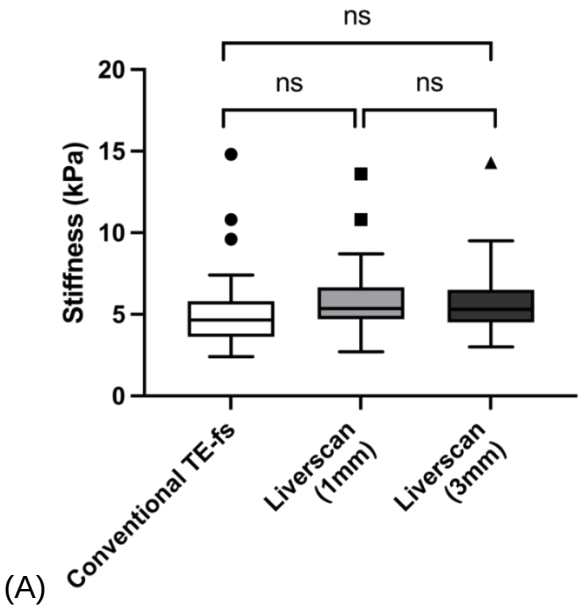

(A)

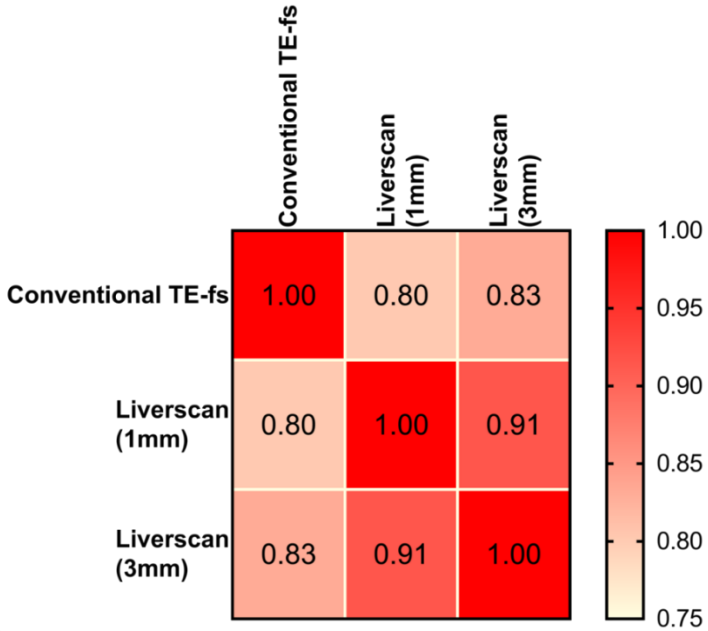

(B)

Figure 2-10. Effect of vibration amplitude on liver stiffness. (A) Boxplot for comparing the two vibration amplitude conditions of Liverscan; (B) Pearson correlation matrix among the three vibration amplitudes (ns: $p > 0.05$; $p \leq 0.05$ otherwise).

2.5 Discussion

The role of TE in hepatology is well-established and unquestionable; however, challenges persist regarding its accessibility and utility. For example, examination inefficiency and failure related to inadequate imaging guidance is not uncommon during a LSM procedure. The large size and immobility of conventional TE systems also limits their use in contexts where inclusion could optimize patient care workflow, such as ward rounds and office consultations, i.e., point-of-care applications. Addressing these issues requires engineering efforts to further advance the TE examination procedure. This is our motivation to develop a palm-sized wireless TE system with real-time B-mode as a guidance tool, aiming to maximize the efficacy of TE in both inpatient and outpatient settings. This study adopted a head-to-head comparison design, supporting the feasibility and validity of Liverscan as a liver elastography modality compared to three other existing systems. In particular, its performance of LSM was demonstrated by small biases (range 1.1–8.6%) for eight reference phantoms and a high correlation (r = 0.975) between liver stiffness measured by conventional TE-fs and Liverscan in 121 patients with varying degrees of fibrosis severity. Moreover, LSM by Liverscan provided high intra- and inter-operator agreement (ICC range 0.824–0.913). As a secondary analysis, liver stiffness measured using the 1-mm and 3-mm vibration amplitudes were found to be comparable (p = 0.121).

Phantom analysis. The first step toward validating the performance of Liverscan was to perform a study on calibrated phantoms devoid of potential *in vivo* confounders, such as respiratory motion and liver heterogeneity. Experiments involving eight phantoms showed that this system can accurately estimate the Young's modulus.

Discrepancies from the known reference values were considered acceptable, with a bias of less than 10% in all phantoms and a mean bias of 2.9 ± 2.4%. One plausible explanation for the observed bias is that, according to the KS215 T-3 phantom manufacturer, phantom reference values were derived from the shear wave speed-based analysis that employed a broadband frequency range of 50 Hz to 500 Hz. This wide spectrum differed from TE operating at a typical 50-Hz frequency, while the elastic property is dependent of the frequency itself. Of note, small biases of 1.9–2.6% were observed for phantoms within the clinically relevant range of 7 kPa to 16 kPa, representing progressive fibrosis stages. The precision of twenty measurements per phantom proved satisfactory, with the CVs below 16%. The small CVs reflected the homogeneity of the phantom materials, as repeated measurements were taken at different locations. This finding aligned with prior results from two other phantom studies, which had reported CVs of 0.6–9.8% [136] for 2D-SWE and 0–9% for TE [137].

Operator reliability. Our results affirmed that LSM by Liverscan was highly reproducible, characterized by excellent-to-good inter- and intra-operator agreement. The reported ICCs between 0.824 and 0.913 were similar to those shown in one reliability study applying conventional TE to a CHB cohort (ICCs: 0.86–0.96) [138]. The reproducibility of Liverscan was even higher than another large MASLD study [139], with the intra-operator ICC of 0.837 and inter-operator ICC of 0.790 specifically reported for conventional TE and the intra-operator ICC of 0.847 and inter-operator ICC of 0.705 specifically reported for 2D-SWE. Nevertheless, caution is warranted in making such direct comparisons, because the patient samples involved were not exactly the same. Excellent-to-good intra-operator reliability ($ICC_{(3,1)}$ of nearly 0.9 observed in both the experienced and novice operators) suggested that medical background and expertise may not be a necessity for obtaining reproducible results.

Additionally, inter-operator reliability analyses confirmed good agreement in two independent sessions, but inferior to the intra-operator reliability. Inter-operator $ICC_{(2,1)}$ of 0.856 for the second examination appeared slightly higher than that of 0.824 for the first examination, with a minimum 10 min interval between them. Similar trends have been reported by Fang et al. [140], who noted the improved inter-operator reliability for 2D-SWE from the previous to latter session, separated by two weeks. We attributed this improvement to growing operational experience or learning retention. However, it remains debated whether the ICC increase of 0.032 represents a clinically meaningful change. Further validation is warranted in a larger cohort and among new operators with varying training levels.

The range of the CV_{ME} values (9.6–14.0%) suggested an acceptable degree of variability, with less variable measurements observed in intra-operator settings. Although no SEM data exist on the topic of liver elastography for comparison, the SEM values in our study (0.6–0.8 kPa) were deemed quite low. These SEM values were lower than those reported in a previous elastography study on lateral abdominal muscles (SEM: 7.8–10.7 kPa) [141]. Nevertheless, it is pertinent to excise caution in interpreting reliability results because biologic factors (rather than technical factors) may contribute to the variability in LSMs, especially in individuals with nonuniform distribution of liver fibrosis. On the other hand, the absence of overlying subcutaneous tissues that attenuate waves and homogeneous phantom materials may explain the less variable results observed in phantoms compared with human livers.

Validity comparison. This prospective study supported that B-mode guided TE can benchmark with conventional TE with respect to LSM. The Bland–Altman plot of Liverscan relative to conventional TE-fs as the reference technique revealed a minimal

mean difference (−0.77 kPa) and limits of agreement within ±4 kPa. A strong correlation and linearity between liver stiffness measured using both techniques (r = 0.975, R^2 = 0.950) were also established in a CLD cohort diagnosed with ALD, MASLD, CHB, and CHC. We further examined the association of contemporaneous use of different liver elastography techniques. The correlation between conventional TE-fs and 2D-SWE (r = 0.618) was consistent with that of previous literature [118, 142], which in part supported the validity of other pairwise comparisons analyzed in this study. Inter-correlation among the four techniques was observed in 90 CLD patients, with the strongest correlation (r = 0.785), strongest linear relationship (R^2 = 0.617), and highest inter-technique agreement (mean difference = −0.69) found at the pair of conventional TE-fs vs. Liverscan. These findings demonstrated that Liverscan was superior to conventional TE-ft and 2D-SWE when validated against conventional TE-fs.

Previous literature suggested shear wave frequency-dependent discrepancies in LSM between TE and 2D-SWE [68, 117, 118]. This could be explained by the lower frequency used by TE (50 Hz) compared to the broadband of 60 to 600 Hz used by 2D-SWE [67, 143]. Interestingly, our study did not find such a discrepancy to be the case, because 2D-SWE and Liverscan had the tendency to produce not significantly different aggregated LSMs (P = 0.364). This probably relates to their technical similarity that allows LSM under B-mode guidance to avoid interference from other non-liver tissues. Furthermore, previous diagnostic studies [67, 69, 117] suggested that 2D-SWE measurement compared favorably to conventional TE, with a generally higher area under the curve (AUC) in differentiating each fibrosis stage. Future research should compare the diagnostic accuracy of 2D-SWE and B-mode guided TE against histology.

On the other hand, LSMs by Liverscan appeared to be less consistent among individual measurements, as reflected by higher IQR/median values (median: 23%, range: 9–45%). According to the commonly defined reliability criteria and standard practice of using TE in clinical settings, an IQR/median smaller than 30% [75, 76] is necessary for valid and high-quality measurement results. Therefore, the relatively high IQR/median values of Liverscan demonstrated in this study would not affect the measurement, as they nearly align with the acceptable reliability category. One potential reason for Liverscan yielding a relatively larger IQR/median would be the relatively smaller beam width currently used in the device. In the current hardware, we adopted the same beamforming parameters for both TE mode and B-mode imaging, resulting in a beam width of approximately 2.3 mm at the focal zone. This specification is smaller than the 10 mm reported by conventional TE [54] and the ROI width of 10 mm [133] standardized for 2D-SWE in this study. Considering the heterogeneity in hepatic fibrosis, a smaller beam width could lead to greater variation among different measurements, as the liver keeps moving. In future studies, we plan to increase the beam width by adjusting the beamforming parameters to investigate whether the IQR/median value will be reduced accordingly. Meanwhile, maintaining a smaller beam width may provide us with a unique opportunity to map the Young's modulus distribution for assessing liver fibrosis heterogeneity, by steering the beam towards different locations while conducting TE measurements. Our future study will also investigate this possibility.

Factor of vibration amplitude. We concluded no significant difference between liver stiffness obtained using the vibration amplitude of TE chosen at the 1-mm and 3-mm levels. This result can be explained by the fact that a larger shear wave amplitude associates with less extent of wave attenuation, while shear wave speed depending

on the properties of the medium remain unchanged. Prior studies [78, 91, 144] comparing LSM using the 2-mm amplitude of the Fibroscan M probe with the 3-mm amplitude of the Fibroscan XL probe have yielded conflicting findings regarding liver stiffness values. Some reported that liver stiffness changed with probe type, while others found the opposite. These disparities may be arisen from additional contributory factors that complicated the comparison between the two probe types, such as ultrasound frequency (2 MHz vs. 3.5 MHz), diameter of transducer tip (9 mm vs. 12 mm), or measurement depth (25-65 mm vs. 35-75 mm). To our best knowledge, this is the first study to report shear wave amplitude impact within the same probe setting that would contribute to the controlling of other confounders.

The XL probe with a stronger vibration amplitude has proven valuable in reducing examination failure and facilitating LSM in obese patients [91, 144]. This is due to the greater penetration of shear waves travelling throughout the subcutaneous tissues into the liver. In our study, valid LSMs were obtained in all cases (BMI range: 19-39) under both the 1-mm and 3-mm vibration conditions. This data emphasizes the effectiveness of both amplitudes not only in non-obese population but also in the overweight or obese subjects (i.e., a proportion of 35% with mean BMI 28.5). Nevertheless, a B-mode guided procedure, a larger size of the transducer tip, and operator proficiency are postulated to play a joint role in overcoming these difficult cases. In the future, the necessity of applying a 3-mm or larger amplitude to the obese cohort warrants further investigation.

Despite the advantage of a stronger vibration and no significant difference in liver stiffness between vibration amplitudes reported in our study, the vibration setting should be selected with caution. Future vibrator design must compromise with patient

comfort and rib interference risk. Additional research is needed to determine the linearity of the relationship between elastogram quality and vibration amplitude levels, thereby informing optimal level selection. Regarding the suggestion for function optimization of TE, future system iteration may include an adaptive vibration amplitude selection algorithm that can adjust the vibration amplitude accordingly and cater to different BMI categories or skin-liver capsule distances.

Highlight of small footprint. Given the prevalence of fibrosis ≥F2 of 27% in high-risk populations [145] and 7.5% in the general population [18], it is imperative for healthcare providers to have a technique that is not only accurate and reproducible, but also highly accessible and cost-effective for assessing liver fibrosis at the point of care. The alarmingly high prevalence further strengthens the necessity of preventive screening programs for liver fibrosis [130]. However, size constraint has been a practical limitation in the widespread availability of TE systems and the scale-up of liver screening programs, which motivated us to introduce POCUS into a TE examination procedure.

Until this work, no engineering attempt had been made to downsize an ultrasound elastography system into a palm-sized version. Another key innovation is that Liverscan is the first wireless ultrasound elastography system; its small footprint represents only a fraction of the size of conventional ones. This portability opens up new possibilities for conducting home-based primary care in a non-hospital setting and screening on a larger scale. Its cable-free connection and lightweight design greatly enhance operational flexibility. Its high accessibility and ease of use make TE a community-based risk-stratification strategy, allowing for the earlier identification of patients and potentially leading to cost savings for healthcare systems. We believe

this new point-of-care testing method could change the paradigm of how the liver fibrosis epidemic is addressed, making TE a standard of care and maximally beneficial for liver disease sufferers worldwide. Further cost-effectiveness analysis comparing Liverscan against conventional TE and common serum biomarkers is required before its uptake as a point-of-care screening method.

Supplementing TE with B-mode guidance. Unlike conventional TE using a single-element transducer [74], Liverscan is configured with a phased transducer array for simultaneous sector B-mode image acquisition and LSM. Traditionally, operators solely relied on the difficult-to-interpret M-mode for liver localization. The incorporation of real-time B-mode imaging guidance provides multiple advantages over the current M-mode setting. First, B-mode possesses 2D spatial information, making it easier to differentiate the liver from the right kidney, gallbladder, or artifacts from nearby cardiac movement and lung or intestine gas. This eases the procedure of liver localization, thereby improving TE examination efficiency. The literature recognizes extreme BMI, higher liver stiffness, and chronic pulmonary disease as the risk factors of TE failure [75, 90]; yet these linkages are poorly understood. One similarity in these conditions is the liver considerably deviates from its commonly located region, making the acoustic window challenging to search for. Therefore, we postulate that B-mode guidance is of particular value to localizing the liver in those patients with post-partial hepatectomy, cirrhosis (shrunken liver size), emphysema (hyperinflated lung size), and extreme obesity. Second, the presence of intra-hepatic blood vessels, bile ducts, and focal masses could distort shear wave propagation trajectory [87] and pulsations around large vasculatures could lead to erroneously elevated shear wave speed [69]. Real-time guidance allows monitoring what intra-hepatic tissues are being measured without the inclusion of non-parenchymal components. This helps ensure the accuracy

of LSM results. Third, the ability to capture anatomic images enables the recording of the exact location or landmark in the liver from which the LSM is made. This facilitates longitudinal monitoring and procedural standardization. Furthermore, Castera et al. [75] reported that limited operator experience (i.e., operation of <500 examinations) is the main determinant of LSM failure or unreliable results, probably due to the lack of B-mode guidance. Direct visualization of liver anatomy may contribute to shortening the learning curve, particularly for those without prior TE experience [119]. Finally, beyond LSM, additional B-mode imaging could serve as a stand-alone modality for routine sonographic assessment of fatty liver and focal lesions (e.g., cyst, hemangioma, or hepatocellular carcinoma) [69].

In contrast, the phased array design presented in our study increases the geometry of the transducer face compared to the conventional single-element design. Although we have demonstrated the feasibility of using a larger transducer face for TE, future transducer design should consider dimensional specification to provide a compromise between a wider FOV and a higher risk of rib interference. Physical artifacts caused by diffraction and coupling of compression and shear wave [146-148] are another consideration, as they can lead to complex elastogram patterns that overestimate stiffness results. Sandrin's team [146] shed light on the relationship between circular vibrator diameter (from 1 to 20 mm) and the extent of these artifacts. The rectangular piston used in Liverscan does not necessarily create a point-like source of an elastic field, as the conventional circular vibrator does. Hence, the shape and size of a vibrating source should be carefully devised to minimize both diffraction and coupling effects. In practice, operators should be aware of the difference between the examination procedures performed by conventional TE and Liverscan (e.g., larger size of the transducer face and the addition of B-mode). Adequate training is necessary to

determine optimal probe placement conditions to avoid ribs and large vessels.

Previous studies explored the incorporation of B-mode guidance into TE, but they have some pitfalls. In 2013, our team developed a TE probe that encapsulates a 4.5-MHz linear array with a miniature electrodynamic shaker [87]. However, this integrated design only allowed linear image acquisition and provided very narrow FOV unsuitable for abdominal sonography. In light of this obstacle, subsequent attempts were made to implement a TE modulus on a conventional B-mode system equipped with a curvilinear array probe to offer a wider and deeper FOV. Azar et al. [149] affixed a vibration actuator on the side surface of a conventional convex probe. Although this design offers a wider FOV, its curvilinear shape is subject to increased rib interferences due to a larger footprint and may lead to complex vibration sources. Another method involved physically coupling a TE probe with a conventional B-mode system equipped with a default convex probe [118, 150]. However, this dual-probe setup required probe swapping during the procedure, and thus limited imaging guidance to a non-real-time basis. Probe swapping is also needed; however, this procedure may introduce variations between sites where the two probe are positioned. Our study was the first to report a fully integrated probe utilizing real-time sector B-mode as a procedural guidance technique.

Limitations and prospects. We acknowledge the following limitations in this study. First, our study lacked histological data which serves as gold standard for liver fibrosis diagnosis. However, given the extensive validation and established status of Fibroscan as the leading non-invasive test of reference in the liver elastography field [69], the choice not to compare against histology can be justified [87, 151, 152]. Future studies should focus on establishing cutoffs for different fibrosis stages in biopsy-

proven CLDs. Second, our cohort included patients with various liver diseases which may limit the generalizability of the finding to a specific etiology. Moreover, there might be a spectrum bias, because MASLD and CHB carriers accounted for 96% of the subjects in this study. Larger studies that adjust for important demographic variables (e.g., etiology, morphotype, and ethnicity) are necessary to further validate the performance of Liverscan. This will be critical for the roll-out and implementation of this technique in a range of clinical settings. Third, we did not specifically examine the added value of B-mode guidance to a TE examination procedure. This aspect had been in part addressed in a prior study by Lee et al. [118]. They confirmed the effectiveness of B-mode addition to mitigate TE failure, notably in a non-real-time format. Rather, our focus was on introducing an integrated probe that allows B-mode visualization of the liver while measuring its stiffness. Nevertheless, a thorough comparison of success rate and time consumption should be made among TE examinations with (a) real-time guidance, (b) non-real-time guidance, and (c) no guidance. Additionally, the applicability of the current probe setting to the pediatric population or adults of small stature remains unknown. The Fibroscan M probe has been reported to interfere with patients with narrow intercostal spaces, causing TE failure, unreliable results, and liver stiffness overestimation [92]. Since B-mode guided TE typically operates with a larger probe tip, rib interference due to changing anatomical relationships needs further verification.

Extending from the existing 1D-TE to 2D- or 3D-TE remains a topic for future research. The current system lacks the capability to map the Young's modulus and it only reports a single value corresponding to the Young's modulus of a 40-mm liver tissue length. Owing to the 32-element array configuration, simultaneous RF acquisition from multiple scan lines opens the possibility for LSM at multiple locations.

This facilitates the visualization of the spatial distribution of the Young's modulus throughout the liver that can better reflect the fibrosis state. Such a modification signifies a TE advancement, because it transforms the single-value nature into a multi-dimensional measurement to improve examination efficiency and reduce sampling error. Lefebvre et al. [143] pointed out the underlying spatial heterogeneity of fibrosis possibly contributing to lesser diagnostic performance and higher unreliable rates. Future 2D-TE can be clinically adopted to characterize fibrotic distribution over a larger liver region for ultrasound assessment of heterogenous stiffening. by steering the beam towards different locations while conducting TE measurements.

2.6 Summary

Chapter 2 introduced and evaluated a new point-of-care tool, named ‘Liverscan’, for assessing liver fibrosis. The Liverscan system incorporates a wireless phased array probe to allow for B-mode guided TE in real-time. Its feasibility and performance of LSM have been evaluated in both phantoms in laboratory tests and human subjects in clinical settings. Our phantom study demonstrated the accuracy of Liverscan in characterizing tissue-mimicking elasticity phantoms across 2 kPa to 75 kPa, representing a spectrum from normal through cirrhotic livers. Using a well-characterized, prospective cohort of Chinese adults with known CLD (n = 121), we compared the performance of Liverscan against other established liver elastography techniques. The clinical results indicated that LSM by Liverscan was comparable to conventional TE and 2D-SWE, and exhibited excellent to good operator reliability. As a secondary analysis, we also concluded that the different vibration amplitudes did not affect liver stiffness. Liverscan introduces two technical advancements over existing modalities. Real-time B-mode imaging allows direct visualization of liver anatomy, enhancing the examination efficiency and shortening the learning curve for inexperienced operators. This feature is of particular benefit for the procedures of liver localization and subsequent confirmation of an optimal anatomical site for measurement. Additionally, the small footprint of the probe paves the way toward point-of-care assessment and mass screening for liver fibrosis. Future research should include more patients stratified by various etiologies and investigate diagnostic accuracy in staging liver fibrosis using biopsy as the reference standard.

Chapter 3. Determining the Ideal Measurement Site and Respiratory Condition for TE: Morphological and Biomechanical Characterization of Intercostal Spaces Using 2D and 3D Ultrasound

This chapter has been published as:

Determining the Ideal Measurement Site and Respiratory Condition for Liver Transient Elastography: Toward Clinical Practice Standardization.

Huang, Z.-H., Lam, S.-K., Cheng, L.-K., Lin, Y.-M., & Zheng, Y.-P.

Insights into Imaging, vol. 15, no. 1, p. 114, 2024, doi: 10.1186/s13244-024-01692-x.

3.1 Background

The severity of liver fibrosis is linked with all-cause and liver-related mortality, necessitating early diagnosis and continuous monitoring [153]. Transient Elastography (TE) is an emerging technological advance in ultrasound imaging for assessing the presence and degree of liver fibrosis via stiffness measurement [53, 54, 74, 77, 78]. Its superior features of being non-invasive, easy to operate, low cost, rapid, and reliable, having high patient compliance, as well as being proven to offer histopathological correlations, have provided the community with a favourable alternative, compared to the current clinical standard of liver biopsy. According to major clinical guidelines [53-55, 95] and the WHO [126, 127], TE has been endorsed as the first-line assessment for chronic liver diseases [154], and its popularity is on a rapid rise in the field of hepatology globally.

Nevertheless, the factors affecting the harvest of reliable and valid examination

results during the implementation of TE technique remain incompletely elucidated. During a TE procedure, an operator places a cylinder-like single-element transducer at a location between the ribs, in which the transmission of both ultrasound and shear waves take place from the skin surface through the intercostal space (ICS) and its overlying abdominal wall layers, and ultimately into liver parenchyma for liver stiffness measurement. Following this line of principle, a successful TE examination relies heavily on the morphological and biomechanical characteristics of the ICS where the ultrasound probe is placed, which may in concert influence the effectiveness of wave propagation.

In the current body of literature, there is accumulating evidence illuminating the deficiencies of the TE examination when it comes to patients with a narrow ICS [74, 88, 92] or obesity [74, 75, 88, 90], and operators with inadequate experience [75, 90]. A transducer under a sub-optimal positioning condition tends to interfere with the ICS configuration in lean and obese patients, even in normal-BMI individuals. Lean individuals with limited rib spacing (i.e., narrow ICS) may experience invalid mechanical excitation of shear waves primarily at rib bones instead of intercostal tissues, resulting in minimal wave generation. Additionally, the presence of ribs is prone to de-focalization of the travelling waves, leading to complex wave propagation patterns and miscalculations of results. On the other hand, obese individuals present excessive subcutaneous adipose accumulation, severely attenuating the waves before reaching the liver. Apart from specific patient subpopulations, TE results could be difficult to obtain from normal-BMI patients due to operator inexperience (i.e., operation on < 500 examinations) [75, 90]. In the largest longitudinal study to date [75], a French team examining 7,261 patients over a 5-year period, reported that the frequency of failure and unreliable TE results could reach as high as 3.1% and 15.8%,

respectively. Similar results have been reported in another Asian cohort (n = 3205) with failures observed in 2.7% of cases and unreliable results in 11.6% [155]. In light of the above evidence, there is an urgent demand in the community for guiding operators in the placing of the transducer, for the sake of mitigating failure or unreliable rate of TE and ultimately maximizing its efficacy in the general population.

Nonetheless, there is no existing guideline on the selection of measurement sites for a standard practice in this regard [123]. Under this circumstance, operators could only rely on their own experience or a trial-and-error method during the procedure, which may largely reduce examination efficiency, as well as patient comfort **(Figure 3-1)**. On top of that, there is no research on the potential respiratory effects on the TE examination procedure. All things considered, it is imperative to investigate the anatomical characteristics of those commonly used ICSs over the liver, and specify an ideal probe placement condition for TE practitioners.

(A) 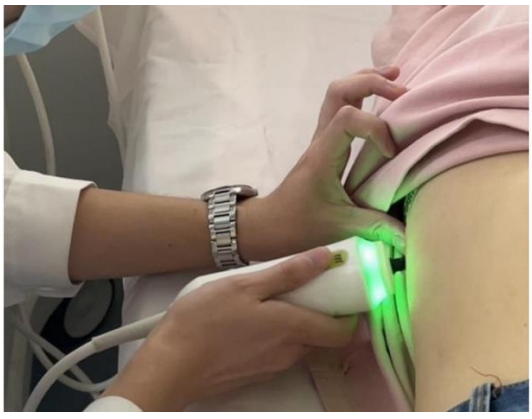 (B) 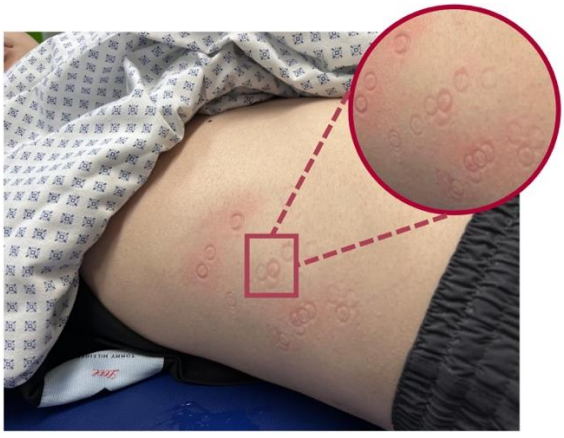

Figure 3-1. TE examination. (A) Setup of the placement of the TE probe in an ICS; (B) A representative patient in real-world practice, who was undergoing the TE examination using a trial-and-error method due to the absence of clear guidelines for selecting a measurement site. Each red mark on the patient's skin surface corresponds to a single measurement attempt made using the transducer tip.

The necessity for practice standardization is further emphasized in the context of the new generation of TE. The use of multi-element array transducers is gaining popularity in liver elastography field, because it enables real-time B-mode image guided TE. An example is the system described in Chapter 2. New array design increases the dimension of the transducer face compared to the conventional single-element design. Consequently, a 2D rectangular shape has a higher likelihood of interfering with the ribs, and poses a challenge to successful TE **(Figure 3-2)**. It is thus pertinent to characterize the course of the ICS, so as to further inform an array transducer-specific placement strategy.

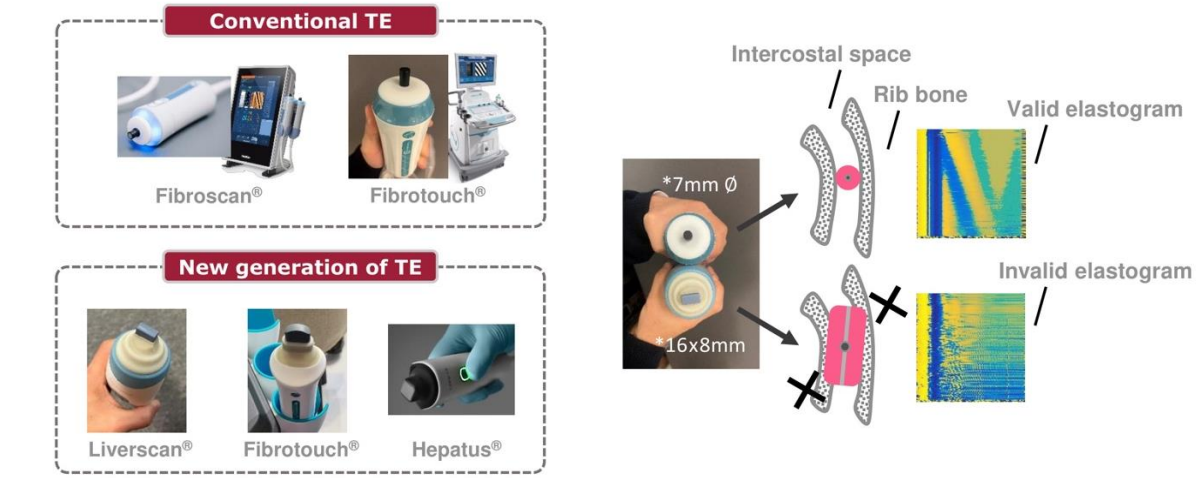

Figure 3-2. Relationship between TE and intercostal space. (A) Iteration of TE techniques: vendor-specific commercial devices; (B) Possible consequences of elastogram acquisition using a TE transducer with the different shapes and dimensions of the contact face.

3.2 Study Aims

The overarching goal of this observational study was to identify an ideal site and respiratory condition for TE probe placement, through the investigation of the anatomical and biomechanical characteristics of the ICSs on the human right inferior rib cage using a combination of two-dimensional shear-wave elastography (2D-SWE), 2D B-mode and 3D ultrasound imaging **(Figure 3-3)**. Specifically, the primary objective of this cross-sectional study was to assess the differences in intercostal width, width-change, angle, stiffness, and skin–liver capsule distance (SCD) among the selected ICSs. Additionally, the study investigated the differential effects of respiration on intercostal width and stiffness under two different respiratory conditions. We hypothesized that intercostal anatomy varied within individuals, and at least one ideal site would stand out to favour TE. The secondary objective was to analyze the factors associated with intercostal width and stiffness, and examine the anatomical relationship of the ICSs with the presence of the liver.

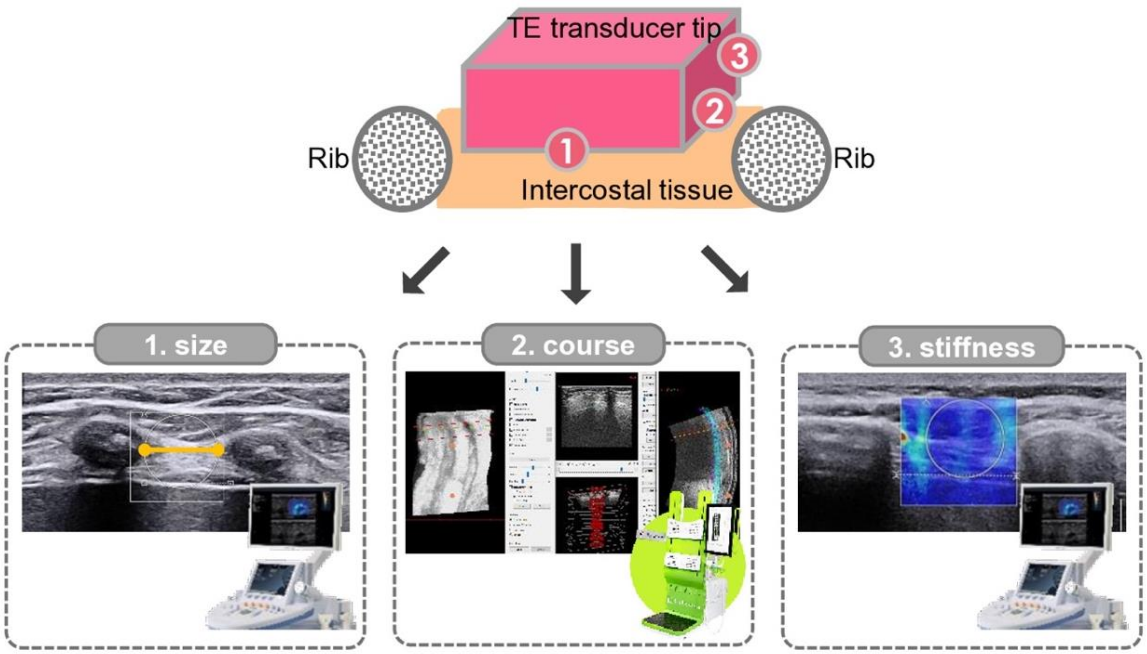

Figure 3-3. Schematic representation of research methodology. 2D and 3D

ultrasound are applied to investigate the spatial relationship between the ICS and the transducer tip positioned upon it. The research project strives to formulate procedure-specific standards for liver TE.

3.3 Methods

3.3.1 Subjects

In this prospective study, adult patients (≥18 years) with known chronic liver diseases of any aetiology who had a clinical indication for TE were eligible. According to the nature of ultrasound technique used for characterizing intercostal spaces, there are two independent groups of study participants: '2D ultrasound cohort' and '3D ultrasound cohort'. In the '2D ultrasound cohort', subjects who underwent 2D ultrasound assessment of the intercostal width, stiffness and SCD participated. The sample size of 52 was estimated using the G*Power software [156], assuming a median effect size of 0.15, statistical power of 0.9, and a two-sided significance level of 0.05 under a two-way repeated-measures design. In the '3D ultrasound cohort', an additional 30 subjects were recruited for 3D ultrasound imaging of the intercostal course. This sample size was projected prospectively and deemed necessary to achieve a median effect size of 0.3, statistical power of 0.95, a two-sided significance level of 0.05, and a dropout rate of 10% under a one-way repeated-measures design. Exclusion criteria consisted of chest wall deformity or a history of previous thoracic or abdominal surgery. This observational cross-sectional study was designed, conducted, and reported in accordance with the STROBE statement [157]. All subjects provided written informed consent prior to enrolment. The research was approved by the institutional review board of The Hong Kong Polytechnic University (HSEARS20210809002), and conformed to the Declaration of Helsinki.

3.3.2 Procedures

The overall rational is depicted in **Figure 3-4**. Four sites of interest in the right inferior part of the rib cage over the liver were selected to investigate a hypothesized

inter-ICS difference. The selection of these four sites was referenced from the locations which were reported in the previous liver ultrasound elastography-related literature and may be commonly used in clinical practice [87, 123, 158-161]. The investigator located and marked the sites using the following standardized anatomical landmarks: Site 1 (intersection between the 8th ICS and anterior axillary line); Site 2 (intersection between the 7th ICS and anterior axillary line); Site 3 (intersection between the 8th ICS and mid-axillary line); Site 4 (intersection between the 7th ICS and mid-axillary line).

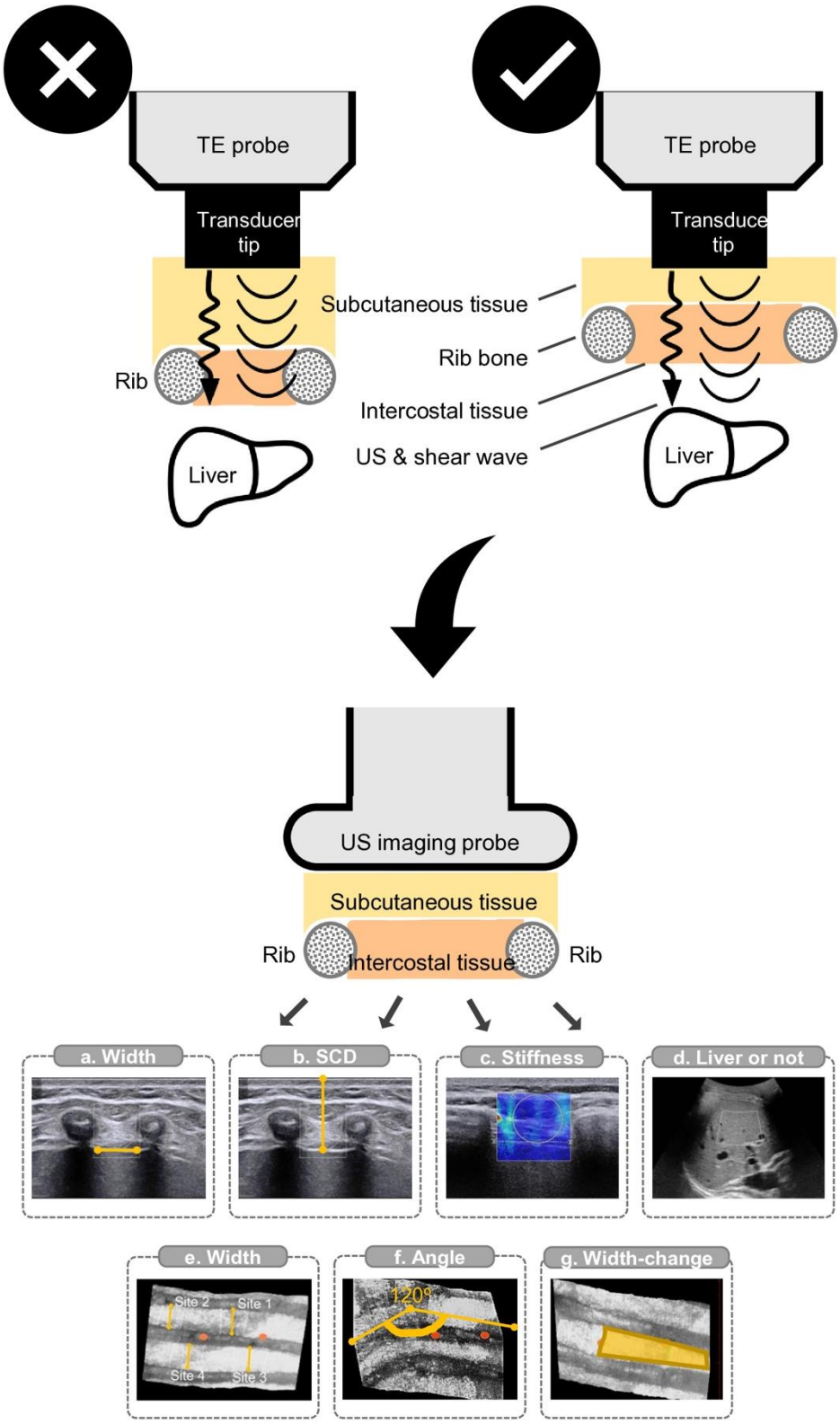

Figure 3-4. Study overview. (A) Clinical problem: the impact of the ICS configuration on the transmission of shear waves into the liver and the ultrasound used to measure their speed of propagation during the TE examination; the left-hand side of

the figure illustrates a failed case, where the transducer is placed on a thick layer of subcutaneous tissue and a narrow ICS; the right-hand side of the figure depicts an ideal situation, where the transducer is placed on an appropriate thickness of subcutaneous tissue and a wide ICS; (B) Research methodology: anatomical characterization of the ICS via 2D ultrasound measurements of intercostal (a) width, (b) SCD, (c) stiffness, and (d) the detection of the presence of the liver and 3D ultrasound measurements of intercostal (e) width, (f) angle, and (g) width-change.

3.3.3 Intercostal 2D Ultrasound Imaging

In the '2D ultrasound cohort', intercostal 2D ultrasound imaging was performed using a linear probe (SL15-4, central frequency: 8.5 MHz) of the Aixplorer® system (SuperSonic Imagine, Aix-en-Provence, France. This US imaging system enables simultaneous B-mode imaging and stiffness mapping, thus both the intercostal B-mode and SWE images displayed as a 2D color-coded elastogram can be obtained for subsequent analyses. Subjects were positioned in the supine posture and raised their right arm maximally, adhering to the standard patient positioning used for liver TE examination [74]. Each subject underwent the simultaneous intercostal SWE and B-mode imaging at each of the four sites under two respiratory conditions: (a) end-inspiration and (b) end-expiration **(Figure 3-5)**, resulting in a total of eight experimental conditions. These conditions were executed as a transient breath-hold during normal breathing. To ensure the consistency of respiratory amplitudes across the conditions, the subjects wore the wearable Go Direct® chest belt (Vernier, Oregon, USA) with a built-in pressure gauge that monitored their real-time respiratory changes during the experiment. The probe was placed with minimal pressure at the skin surface of each site. The probe orientation was fine-tuned around the marked site, until its width was estimated to be minimal, indicating that the probe was perpendicularly oriented to the

ribs. A 6-s video, comprising sequential images of one half-respiratory cycle, was acquired from the eight experimental conditions. A linear probe (SL15-4, central frequency: 8.5 MHz) was also employed to observe the presence of the liver underneath each site. Settings for depth and time-gain compensation (TGC) were fined-tuned to achieve a deeper field of view of the underlying organ. A binary criterion (i.e., presence or absence) was utilized to determine whether a liver parenchymal portion with at least 4-cm thickness could be visualized in the cross-sectional B-mode images.

We further analyzed the intra- and inter-observer reliability of the intercostal width, SCD, and stiffness measurement, respectively. The protocol is detailed as follows. Site 1 was imaged twice by Operator 1 under the two respiratory conditions to allow for assessment of intra-observer reliability, with the probe removed from the patient and repositioned between scans. The interval was approximately 1 minute, with no change in patient condition or positioning. To establish inter-observer reliability, two operators (i.e., Operators 1 and 2) independently performed one set of intercostal acquisitions at Site 1. The first set of data collected by Operator 1 was used to assess inter-site differences.

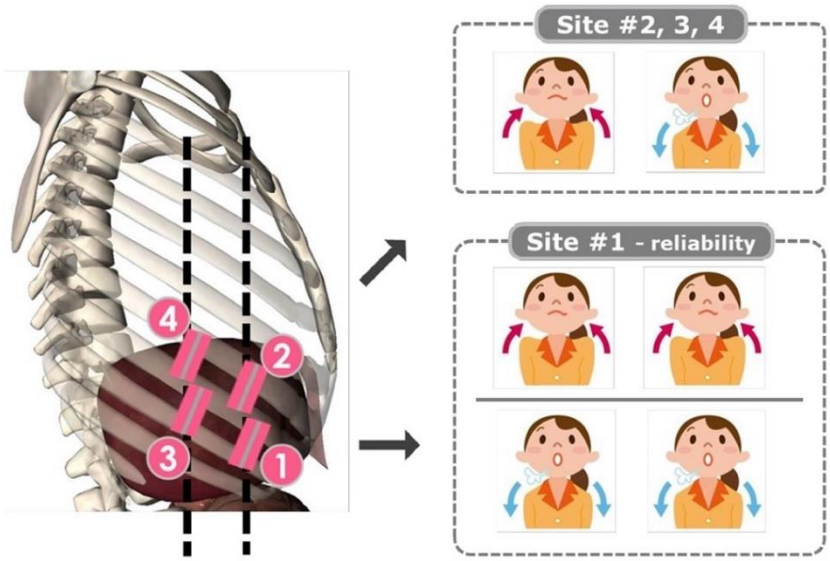

Figure 3-5. Experimental protocol. Selection of the four measurement sites and the two respiratory conditions.

3.3.4 Intercostal 3D Ultrasound Imaging

In the '3D ultrasound cohort', freehand 3D ultrasound imaging of the ICSs was performed using the Solioscan® system (Telefield Medical Imaging Ltd., Hong Kong, China), with subjects in the supine position and their right arm raised maximally. This patient positioning was same as what was adopted in the '2D ultrasound cohort'. Before the freehand 3D scans, surface marking of measurement site was performed **(Figure 3-6, A)**. The investigator located and marked the pre-determined four ICSs by attaching the stickers on their skin surface correspondingly. The sticker, which is a self-adhesive plastic film, enables specular reflection and acoustic shadowing in sequential B-mode images. These appearances aid in searching for and locating the specific ICS of interest within a stack of images comprising the entire volume **(Figure 3-6, B)**.

The volume data of the 7^{th} to 9^{th} ribs during the end-inspiratory breath-holds was acquired by sweeping the 3D ultrasound probe along the long axis of the ribs from the

posterior to the anterior axillary line. As a result, the 7th and 8th ICSs containing Sites 1 to 4 were covered. Following the standardization efforts of the '2D ultrasound cohort', the amplitude of end-inspiratory motion was monitored in real-time by the respiratory belt. It helps ensure the comparable dynamic changes in lung volume during 3D scanning. In case that the FOV couldn't contain two ICSs simultaneously, two independent sweeps were administrated.

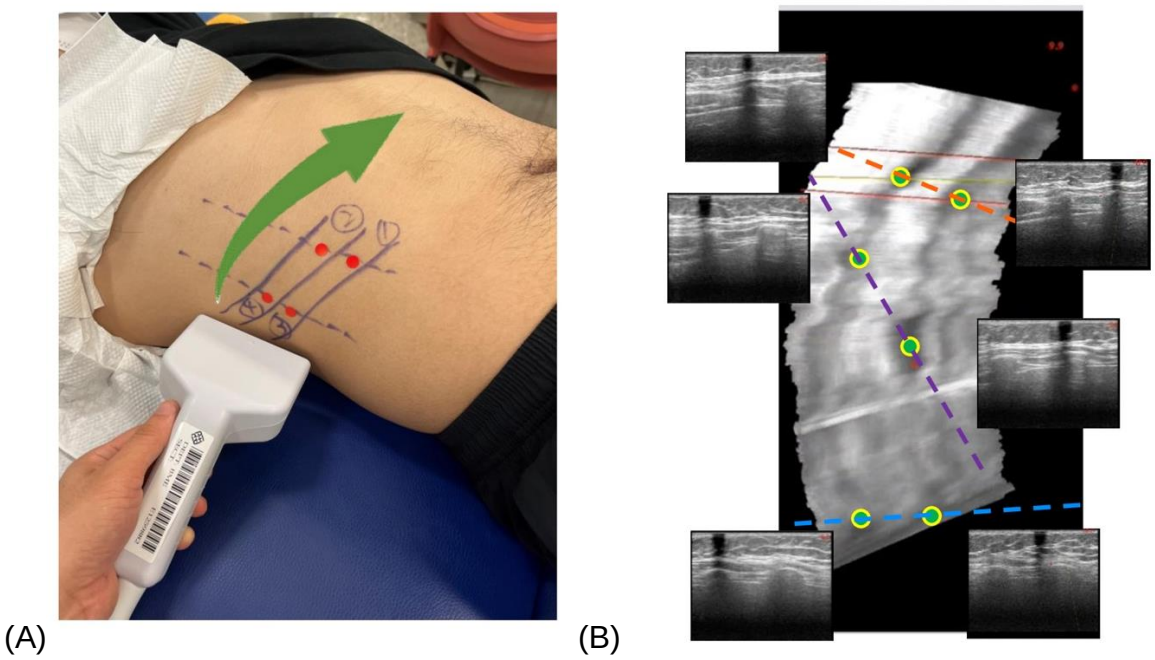

Figure 3-6. Experimental setup of intercostal 3D ultrasound. (A) 3D data of the ICSs were obtained along the ribs, during which the subject was instructed to suspend the breath at the end-inspiratory phase; (B) Procedure of locating multiple pre-defined sites by using ultrasound visualization and depiction of stickers in the 3D reconstructed images.

3.3.5 Outcome Measures

This anatomy research contains a series of outcome measures. By utilizing various ultrasound techniques, we characterized the ICSs from the perspectives of morphology, biomechanics, and physiology.

2D B-mode-derived intercostal width and SCD. The width of the ICS was measured to examine its geometric relationship with the size of a TE transducer. It was defined as the horizontal length between the inferior border of the upper rib and the superior border of the lower rib, where acoustic shadowing caused by rib bones is widest **(Figure 3-7, A)**. Linear measurements of the width were consistently taken at the level of an innermost echogenic layer of the diaphragmatic border. The SCD of the ICS corresponds to abdominal wall thickness, which was measured from the skin surface to the pleural line **(Figure 3-7, B)**. Due to the varying shape of intercostal tissues, the SCD value is not necessarily the same within one ICS. Thus, we repeated SCD measurements at three different locations within the ICS (i.e., its centre, left-most boundary, and right-most boundary). These three measurements were then averaged, which became the representative SCD for that ICS.

(A) 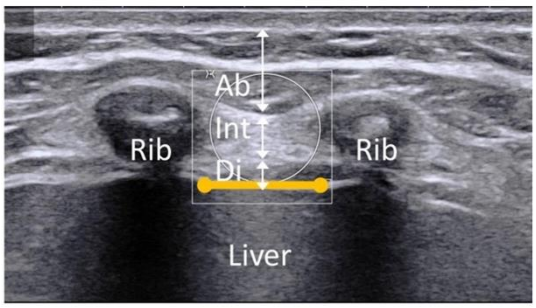

(B) 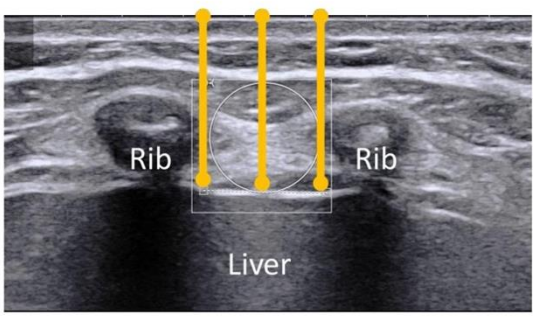

Figure 3-7. Illustration of morphological imaging of the ICSs. (A) Width and (B) SCD measurements in the B-mode image of the ICSs (Ab: abdominal muscles; Int: intercostal muscles; Di: diaphragm muscle).

2D SWE-derived intercostal stiffness. During the SWE acquisition process, an SWE box was placed at the centre of an ICS and customized to include the cross-sectional area of the external oblique, intercostal muscles, diaphragm, and portions of ribs and subcutaneous fat **(Figure 3-8)**. Intercostal stiffness represents the axial strain

of the ICS in response to the probe pressure. This biomechanical parameter assesses the degree to which the ICS is accommodating to the placed transducer tip.

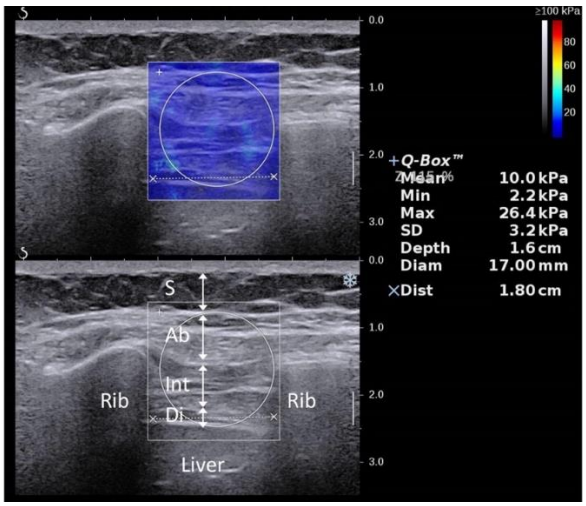

Figure 3-8. Illustration of elasticity imaging of the ICSs. Stiffness measurement in the SWE image of the ICSs (S: subcutaneous fat; Ab: abdominal muscles; Int: intercostal muscles; Di: diaphragm muscle).

3D ultrasound-derived intercostal course. The width of the ICSs (mm) was quantified in the 3D-constructed coronal images. In addition to point estimate of intercostal width, interval estimate of the ICSs was applied, which is specifically relevant to 2D array transducers. The intercostal angle (°) and width-change (%) represent the anatomical course of the ICSs. The angle of the ICS was measured at each of the four sites to assess intercostal curvature and degree of angularity. The percentage change of the intercostal width (%) for each site characterizes the dimensional change and the degree of irregularity of the rib cage overlying the liver. This metric is computed based on the ratio of the two different widths apart.

Benchmark test for intercostal width. Both the 2D and 3D ultrasound-derived intercostal width measurement detailed above were based on operators' estimation on the probe's perpendicularity to the long axis of the ICS. Visual approximation,

however, may not guarantee what has been a minimal width. Therefore, it is worthwhile to test the validity of these currently used methods against a more accurate method. An alternative method for width measurement was adopted as the benchmark in this regard. It is named ‘probe rotation method’ in this study which involves capturing a clip of rotating the probe 180 degree at the site. Compared to the ‘visual approximation method’, this data collection method enables more accurate and precise identification of the exact frame that contains the minimal width. The further data analysis for linear measurement of width was done in an offline manner (See **Chapter 3.3.4** for details).

The overall experimental workflow is depicted in **Figure 3-9**.

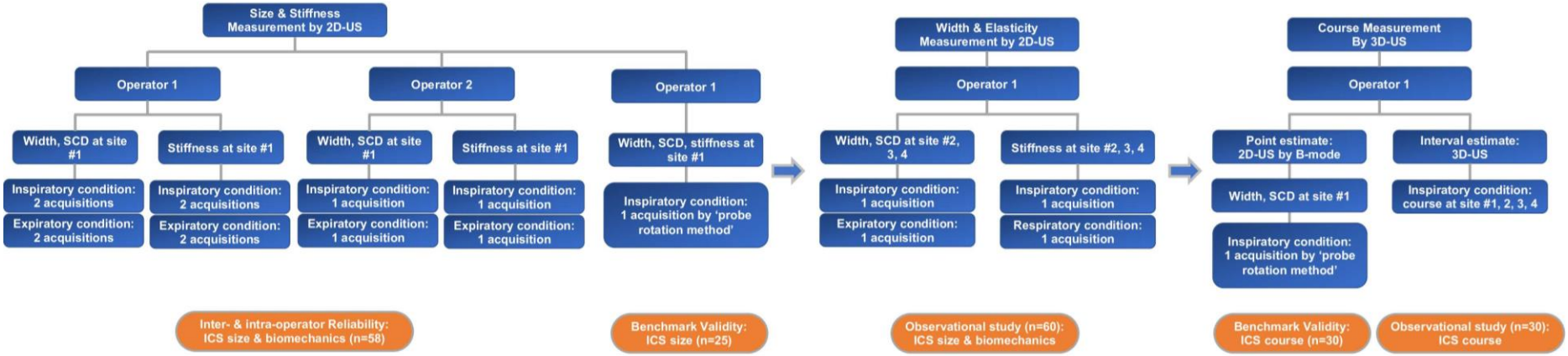

Figure 3-9. Schematic diagram of study design. Characterization of the ICSs via (A) 2D ultrasound and (B) 3D ultrasound for measuring intercostal size, course and stiffness.

3.3.6 Data Analyses

Image post-processing was performed to quantify the width, stiffness, angle and SCD of the ICS in the intercostal ultrasound images, using a dedicated workstation provided by the manufacturers. The measurement data were collected by the third-party rater, who was blinded to the actual experimental condition of the images being analyzed. Details of these quantification procedures are described as follows:

In the '2D ultrasound cohort', the post-processing was made in the 2D B-mode and SWE images. To minimize the measurement error, a repeated measurement strategy was implemented offline on the separate images of each captured 6-s video. For the quantification of intercostal width, three individual linear measurements using the built-in calliper were conducted in the respective frames at 2 s, 4 s, and 6 s of the video, resulting in three measurement values. The average of these three measurement values was used to represent the intercostal width of that experimental condition. For the quantification of intercostal SCD, the same methodology as outlined above was applied to measure the SCDs in the same three frames (i.e., 2 s, 4 s, 6 s). For the quantification of intercostal stiffness, the Young's moduli of the intercostal tissues were derived from the SWE images that pair with the previously measured B-mode image frames **(Figure 3-8)**. For each SWE image, the rater placed the largest possible circular region of interest (i.e., Q-box), avoiding bone-proximity artifacts and inclusion of subcutaneous fat within the ICS. In this fashion, the upper and lower limits of Q-box encompassed the superior border of the abdominal muscle and the inferior border of the diaphragm, respectively. The mean Young's modulus value derived from three SWE images was calculated for each experimental condition.

In the '3D ultrasound cohort', data analyses of the 3D reconstructed cut-plane of

the ICSs were conducted offline in a custom workstation – Scoliostudio® (Telefield Medical Imaging Ltd., Hong Kong, China) **(Figure 3-10)**. Specifically, the 3D reconstruction of the coronal images of the ICSs was standardized at the level of the inner border of the diaphragm. The 3D reconstructed coronal views of the 7th and 8th ICS were used for measuring the minimal width, angle, and width-change of the ICS. The four ICSs at the levels of the anterior and midaxillary lines were identified accordingly, based on acoustic shadowing caused by the attached stickers on the skin surface. Using visual approximation, the third-party rater measured what had been estimated to be minimal and become the width of that ICS in mm. The intercostal angle, expressed in degrees, was determined by drawing two lines along the long axis of the ICS around the designated point. The intercostal width-change (%) was calculated as the percentage change from a wider to narrower space within a 20-mm course of the ICS. The following equation is used:

$$Width - change\ (\%) = \frac{|Greater\ width\ (mm)\ -\ Smaller\ width\ (mm)|}{Smaller\ width\ (\mathrm{mm})} \times 100\%$$

(A) 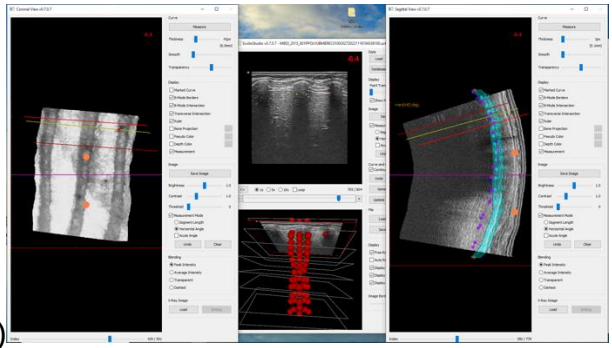 (B) 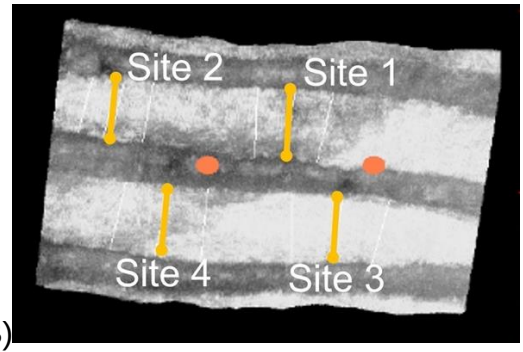

(C) 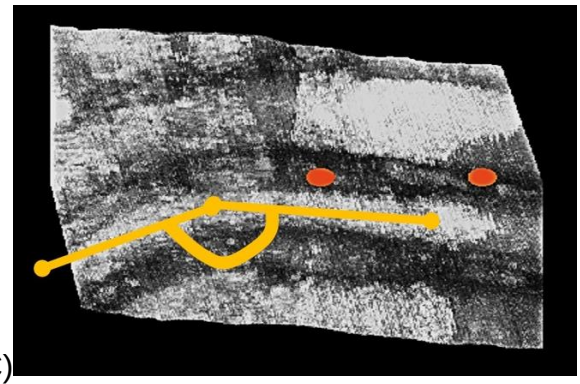 (D) 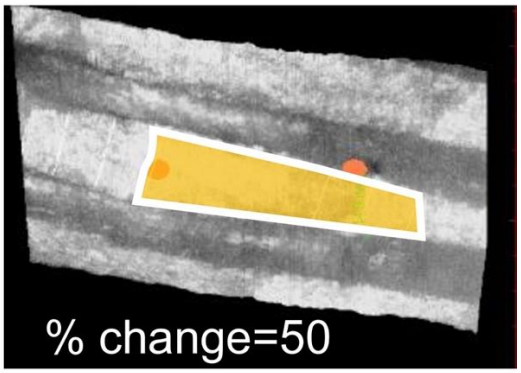

Figure 3-10. Post-processing of intercostal 3D ultrasound data. (A) User interface of Scoliostudio®: customized reconstruction of the volume projection image in the coronal view; Illustration of the 3D ultrasound-derived measurements of (B) width, (C) width-change, and (D) angle in the reconstructed coronal images of the ICSs.

3.3.7 Statistical Analyses

Descriptive statistics. Cohort characteristics were descriptively summarized and reported as medians (IQRs) for continuous variables and proportions (frequencies) for categorical variables. Two-sided P-values less than 0.05 were considered statistically significant.

Effect of respiration and site on 2D ultrasound measurement. Two-way repeated measures ANOVAs were conducted to analyze the main and interaction effects of two factors: (a) ‘respiration’ factor (end-inspiratory vs. end-expiratory conditions) and (b) ‘measurement site’ factor (Site 1, 2, 3, 4) on the US-derived width, stiffness and SCD of the ICSs, respectively.

Effect of site on 3D ultrasound measurement. One-way analysis of variance (ANOVAs) with repeated measures was used for comparing three 3D ultrasound-derived morphological parameters (i.e., width, width-change, and angle of the ICS) among the four sites of interest. Post-hoc comparisons between sites were performed

using a Bonferroni test.

Likelihood of visualizing the liver underneath sites. Cochran's Q test was applied to test the differences in detecting the presence of the liver across the sites.

Validity statistics for 2D and 3D ultrasound measurement. In the '2D ultrasound cohort', Pearson correlation between intercostal width measured using 2D ultrasound vs. 'probe rotation method' was determined. Simple linear regression was also used to examine the strength of the relationship between the two methods. In the '3D ultrasound cohort', the Pearson correlation coefficient (*r*) and coefficient of determination (R^2) were also computed. These metrics establish the validity of 3D ultrasound-derived width measurement against 'probe rotation method' as the reference technique.

Reliability statistics for 2D ultrasound measurement. Operator repeatability was assessed for respective width, stiffness, and SCD measurements using intra-class correlation coefficients (ICC). Repeatability was evaluated by comparing two repeated trials collected by one operator and two separate trials by two individual operators. Intra-observer ICC with two-way mixed model and consistency was calculated based on two repeated trials by the same operator, while inter-observer ICC with two-way random model and consistency was assessed in a two-operator setting. The repeatability was classified based on ICC values as follows: poor (ICC: 0–0.5), fair/moderate (ICC: 0.5–0.75), good (ICC: 0.75–0.9), and excellent (ICC: 0.81-1.00) [135].

Factor analysis. To evaluate the demographic and anthropometric factors that possibly influenced the width and stiffness of the ICS, we performed univariate analysis using Spearman's correlation test for continuous candidate variables, and the

Mann-Whitney U test for categorical candidate variables. Variables that achieved statistical significance ($p < 0.05$) in univariate analysis were included in a multivariate model. The multiple regression model was constructed with age, height, weight, BMI, SCD, waist circumference, sex, and metabolic syndrome as candidate covariates, and the width and stiffness as the outcome variables.

3.4 Results

3.4.1 Subject Demographics

Between May and December 2022, 92 consecutive adult patients with known chronic liver diseases were screened for eligibility of the study. Three subjects were excluded due to withdrawal of consent (n = 2) and accidental data loss (n = 1). The remaining 89 subjects included in the analyses comprise of the '2D ultrasound cohort' (n = 59) and '3D ultrasound cohort' (n = 30). **Table 3-1** outlines the patient characteristics of the two cohorts; the aggregated anatomical data for each site of interest are presented for comparison. In the '2D ultrasound cohort', the median age was 57 years (IQR: 43–64; range: 27–71) with 51% females. The median BMI was 24 kg/m^2 (IQR: 21–26; range: 17–39); 27% and 7% of patients were classified as overweight (BMI ≥ 25 kg/m^2) and obese (BMI ≥ 30 kg/m^2), respectively. The majority (78%) were experiencing chronic hepatitis B (32% with coexistent steatosis) and 22% had metabolic dysfunction-associated steatotic liver disease (MASLD). In the '3D ultrasound cohort', 10% of patients were overweight or obese with the median BMI range between 16–27 kg/m^2.

Table 3-1. Baseline characteristics comparison between the two study cohorts.

Variable	2D-US cohort (n=59)	3D-US cohort (n=30)
• Demographics		
Male gender	49% (29)	50% (15)
Age, years	57 [21; range 27–71]	59 [12; range 29–70]
Overweight & obese	34% (20)	10% (3)
Central obesity	51% (30)	60% (18)
Metabolic syndrome	12% (7)	10% (3)
• Anthropometrics		
BMI, kg/m^2	24 [5; range 17–39]	23 [4; range 16–27]

Waist circumference, cm	87 [15; range 66–115]	82 [14; range 65–98]
• ICS morphology by 2D-US		
Width at Site 1†, mm	14.9 [6; range 6–26]	-
Width at Site 2†, mm	18.0 [6; range 8–53]	-
Width at Site 3†, mm	17.4 [7; range 5–32]	-
Width at Site 4†, mm	15.4 [5; range 7–25]	-
SCD at Site 1, mm	19.3 [5; range 13–39]	-
SCD at Site 2, mm	16.6 [6; range 11–38]	-
SCD at Site 3, mm	17.6 [6; range 11–39]	-
SCD at Site 4, mm	19.6 [7; range 10–37]	-
• ICS morphology by 3D-US		
Width at Site 1‡, mm	-	14.9 [8; range 8–25]
Width at Site 2‡, mm	-	20.5 [5; range 13–27]
Width at Site 3‡, mm	-	18.6 [4; range 8–26]
Width at Site 4‡, mm	-	18.0 [4; range 12–24]
Angle at Site 1, °	-	158 [21; range 120–178]
Angle at Site 2, °	-	170 [13; range 138–179]
Angle at Site 3, °	-	176 [6; range 156–180]
Angle at Site 4, °	-	177 [4; range 157–180]
Width-change at Site 1, %	-	18 [27; range 0–96]
Width-change at Site 2, %	-	9 [12; range 1–39]
Width-change at Site 3, %	-	6 [11; range 0–80]
Width-change at Site 4, %	-	12 [13; range 2–32]
• ICS biomechanics		
Stiffness at Site 1, kPa	15.1 [9; range 6–51]	-
Stiffness at Site 2, kPa	12.6 [8; range 4–46]	-
Stiffness at Site 3, kPa	11.7 [7; range 5–48]	-
Stiffness at Site 4, kPa	10.0 [6; range 4–40]	-

All data are median [IQR] or % (n), unless otherwise indicated.

BMI = body mass index; US = ultrasound; ICS = intercostal space; SCD = skin–liver capsule distance.

† Width measured by 2D ultrasound; ‡ width measured by 3D ultrasound.

3.4.2 Reliability of 2D Ultrasound Measurement

Of the 59 subjects, 34 participated in the intra-operator reliability analysis, while 24 were assessed for the inter-operator reliability **(Table 3-2)**. Intercostal width and SCD

measurements are highly reproducible irrespective of respiratory conditions (ICC ≥ 0.97), while intercostal stiffness measurement demonstrated fair to good reliability (inter-operator $ICC_{(2,3)}$: 0.593–0.683; intra-operator $ICC_{(3,3)}$: 0.790–0.896). Specifically, regarding the intra-operator reliability of width and SCD measurements, the $ICCs_{(3,3)}$ of end-inspiratory and end-expiratory conditions ranged between 0.972 and 0.992. Additionally, all $ICCs_{(2,3)}$ for inter-operator reliability were greater than 0.97. Both measures reflected excellent observer reliability. In comparison, inter- and intra-observer reliability for intercostal stiffness measurements were fair to good, with higher intra-operator $ICC_{(3,3)}$ (between 0.790 and 0.896) than inter-operator $ICC_{(2,3)}$ (between 0.593 and 0.683). This may imply the impact of operator experience, as the operator gained experience across two successive scans in an intra-operator setting. The lowest $ICC_{(2,3)}$ of 0.593 (95% CI: 0.060–0.824) was noted in the inter-observer reliability at end-inspiration.

Table 3-2. Intra- and inter-operator reliability results for 2D ultrasound measurements of the intercostal space.

	Intra-operator reliability (n=34)		**Inter-operator reliability (n=24)**	
Intercostal 2D-US measurement	**$ICC_{(3,3)}$[a]**	**95% CI**	**$ICC_{(2,3)}$[b]**	**95% CI**
Width at end-inspiration (mm)	0.981	(0.963–0.991)	0.978	(0.950–0.991)
Width at end-expiration (mm)	0.986	(0.972–0.993)	0.977	(0.948–0.990)
SCD at end-inspiration (mm)	0.992	(0.985–0.996)	0.976	(0.944–0.989)
SCD at end-expiration (mm)	0.972	(0.943–0.986)	0.986	(0.969–0.994)
Stiffness at end-inspiration (kPa)	0.896	(0.791–0.948)	0.593	(0.060–0.824)
Stiffness at end-expiration (kPa)	0.790	(0.580–0.895)	0.683	(0.268–0.863)

CI = confidence interval; ICC = intraclass correlation coefficient; US = ultrasound; SCD = skin-liver capsule distance.

[a]ICC computed using two-way mixed model and consistency; [b]ICC computed using two-way random model and consistency.

3.4.3 Validity of 2D and 3D Ultrasound Measurement

We further validated the 2D and 3D methods before adopting them for analyses of the inter-ICS difference. Excellent correlation with the 'probe rotation method' was demonstrated for both the 2D and 3D ultrasound-based width measurements (r = 0.901 and 0.922, respectively). On subgroup analysis, the linearity between width measurements was higher for 3D ultrasound (R^2 = 0.922) than 2D ultrasound (R^2 = 0.812). The results indicated that the currently used 2D and 3D ultrasound methods were valid for intercostal width measurement. Pairwise comparisons of intercostal width measurement are presented in **Figure 3-11**.

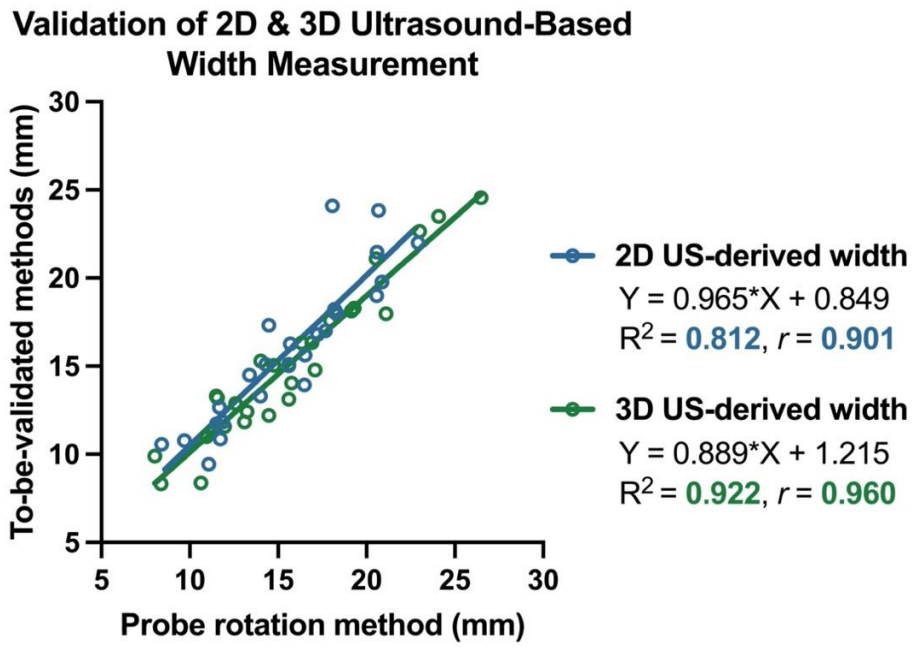

Figure 3-11. Relationship between intercostal width measured by (A) 2D ultrasound and (B) 3D ultrasound relative to the 'probe rotation method' as a reference

standard.

3.4.4 Comparison of Respiration and Site in 2D Ultrasound Measurement

Intercostal width measurement. No significant interaction effect was found between the factor of 'site' and 'respiration' on intercostal width ($F(1,80) = 3.07$; $p = 0.07$). The results showed a significant main effect of 'respiration' ($F(1,58) = 75.27$; $p < 0.001$), with inspiration producing greater intercostal width values **(Figure 3-12, A)**. The main effect of 'site' was also significant ($F(2,129) = 17.25$; $p < 0.001$). Post-hoc comparisons among all sites revealed that the ICSs at Site 2 (18.4 mm, 95%CI: 17.3–19.6) and Site 3 (17.8 mm, 95% CI: 16.6–19.0) were significantly wider than those at Site 1 (15.2 mm, 95% CI: 14.2–16.2) and Site 4 (15.6 mm, 95% CI: 14.7–16.5).

Intercostal stiffness measurement. Similarly, although there was no two-way interaction between two factors ($F(2,138) = 0.05$; $p = 0.967$), the significant main effects of 'respiration' ($F(1,58) = 15.24$; $p < 0.001$) and 'site' ($F(3,161) = 10.78$; $p < 0.001$) factors were identified on the stiffness values **(Figure 3-12, B)**. Respiratory movement generally increased intercostal stiffness from the end-expiratory to end-inspiratory phase. Intercostal stiffness was significantly lower at Site 4 (12.2 kPa, 95% CI: 10.7–13.7) than at Site 1 (16.6 kPa, 95% CI: 14.9–18.3) and Site 2 (14.4 kPa, 95% CI: 12.7–16.1). The intercostal stiffness values of Sites 3 and 4 were observed to be similar (a mean difference of 1.3 kPa, $p = 0.335$), irrespective of respiratory conditions.

Intercostal SCD measurement. An interaction effect between 'site' and 'respiration' existed in explaining the difference in intercostal SCD **(Figure 3-12, C)**, $F(3,174) = 9.75$; $p < 0.001$. This implied that the effect of respiration is site dependent. Therefore, simple main effects of 'site' were run separately for the end-inspiratory and end-expiratory conditions. While Site 2 (17.8 ± 4.2 mm) and Site 3 (17.9 ± 4.1 mm)

shared significantly shorter end-inspiratory SCDs, Site 2 (18.4 ± 4.8 mm) exhibited the shortest end-expiratory SCD.

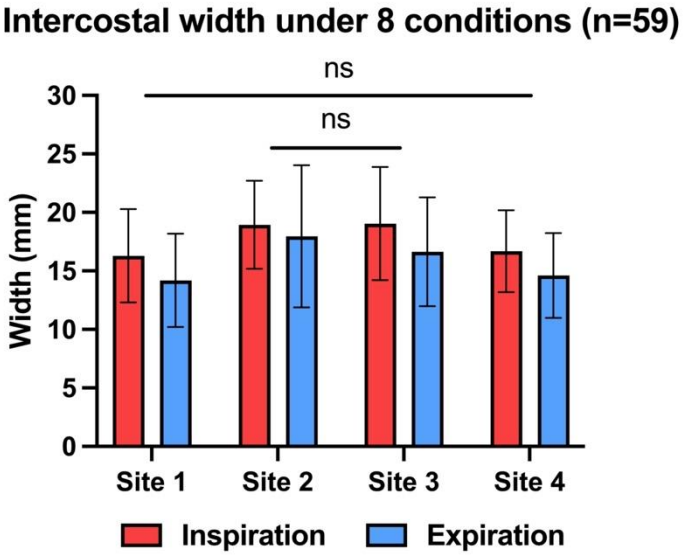

(A)

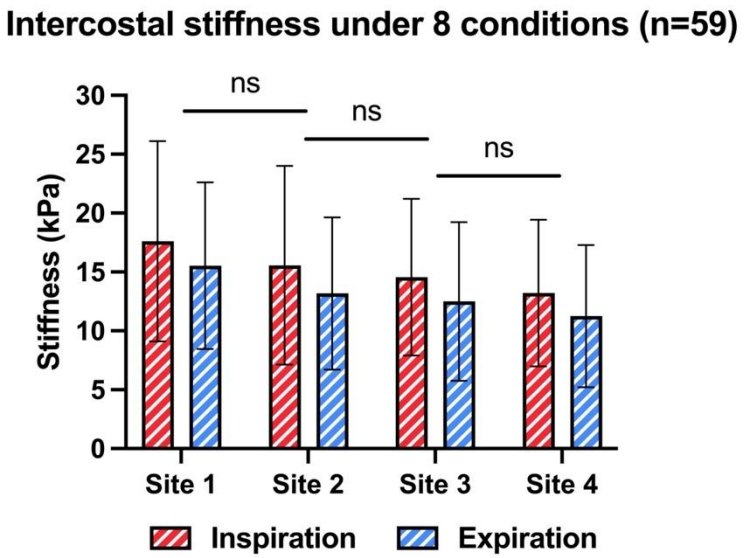

(B)

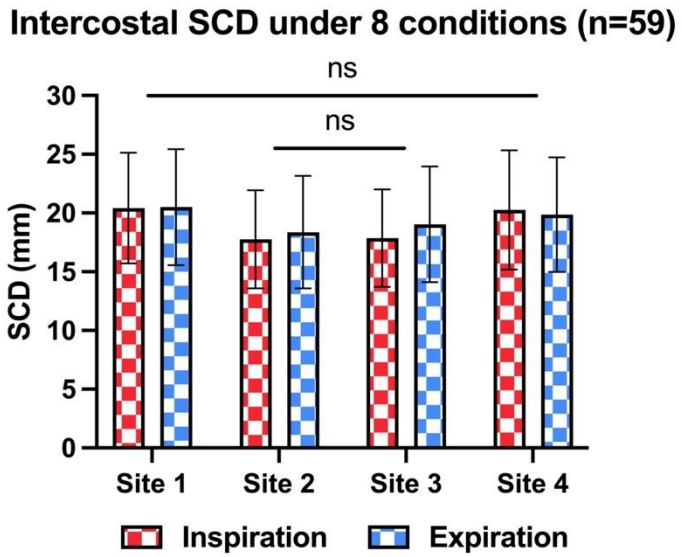

(C)

Figure 3-12. Morphological and biomechanical data of the ICSs show the 2D ultrasound-derived intercostal (A) width, (B) stiffness, and (C) SCD under eight experimental conditions (ns: $p > 0.05$; $p \leq 0.05$ otherwise).

3.4.5 Comparison of Site in 3D Ultrasound Measurement

Intercostal course measurement. Among the four measurement sites, one-way repeated measures ANOVAs demonstrated statistically significant differences of the course of the ICSs, as characterized by intercostal angle and width-change **(Figure 3-13)**. Specifically, Sites 3 and 4 were found to have significantly greater angles of the ICS ($F(2,59) = 30$, $p < 0.001$), with higher degrees indicating less angular ICSs. The width-change (%) of the ICSs was significantly greater with Site 1 than Sites 2 to 4 ($F(2,59) = 7$, $p = 0.002$). Similar to what 2D ultrasound measured, the 3D ultrasound-derived width of the ICS was significantly different among sites ($F(2,65) = 15$; $p < 0.001$). Post-hoc Bonferroni's analysis confirmed the significant difference in width values between each pair of sites, except for Site 3 vs. Site 4 ($p = 1$). Among them, the width of the ICS was highest at Site 2 (20.4 ± 3.3 mm), followed by Site 3 (18.3 ± 4.2 mm).

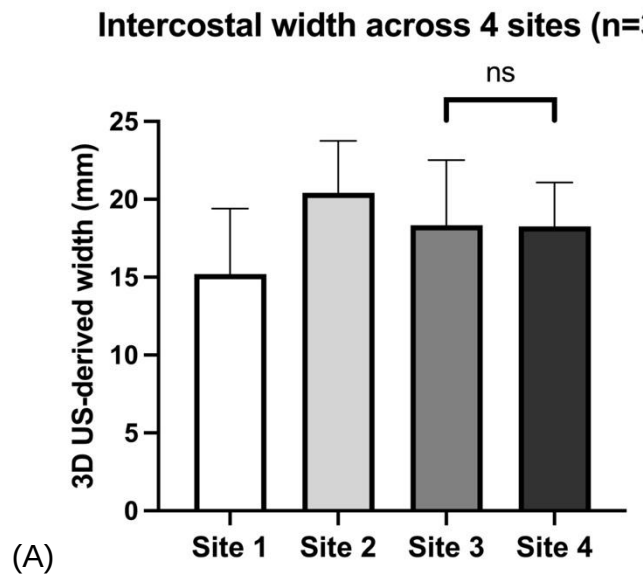
Intercostal width across 4 sites (n=30)
ns
3D US-derived width (mm)
25
20
15
10
5
0
Site 1
Site 2
Site 3
Site 4

(A)

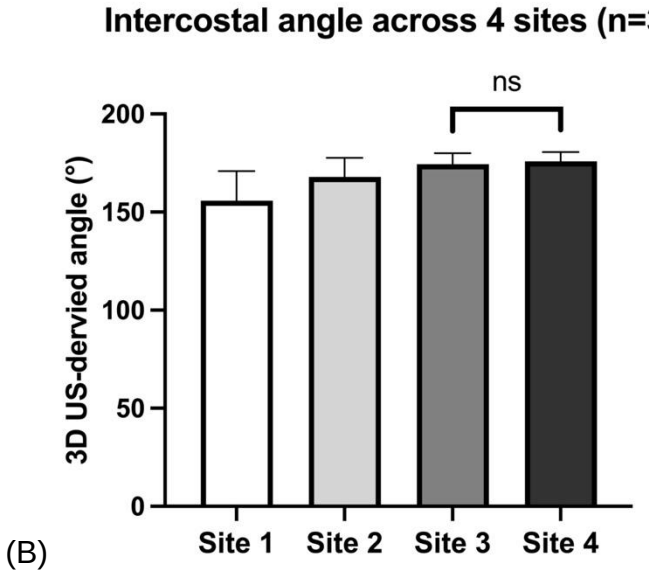
Intercostal angle across 4 sites (n=30)
ns
3D US-dervied angle (°)
200
150
100
50
0
Site 1
Site 2
Site 3
Site 4

(B)

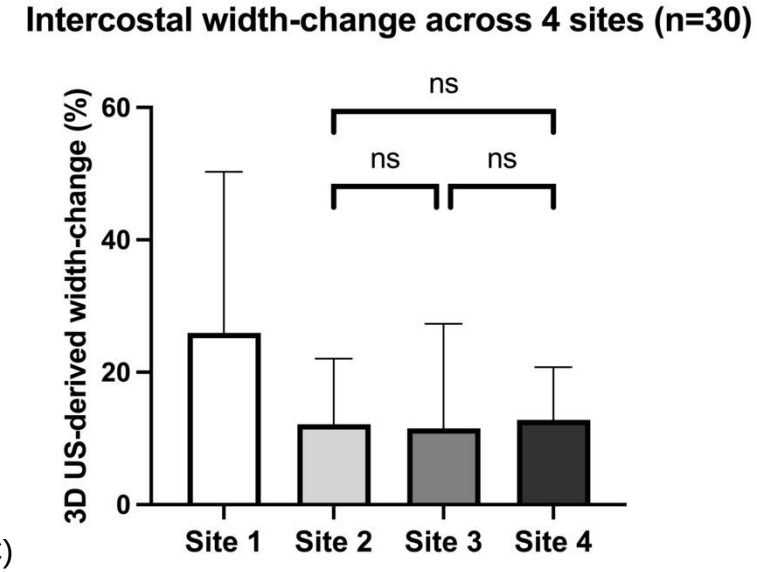
Intercostal width-change across 4 sites (n=30)
ns
ns
ns
3D US-derived width-change (%)
60
40
20
0
Site 1
Site 2
Site 3
Site 4

(C)

Figure 3-13. Morphological data of the ICSs show the 3D ultrasound-derived intercostal (A) width, (B) angle, and (C) width-change under four experimental conditions (ns: $p > 0.05$; $p \leq 0.05$ otherwise).

3.4.6 Factor Analyses of Intercostal Width and Stiffness

Detailed investigations about the influencing factors of intercostal width and stiffness were done. **Table 3-3** and **Table 3-4** show the results of the respective univariate and multivariate analyses evaluating the factors associated with the 16 experimental conditions. In univariate analysis **(Table 3-3)**, greater weight, higher BMI, and larger waist circumference were strongly associated with larger width values (p <0.001 in all conditions). Height was positively correlated to the width of the ICS at Sites 1 to 3, but not at Site 4 (end-inspiratory condition: $p = 0.140$, end-expiration condition: $p = 0.201$). An increase in SCD was fairly associated with an increase in the width of the ICS at all sites ($r_s = 0.27–0.35$). Wider ICSs were more likely to be identified in patients with metabolic syndrome (Site 1, end-expiratory condition: $p = 0.012$; Site 2, end-inspiratory condition: $p = 0.002$; Site 3, end-expiratory condition: $p = 0.027$; Site 4, end-inspiratory and end-expiratory conditions: $p < 0.001$ and $p = 0.003$). There was a significant influence of gender on width values, with males having wider ICSs except for Site 3 (end-inspiratory condition: $p = 0.138$, end-expiratory condition: $P=0.124$). Whereas no association between age and width was seen, older age fairly correlated with greater stiffness at one site (Site 3: $r_s = 0.37$, $p = 0.004$). With the exception of height (Site 3: $r_s = -0.30$, $p = 0.021$), none were significant predictors of the stiffness of the ICS.

Table 3-3. Factors associated with the width and stiffness of the intercostal space in univariate analyses (n=59).

		Age		Height		Weight		BMI		SCD		Waist circumference		Sex		Metabolic syndrome	
		r_s	*P*	r_s	*P*	r_s	*P*	r_s	*P*	r_s	*P*	r_s	*P*	Mean ± SD	*P*	Mean ± SD	*P*
Width (mm)																	
Site 1	Inspiration	-	0.478	-	0.085	0.485	**<0.001***	0.514	**<0.001***	0.269	**0.039***	0.563	**<0.001***	Male, 17.0±4.1; Female, 15.6±3.8	0.197	Absent, 16.0±3.9; Present, 18.5±4.0	0.128
	Expiration	-	0.496	0.301	**0.021***	0.545	**<0.001***	0.523	**<0.001***	0.297	**0.022***	0.601	**<0.001***	Male, 15.2±4.2; Female, 13.2±3.6	**0.050***	Absent, 13.7±3.7; Present, 17.7±4.5	**0.012***
Site 2	Inspiration	-	0.561	0.275	**0.035***	0.526	**<0.001***	0.544	**<0.001***	0.266	**0.042***	0.532	**<0.001***	Male, 20.1±4.1; Female, 17.8±3.1	**0.019***	Absent, 18.4±3.5; Present, 22.9±3.7	**0.002***
	Expiration	-	0.774	-	0.174	0.482	**<0.001***	0.529	**<0.001***	-	0.101	0.510	**<0.001***	Male, 18.7±4.2; Female, 17.2±7.5	0.370	Absent, 17.5±6.2; Present, 21.1±3.6	0.141
Site 3	Inspiration	-	0.267	0.272	**0.037***	0.551	**<0.001***	0.585	**<0.001***	0.314	**0.015***	0.563	**<0.001***	Male, 20.0±4.5; Female, 18.1±5.1	0.139	Absent, 18.7±4.9; Present, 22.0±3.6	0.089
	Expiration	-	0.199	0.259	**0.048***	0.584	**<0.001***	0.632	**<0.001***	0.354	**0.006***	0.580	**<0.001***	Male, 17.6±4.3; Female, 15.7±4.9	0.124	Absent, 16.1±4.6; Present, 20.2±3.5	**0.027***
Site 4	Inspiration	-	0.711	-	0.140	0.418	**<0.001***	0.454	**<0.001***	-	0.067	0.489	**<0.001***	Male, 17.8±3.4; Female, 15.7±3.4	**0.019***	Absent, 16.1±3.2; Present, 20.8±2.9	**<0.001***
	Expiration	-	0.941	-	0.201	0.466	**<0.001***	0.540	**<0.001***	0.296	**0.023***	0.526	**<0.001***	Male, 15.8±3.6; Female, 13.4±3.3	**0.010***	Absent, 14.1±3.4; Present, 18.3±3.4	**0.003***
Stiffness (kPa)																	
Site 1	Inspiration	-	0.876	-	0.973	-	0.364	-	0.380	-	0.892	-	0.323	Male, 17.5±7.7; Female, 17.7±9.3	0.779	Absent, 17.7±9.0; Present, 17.3±2.7	0.542
	Expiration	-	0.465	-	0.389	-	0.716	-	0.428	-	0.282	-	0.365	Male, 14.1±3.6; Female, 17.0±9.1	0.481	Absent, 15.6±7.5; Present, 15.3±3.0	0.573
Site 2	Inspiration	-	0.646	-	0.657	-	0.843	-	0.386	-	0.710	-	0.865	Male, 15.6±8.0; Female, 15.6±9.0	0.628	Absent, 15.7±8.7; Present, 14.8±6.8	0.954
	Expiration	-	0.164	-	0.675	-	0.305	-	0.114	-	0.055	-	0.409	Male, 14.0±7.5; Female, 12.4±5.3	0.539	Absent, 13.0±6.6; Present, 14.4±5.4	0.441
Site 3	Inspiration	-	0.646	-	0.200	-	0.692	-	0.733	-	0.860	-	0.956	Male, 13.0±5.7; Female, 16.1±7.2	0.065	Absent, 14.2±5.8; Present, 17.6±11.4	0.705
	Expiration	0.371	**0.004***	-0.299	**0.021***	-	0.301	-	0.876	-	0.503	-	0.773	Male, 11.8±8.0; Female, 13.2±5.3	0.057	Absent, 12.5±7.1; Present, 12.9±3.8	0.413
Site 4	Inspiration	-	0.633	-	0.396	-	0.480	-	0.375	-	0.671	-	0.861	Male, 11.7±4.8; Female, 14.7±7.1	0.072	Absent, 12.8±5.3; Present, 16.4±11.0	0.441
	Expiration	-	0.821	-	0.394	-	0.930	-	0.737	-	0.782	-	0.785	Male, 10.2±5.0; Female, 12.2±6.8	0.246	Absent, 11.0±5.7; Present, 13.7±8.3	0.441

Note: age, height, weight, BMI, SCD and waist circumference were analysed by Spearman's correlation test; sex and metabolic syndrome were analysed by unpaired t-test or Mann-Whitney U test, where appropriate.

* $p \leq 0.05$; BMI = body mass index; SCD = skin-liver capsule distance; ICS = intercostal space; r_s = Spearman's rank correlation coefficient.

In multivariate analysis **(Table 3-4)**, height, weight, BMI, SCD, gender, and the presence of metabolic syndrome remained independent factors associated with intercostal width. Waist circumference no longer provided a significant contribution to the width values in this model. The beta weights showed that weight (Site 1, end-inspiratory condition: β = -2.91, p = 0.041) had the greatest influence on the regression model, followed by BMI (Site 1, end-inspiratory condition: β = 2.75, p = 0.011; end-expiratory condition: β = 2.47, p = 0.018). However, only SCD and BMI were independently associated with the width values at most sites and appeared to be the most general determinants. The only covariate influencing the stiffness values was height (β = -2.03; p = 0.029), which was in line with the result of univariate analysis.

Table 3-4. Factors associated with the width and stiffness of the intercostal space in multivariate analyses (n=59).

		Age		Height		Weight		BMI		SCD		Waist circumference		Sex		Metabolic syndrome	
		β	*P*	β	*P*	β	*P*	β	*P*	β	*P*	β	*P*	β	*P*	β	*P*
Width (mm)																	
Site 1	Inspiration	-0.040	0.752	1.556	**0.047***	-2.909	**0.041***	2.753	**0.011***	-0.441	**0.026***	0.310	0.324	0.005	0.980	0.090	0.513
	Expiration	-0.082	0.502	1.423	0.062	-2.576	0.062	2.471	**0.018***	-0.389	**0.042***	0.232	0.448	-0.049	0.783	0.228	0.093
Site 2	Inspiration	0.011	0.927	0.513	0.466	-0.919	0.471	1.284	0.166	-0.579	**0.004***	0.301	0.336	-0.068	0.709	0.264	**0.041***
	Expiration	0.102	0.495	-0.813	0.354	1.150	0.467	-0.387	0.735	-0.338	0.160	0.013	0.974	-0.171	0.448	0.149	0.347
Site 3	Inspiration	-0.076	0.540	0.854	0.245	-1.332	0.317	1.904	0.059	-0.693	**0.002***	0.172	0.574	0.073	0.679	0.095	0.459
	Expiration	-0.070	0.541	1.101	0.109	-1.809	0.146	2.391	**0.012***	-0.668	**0.001***	0.037	0.895	0.028	0.862	0.181	0.132
Site 4	Inspiration	-0.025	0.829	0.354	0.592	-1.008	0.401	1.462	0.095	-0.705	**0.001***	0.280	0.356	-0.310	0.065	0.322	**0.009***
	Expiration	-0.023	0.838	0.478	0.449	-1.437	0.211	1.897	**0.025***	-0.676	**0.001***	0.180	0.532	-0.457	**0.005***	0.275	**0.019***
Stiffness (kPa)																	
Site 1	Inspiration	-0.025	0.871	-0.007	0.994	-0.245	0.887	0.820	0.524	-0.132	0.578	-0.386	0.317	-0.150	0.507	0.049	0.770
	Expiration	0.059	0.688	-2.030	**0.029***	3.282	0.051	-2.225	0.076	0.315	0.170	-0.334	0.368	-0.075	0.728	-0.032	0.845
Site 2	Inspiration	-0.023	0.885	0.024	0.980	-0.277	0.871	0.053	0.965	0.180	0.484	-0.009	0.982	-0.134	0.583	-0.037	0.826
	Expiration	0.109	0.471	0.328	0.709	-1.324	0.407	1.116	0.335	-0.177	0.461	-0.063	0.872	-0.430	0.063	0.115	0.469
Site 3	Inspiration	0.106	0.467	0.735	0.397	-1.505	0.339	1.139	0.334	0.404	0.107	-0.244	0.501	0.101	0.627	0.205	0.179
	Expiration	0.248	0.090	0.356	0.677	-1.656	0.287	1.419	0.224	0.029	0.905	0.047	0.896	-0.326	0.117	-0.030	0.841
Site 4	Inspiration	0.049	0.749	0.361	0.679	-0.827	0.600	0.349	0.759	0.241	0.366	0.238	0.552	0.264	0.229	0.136	0.390
	Expiration	0.079	0.615	-0.287	0.745	0.182	0.909	0.164	0.887	0.204	0.450	-0.313	0.440	-0.008	0.972	0.179	0.265

Note: age, height, weight, BMI, SCD, waist circumference, sex and metabolic syndrome were analysed by multiple linear regression.

* $p \leq 0.05$; BMI = body mass index; SCD = skin-liver capsule distance; ICS = intercostal space; β = standardized regression coefficient.

3.4.7 Differences in Liver Detection Rates

Table 3-5 presents the relationship between the site and the presence of the liver under the two respiratory conditions. Cochran's Q test determined statistically different proportions among the four sites below which the liver is visible at end-inspiration, $\chi^2(3) = 44.357$, $p < 0.001$. The post hoc Dunn's test found that the liver was significantly better visualized at Sites 1 and 3 (100% and 90%, $p = 0.989$) than Sites 2 and 4. On the other hand, the test did not indicate any differences among the four proportions during the end-expiratory phase, $\chi^2(3) = 0.857$, $p = 0.836$.

Table 3-5. Liver detection rates across four measurement sites under two respiratory conditions (n = 59).

	Is the liver the underlying organ visible in B-mode images?			
	7th ICS		**8th ICS**	
	Site 2	**Site 4**	**Site 1**	**Site 3**
End-inspiration†	75% (44)	54% (32)	100% (59)	90% (53)
End-expiration‡	95% (56)	95% (56)	93% (55)	97% (57)

Data were presented as proportion % (n); ICS = intercostal space.

† $p > 0.05$ for Site 1 vs. 3 and Site 2 vs. 3; $p \leqslant 0.05$ for remaining pairs otherwise.

‡ $p > 0.05$ for all pairs.

3.5 Discussion

A right lateral intercostal approach is commonly used in the TE examination procedure to access the liver. Understanding the anatomical relationship between the ICS and transducer is of clinical importance, as it influences the success and efficiency of the examination. Knowledge of intercostal anatomy can assist in managing transducer–rib interferences, but is lacking in the literature. Hence, this ultrasound-based observational study sought to establish evidence-based recommendations for a TE measurement protocol, including a specific measurement site and respiratory condition. It is the first work towards the standardization of the TE examination procedure, ultimately maximizing its effectiveness for liver disease sufferers.

Measurement validity and reliability. Excellent intra- and inter-operator agreement of the morphological measurements of width and SCD were observed, with all ICCs exceeding 0.97. In contrast, the measures of intercostal stiffness were less reliable, with ICCs ranging between 0.593 and 0.896. This reduction in ICCs may be attributed to SWE signal interference from adjacent ribs. A previous study [162] also reported the relatively low repeatability for SWE of the diaphragm ($ICC_{(3,1)} = 0.68$) and intercostal muscles ($ICC_{(3,1)} = 0.44$). Inter-operator $ICCs_{(2,3)}$ of intercostal SWE was found to be lower than intra-operator $ICCs_{(3,3)}$. We postulated that this variation may be due to discrepancies in the actual measurement site or differences in probe pressures applied between operators. It is worth noting that we attempted to minimize this measurement error by marking the investigated sites with a surgical skin marker to achieve higher repeatability. Placing the probe with minimal pressure was also required to prevent deformation of the intercostal tissues being examined. Despite these efforts, there is still room for improvement in terms of standardizing probe

positioning to ensure reliable intercostal measurements by ultrasound.

The acquisition of width data in this study may be error-prone and biased, as the investigator visually approximated and determined the probe orientation corresponding to the minimum width. Consequently, we conducted further validation of the existing 2D and 3D methods used for analyzing the inter-ICS difference by comparing them with a reference method. Our results indicated that the errors may be considered negligible, as supported by excellent inter-method correlation ($r > 0.9$). Nevertheless, future research warrants other compelling data collection methods, such as CT [163-165] and MRI [166] for the morphometry of the ICS-related anatomy. Future validation against non-ultrasound modalities will enhance the validity of the existing ultrasound-based measurement data.

Intercostal anatomy and implication for site choice. To better accommodate the transducer tip and mitigate interferences from adjacent ribs and overlying fat layers, we anticipated the ICS to be wider, thinner, softer, less angular and have a regular shape. Our anthropometry analyses revealed that the anatomical characteristics of the ICSs are site-dependent, with significantly greater intercostal width at Sites 2 and 3, lower intercostal width-change at Sites 2 and 3, shorter intercostal SCD at Sites 2 and 3, lower intercostal stiffness at Sites 3 and 4, and greater intercostal angle at Sites 3 and 4.

Previous studies on ICS anatomy are scarce, with limited published data available concerning intercostal width over the liver region. Only one related work carried out by Kim et al. [164] showed substantial variation in the widths of the six ICSs on the right inferior rib cage, with the 7th ICSs on the anterior axillary line being widest (mean width of 18.3 ± 3.4 mm). Notably, this reported width closely matched our data for that

particular ICS (Site 2: mean width of 18.1 ± 4.5 mm; median width of 18.0 mm with IQR 5.8 mm). Moreover, our demographic analysis revealed that 6.8% and 44.1% of the subjects in our cohort had intercostal width values smaller than 9 mm (diameter of the M probe tip for standard morphotype [74]) and 12 mm (diameter of the XL probe tip for obesity [91]), respectively. These relatively narrow ICSs might partly account for the previously reported TE failure or unreliable results in the literature. This finding further emphasizes the importance of considering intercostal dimensions when designing future transducer specifications. Pradhan et al. [92] were also aware of the limitation of TE in small adults who frequently have narrow ICSs; they proposed a solution to utilize the S probe which configures a smaller 7-mm diameter tip to minimize rib interference. In contrast, our study introduced a more universal and adaptive approach to the community by providing TE practitioners with an ideal probe placement site, even for patients of small stature with generally narrower ICSs. This effectively waives the need to modify the type of TE probe in practice. Intercostal elastography also remains an unexplored territory in the literature. Only two recent studies [167, 168] demonstrated the feasibility of biomechanical characterization of the ICS by SWE. The reported biomechanical values (an approximation of 10 to 20 kPa) were of the same order of magnitude as our data, which supports the validity of our intercostal SWE results. However, those studies were limited to measuring only one representative ICS in the adolescent scoliosis cohort. In contrast, our study presented a distinct research question and was the first attempt to investigate the biomechanical differences among multiple ICSs in adults. Additionally, abdominal wall thickness is the determinant of TE failure, as it relates to the hindrance of propagation of ultrasound and shear waves [91]. To adapt to a greater amount of subcutaneous tissues in obese patients, the XL probe with a lower ultrasound frequency and a higher

vibration amplitude was specifically designed [78, 91]. Our study identified two specific ICSs with relatively thinner abdominal walls, which may provide another insight into addressing overweight population, particularly when an XL probe is not available.

It is worth noting that our 2D ultrasound results can, at most, imply the placement of a single-element transducer, as we collected only 1D information regarding intercostal size, specifically its width. This anatomical information is insufficient in the context of array transducers, which are commonly fabricated with a larger footprint. In this case, we further conducted an intercostal 3D ultrasound study to supplement the selection of an ideal site, taking into account the course of the ICS. Results derived from 3D ultrasound showed that the less angular and less irregular ICSs lie at Sites 3 and 4 and Sites 2 and 3, respectively. The 3D ultrasound-derived width was greater at Sites 2 and 3 than the other two. The order of approximately 18 mm and the trend of the 3D ultrasound results coincide with those of 2D ultrasound, supporting the validity of the methods used in this study. To our best knowledge, this is the first work toward 3D ultrasound imaging of the rib cage and associated ICSs.

To sum up both the 2D and 3D ultrasound results, Site 3 consistently emerged as the superior site for TE probe placement, given its greater width, lower width-change, greater angle, lower stiffness, and shorter SCD.

Respiratory effect on intercostal anatomy. End-inspiration appeared to consistently yield the wider and stiffer ICSs across all measurement sites in the present study. We speculated that an increased thoracic perimeter and inspiratory muscle activation during inhaling played a role. The finding is consistent with the previous studies that reported an increase in intercostal width [167], stiffness [167-169], muscle cross-sectional area [163], and muscle thickness [170] during inspiration.

On the other hand, the impact of respiration on the intercostal SCD values exhibited a non-linear pattern, because the ANOVA suggested a site-dependent interaction. This observation implies that respiratory movement behaved differently at various sites. Factors such as lung volume, intercostal muscle recruitment and pleural pressure collectively contribute to the overall shape of intercostal tissues [171], influencing the derived SCD.

Influencing factors and implication for patient selection. Height was the only predictor of intercostal stiffness. Intercostal width, on the other hand, varied considerably depending on gender, BMI, and SCD. Only SCD had a homogeneous influence on the width across all sites, suggesting that subcutaneous fat accumulation contributes to a wider ICS. We also confirmed narrower ICSs in women which aligns with a previous study [164]. Our findings have clinical implications for patient selection and stratification based on patient characteristics: taller males with greater SCD and BMI tend to favour TE probe placement. However, a dilemma arises, as the risk of TE failure might increase in this population due to the associated overmuch fat layers. Consequently, hepatologists are strongly urged to exercise caution when applying these regression results in pre-TE planning.

Presence of the liver and implication for site choice. Compared to the 7th ICS, there seemed to be a higher likelihood of visualizing the liver via the 8th ICS. In the 7th ICS, the frequency of occurrence of the liver was lower at end-inspiration, whereas no such trend was observed in the 8th ICS. This phenomenon can be explained by lung inflation during the inspiratory phase, causing the liver to move cranio-caudally. Consequently, the upper ICSs are more likely to present the lung rather than the liver. Our analysis was not attempting to describe a comprehensive distribution of all the

ICSs overlying the liver, but rather to justify the choice of the four investigated sites. Although the data may not be complete, they did not compromise the validity of recommending Site 3 (90% liver detection rate at the end-inspiratory condition, 97% at the end-expiratory condition).

Novelty and clinical contribution. Anatomical research on ICSs has received very limited attention, possibly due to the unavailability of a standard morphometric analysis method. Since ICSs are anatomically located in subcutaneous regions, in vivo manual morphometry is practically challenging. CT with multiplanar reformation (MPR) has showed its ability to quantify intercostal size (as measured by vertical width [164]), intercostal muscle quality (as measured by CT attenuation [172]), and quantity (as measured by cross-sectional area [163, 172]). Yet, intercostal CT assessment is resource intensive, and generally requires specialized expertise. Furthermore, conducting a large-scale CT study to derive anatomical information of the ICSs is deemed unethical as it exposes participants to ionizing radiation. Given its highly accessible and radiation-free nature, ultrasound has the promising potential to map the ICSs. Our study demonstrated the feasibility of utilizing ultrasound imaging to characterize multiple ICSs both morphologically and biomechanically. To our best knowledge, this study was the first to report the relevance of intercostal anatomy to the TE examination procedure. Among the four candidate sites, Site 3 is recommended as the ideal site for TE probe placement. Additionally, we propose performing TE at end-inspiration to allow for less transducer–rib contact. It is an important advance because our finding has the potential to address operator-related dependencies and inexperience, which have hindered the broad applicability of TE. Prior to our work, site selection relied on subjective judgment and operators' expertise, lacking standardized clinical practice guidelines. Our recommendations could serve

as a guide for novices and be incorporated into operational workflows to enhance procedural efficiency of liver elastography. Moreover, these findings may be extrapolated to other liver elastography techniques, such as point ARFI or 2D-SWE, for which an adequate acoustic window is also the requisite.

While most studies did not specify the exact measurement site, some have reported using somewhere between the 5th and 8th ICSs [87, 123, 158, 161]. We postulated that these choices might reflect common real-world clinical practices. Surprisingly, the reported range contradicts the existing clinical guidelines recommending probe placement in the 9th to 11th ICS [54, 55, 95]. Moreover, the consideration of a breathing technique used is also lacking in these recommendations. It was the motivation of our study that provided anatomical considerations in the context of TE. Yet, one study is rarely sufficient evidence on which to base a change. Thus, our study advocates for more rigorous scientific evaluation of what those guidelines recommended before their widespread uptake.

Limitation and prospect. This study has several limitations. First, the sample size of 59 subjects enrolled appears to be relatively small. However, a *priori* analysis for the repeated measures ANOVA was performed and determined that this sample size was statistically sufficient to test our hypothesized inter-ICS differences; and it is worth noting that we have successfully demonstrated the feasibility to identify the ideal site and respiratory condition for TE. However, to consolidate the spatial distribution information and further whether other comparably ideal sites existed, mapping additional ICSs is necessary in the future. Second, the scope of this study was confined to Chinese adults, which may raise questions about the generalizability of our findings across diverse racial demographics. Future research should encompass

subjects representing varying races, geographical regions, and BMI categories. Additionally, follow-up studies could evaluate the improvement in the successful rate and time consumption of the TE examination when applying the guideline outlined in this study, in comparison to the common experience-based clinical practice. Third, we did not standardize the type of the breathing performed during the data acquisition among all enrolled subjects. This may lead to the concern that the difference between thoracic and diaphragmatic breathing could affect intercostal anatomy. Future investigation is need to address the potential impact of different breathing exercises. Another future research direction is to determine the relative accuracy of TE measurements obtained from different sites for staging liver fibrosis, using liver histology as the reference standard.

Despite the aforementioned shortcomings, it is worth noting that the overarching goal of this feasibility study was to provide an evidence-based recommendation for ideal place placement and patients' breathing technique during the TE examination. We hope these findings would not only serve to increase the awareness of TE practitioners and the liver research community, but also encourage concerted efforts for pressing ahead the TE examination procedure to the next rung on its developmental ladder.

3.6 Summary

Chapter 3 adopted a within-subject design attempting to demonstrate the anatomical differences among the four investigated measurement sites and between the two respiratory conditions. Notably, this is the first study to demonstrate the feasibility of applying 3D ultrasound imaging for the characterization of intercostal course. We observed site-dependent differences in the intercostal width, width-change, angle, SCD, and stiffness, indicating that ICS configuration is highly variable. Our accumulating evidence supported performing TE at Site 3 (the 8th ICS on the mid-axillary line) during the end-inspiratory phase as the measurement protocol of choice. It serves as a practical solution for challenging cases involving patients with narrow ICSs or obesity, potentially offering a universally applicable strategy without requiring technological modifications of the TE probe. Additionally, this streamlined procedure can assist inexperienced TE practitioners and even non-specialists in shortening the learning curve. We would welcome its validation in the real-world clinical context. Larger studies encompassing diverse racial demographics are warranted to contextualize the findings on a global scale.

Chapter 4. Determining the Ideal Patient Positioning for TE: Effect of Body Posture on Liver Stiffness Measurement

This chapter has been derived from the manuscript that has been submitted to a journal:

Can Body Posture Modulate Liver Stiffness Measured by Transient Elastography?

Huang, Z.-H., Deng, M.-Q., Lin, Y.-M., Ye, C.-H., Zheng, M.-H., & Zheng, Y.-P.

Submitted and under review, 2024.

4.1 Background

Currently, liver biopsy is considered the gold standard for diagnosing the excessive accumulation of fibrous tissue in the liver. However, this invasive procedure carries the risk of life-threatening complications, and is limited by inter-pathologist variability and sampling error [173]. These drawbacks have prompted the widespread clinical adoption of transient elastography (TE), a technique that quantifies liver stiffness (LS) as a surrogate biomarker for liver fibrosis [74]. TE is a WHO-recommended ultrasound elastography technique for liver stiffness measurement (LSM) [56, 174], and has demonstrated excellent diagnostic accuracy in staging liver fibrosis through meta-analyses [175, 176].

LS below 8 kPa typically indicates the upper limit of normal, which is associated with a high negative predictive value for excluding clinically significant fibrosis (stage F≥2) [154, 177], and possesses up to a 93% sensitivity for ruling out cirrhosis (stage F=4) [178]. At the higher end of the LS spectrum, although increased LS (≥8 kPa) is widely recognized to primarily reflect a degree of fibrotic accumulation, various other

factors can influence LS [56, 97, 98]. In other words, certain pathophysiological conditions have been shown to elevate LS in the absence of liver fibrosis. These confounding factors could be matrix-related (e.g., amyloidosis [179]), histological (e.g., necro-inflammation [102, 103], mastocytosis [180]) or hemodynamic (e.g., congestion [104, 105], cholestasis [106], respiration [181], food intake [100, 101], hepatic arterial and portal pressure [107, 108]). For instance, two European studies have reported that liver damage from acute hepatitis can induce a reversible increase in LS to the level suggestive of cirrhosis (≥12.5 kPa), thus potentially misguiding the diagnosis of pre-existing cirrhosis [102, 103]. Likewise, Millonig et al. [104] identified hepatic congestion due to cardiac insufficiency as another hemodynamic cause that can elevate LS irrespective of the fibrosis stage. Impaired venous drainage and intrahepatic blood stasis may be the primary reasons behind this false-positive result of LSM. Given the existing evidence, there is a pressing need to identify additional confounders for the proper use of TE and the accurate interpretation of LS in assessing liver fibrosis severity.

Body posture may be one such factor to confound LS, as it also influences hepatic hemodynamics. Previous literature has documented morphological and hemodynamic responses of liver-associated vasculatures such as inferior vena cava (IVC) [182, 183], portal vein [184, 185] and aorta [182] to postural changes; however, the causative relationship between posture and LS has not been well explored.

4.2 Study Aims

Along this line, this study aimed to assess the effect of the supine and upright positions (i.e., seated and standing) on LSM using TE. Given the previously established variations in anatomy and pathophysiology between healthy and cirrhotic livers [184, 186], we further hypothesized that the liver would respond differently to an upright posture depending on the degree of fibrosis. To test this hypothesis, we analysed the posture-induced LS differences in healthy individuals and patients across various fibrosis stages.

4.3 Methods

4.3.1 Subjects

In this prospective study, we recruited two independent 'LS groups' via convenience sampling. Adults (≥18 years) who had been diagnosed with chronic liver disease (CLD) of any aetiology and clinically indicated for TE were eligible. Patients were recruited from The First Affiliated Hospital of Wenzhou Medical University and assigned to the patient group. In contrast, a cohort of healthy controls with no history of liver disease were recruited from another participating institute − The Hong Kong Polytechnic University to assemble the control group. Exclusion criteria for both groups included: (1) common contraindications for TE (e.g., ascites, active cardiac implant); (2) previous liver transplantation; and (3) any previously reported confounding conditions (e.g., cholestasis, acute hepatitis, congestive heart failure) to mitigate possible interferences with LS. Because the experiment involves procedures including postural changes, upright positioning, and raising the right arm to expose an acoustic window, individuals with limited shoulder mobility or balance disorders (e.g., Parkinson's disease) were also deemed ineligible and thus excluded from this study.

A *priori* power analysis projected a sample size of 56 under a two-way (3×2) mixed-model design, assuming a medium Cohen's effect size of f = 0.20 (η^2_p = 0.04), 90% statistical power, and a two-tailed significance level of 0.05. The final target sample size was set at 62 to allow for 10% dropout. More importantly, the sample of 62 guaranteed an equal distribution of 31 individuals per group for both patient and control cohorts. The Ethics Committee at The Hong Kong Polytechnic University approved the study protocol (HSEARS20210809002). All subjects provided written informed consent. This observational, cross-sectional study was compliant with the Declaration

of Helsinki and the STROBE criteria.

4.3.2 Procedures

Prior to LSM, demographic, anthropometric, and clinical data were collected according to standard protocols. To evaluate LS under three different postures, TE was conducted with the Liverscan® system (Eieling Technology Limited, Hong Kong, China) which enables simultaneous B-mode imaging of liver anatomy and LSM [187]. All subjects fasted for a minimum of three hours before LSM to avoid a confounding post-prandial increase in LS. As previously described [56, 74], the standard patient positioning for TE examination requires maximal abduction of the right arm, which was consistently maintained across all three posture conditions. Each subject underwent TE in the supine position as the baseline assessment first, followed by the seated or standing positions **(Figure 4-1)**. The examination order of the latter two upright positions were randomized for subjects to eliminate the operator bias resulting from a learning effect. A five-minute interval between different posture conditions was allocated. Assisted by real-time B-mode, an investigator, who was specialized in radiography and had six years of TE experience, identified a representative portion of the right liver parenchyma free of large vasculatures, and selected it as the reference image. The corresponding measurement site was also marked on the subject's skin surface. An attempt was made to collect exact 15 measurements under each of the three postures.

(A)

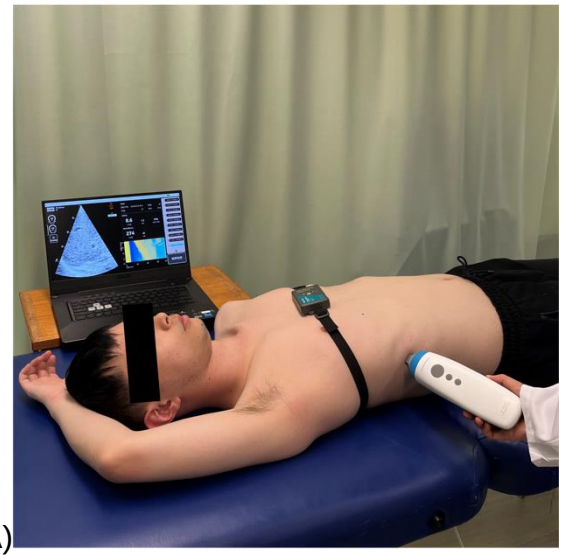

(B)

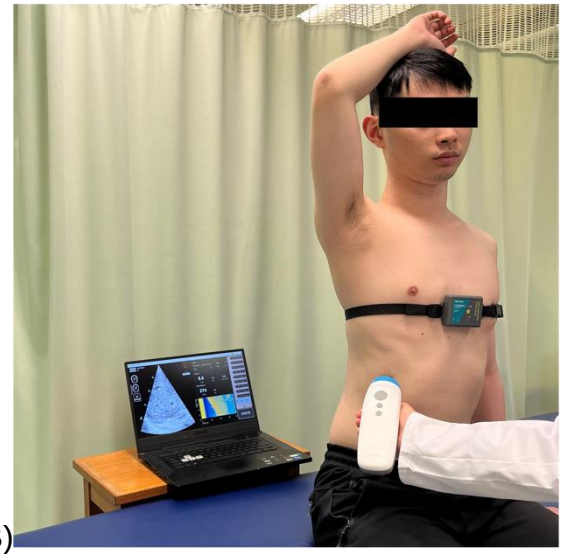

(C)

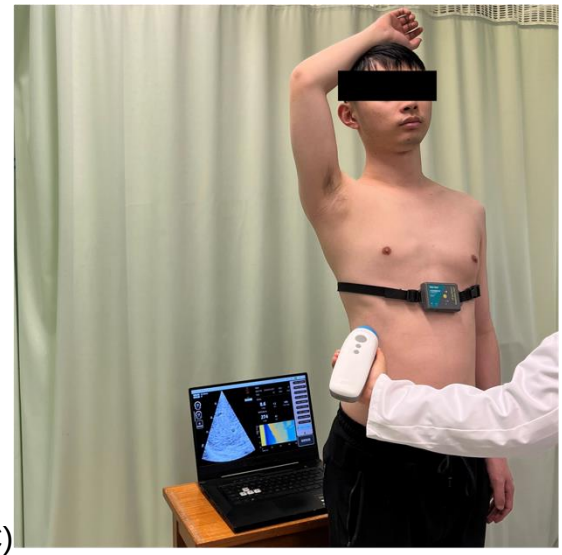

Figure 4-1. Experimental setup for TE-based LSM under three patient positioning techniques. (A) Supine; (B) Seated; (C) Standing.

Considering that the liver is a moving organ and not necessarily uniform, measures were taken in an attempt to limit the confounding factors, i.e., respiratory motion and liver fibrosis heterogeneity **(Figure 4-2)**. To control for the confounder of respiration, subjects wore a Go Direct® respiration chest belt (Vernier, Beaverton, USA) sensing and monitoring respiratory cycles in real-time. LSMs were standardized at the end-inspiratory phase across postures, as suggested by previous studies for improved predictive accuracy and success rate of TE [181]. To control for the confounder of

heterogeneous fibrosis, upright LSM was performed near the initially identified site. Using the captured B-mode images as additional reference, the investigator located the same liver lobe of interest. LS was then obtained with reference to the exact location or landmark within the liver, from which the baseline supine LSM was made.

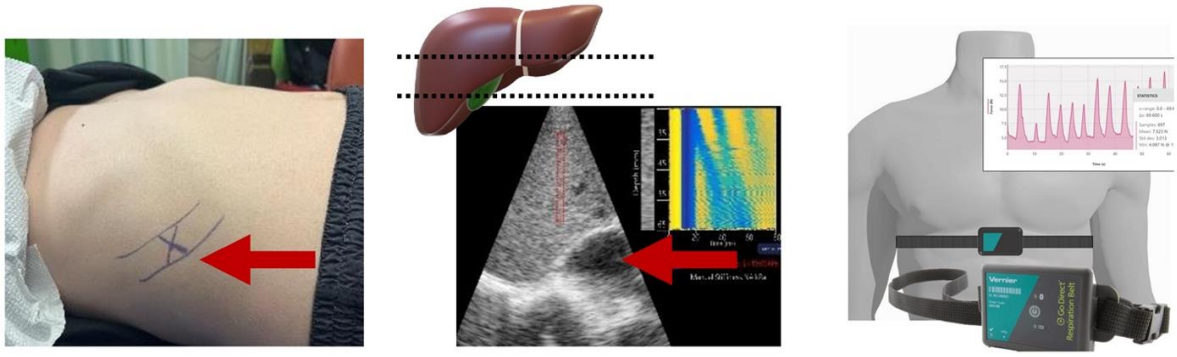

Figure 4-2. Quality control measures of elastogram acquisition to maximize the consistency of the anatomic locations being measured within the liver across postures.

To validate the performance of B-mode guided TE, conventional TE using the widely validated Fibroscan® system (Echosens, Paris, France) was administered to each subject on the same day. Following the previously detailed protocol [56, 74], a minimum of 10 valid acquisitions were made solely in the supine position for benchmark comparison.

4.3.3 Outcome Measures

LSM typically involves not only LS, but also its quality criteria [76]. The median LS of the first 10 successful acquisitions was calculated, and used in this study as the per-subject Young's modulus of the liver for each posture condition. To allow easy implementation, simplified rounded LS of <8 kPa, 8–13 kPa and ≥13 kPa were respectively considered normal, clinically significant fibrosis and cirrhosis [105, 154,

176], and were therefore adopted as cutoffs for the subsequent subgroup analyses. The interquartile range to median LS ratio (IQR/median) was determined as the evaluation metric of variability between the 10 LSMs. The success rate, defined as the ratio of successful acquisitions to the total of 15 measurement attempts, was also computed for each posture. This serves as the metric evaluating whether the feasibility of LSM would vary with posture. To achieve that, elastogram acquisition quality was qualitatively analyzed by a human rater and determined on a binary scale **(Figure 4-3)**. Manual elastogram classification primarily incorporates two criteria: the presence and quality of the shear wave propagation trajectory in an elastogram. Specifically, a rater utilized the dichotomy (i.e., presence or absence) to determine whether a shear wave trajectory was detectable and of sufficient quality for LS computation. A successful LSM was indicated by a high-quality elastogram, whereas a poor-quality elastogram invalidated LSM, potentially compromising the diagnostic accuracy. In this study, two raters, who had six years and six months of experience in interpreting elastogram respectively, independently classified all elastograms. They were blinded to each other's classification results and the actual posture condition of the elastogram being judged. In case of discrepancies between raters, a consensus classification result was assigned for subsequent analysis of inter-posture success rate comparison. Ultimately, the median LS (in kPa), alongside another two measures of IQR/median (%) and success rate (%), were reported for each posture condition.

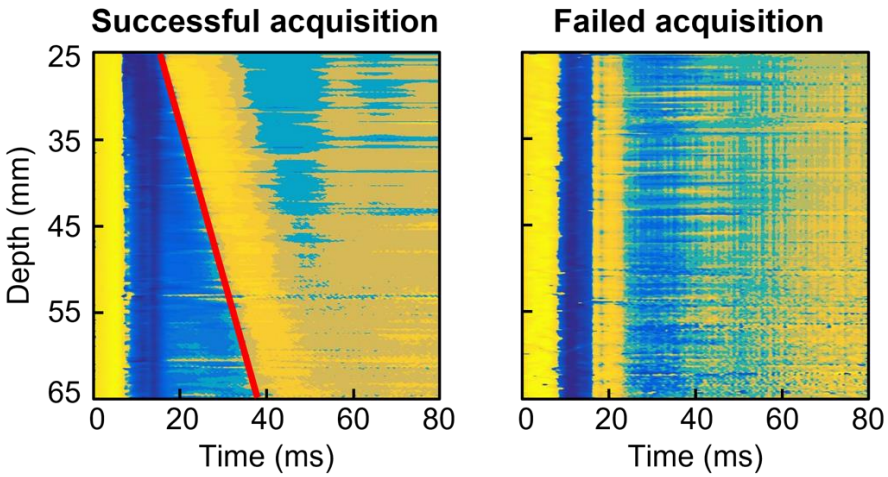

Figure 4-3. A representative example illustrating the manual classification outcomes for both a successful and a failed elastogram acquisition from the same subject. Classification system was devised on the basis of a binary criterion, with shear wave propagation in the liver indicating a successful LSM; and vice versa.

4.3.4 Statistical Analyses

All statistical analyses were conducted using SPSS version 26.0 (IBM Corp., New York, USA) and GraphPad Prism 9 (GraphPad Software Inc., San Diego, USA). The significance level is set at 0.05.

Descriptive statistics. Between-group comparisons were made using Fisher's exact test for categorical data, and Mann-Whitney U test for continuous data. Normality was assessed by Shapiro-Wilks's test.

Posture effect on LSM. A two-way mixed ANOVA was applied to examine the main effects of (a) within-subjects factor 'posture' (supine, seated, standing conditions) and (b) between-subjects factor 'LS group' (patient vs. control groups), and their interaction on LS. The success rate and IQR/median values between three posture conditions were compared separately using a one-way repeated measures ANOVA and non-parametric Friedman test, where appropriate. The relationship between the

LS measured in the benchmark supine position and the magnitude of change in LS from the supine to upright position (i.e., absolute value of stiffness-change [%]) was analysed using both Spearman's correlation and linear regression.

Rater agreement statistics. In a secondary analysis, we examined inter-rater percentage agreement and corresponding Cohen's kappa (κ) for two raters who participated in classification of successful elastogram acquisition. The strength of agreement was interpreted based on Landis & Koch's criteria [188]: poor to fair (κ < 0.4), moderate (κ = 0.4–0.6), substantial (κ = 0.6–0.8), and excellent (κ > 0.8).

Validity statistics. LS measured by conventional TE and B-mode guided TE in different positions were compared pairwise, and Spearman's rank correlation coefficients (r_s) were computed.

4.4 Results

4.4.1 Subject Demographics

Between October 2022 and June 2023, 32 patients and 31 controls were screened for eligibility in the study. A female patient with a BMI of 28 kg/m^2 was excluded because LSM failure occurred repeatedly in all attempts. **Table 4-1** outlines the comparative analysis of the 62 subjects who were successfully enrolled. Overall, the median age of all subjects was 55 years, and 61% of them were male. The patient group consisted predominantly of those with metabolic dysfunction-associated steatotic liver disease (MASLD, the new nomenclature for non-alcoholic fatty liver disease [NAFLD]), among whom 45% had simple steatosis and 6% presented with concurrent hepatitis B virus (HBV) infection. Compared with liver disease patients, controls were less overweight (proportion, 61% vs. 10%; $p < 0.001$) as indicated by a lower BMI (25 kg/m^2 vs. 23 kg/m^2; $p < 0.001$), skin–liver capsule distance (16 mm vs.

11 mm; $p < 0.001$) and waist circumference (96 mm vs. 81 mm; $p < 0.001$), but gender distribution (males, 71% vs. 52%; $p = 0.192$) and age (50 years vs. 58 years; $p = 0.051$) did not differ between the groups. In addition, subgroup analyses by posture (supine vs. seated vs. standing) revealed no differences in IQR/median between the groups. The success rate was not significantly different between the groups, except for those LSMs performed in the supine condition (100% for patients vs. 97% for controls; $p = 0.005$). In contrast, LS was significantly higher in the patient group than in the control group, consistently across the three postures (all $p < 0.001$).

Table 4-1. Baseline characteristics comparison between two liver stiffness groups (n=62).

Variable	Patients (n=31)	Controls (n=31)	Total (n=62)	*p*-value¶
• Demographics				
Male	71% (22)	52% (16)	61% (38)	0.192
Age, years	50 [17]	58 [14]	55 [18]	0.051
Overweight & obese	61% (19)	10% (3)	35% (22)	<0.001*
Metabolic syndrome	29% (9)	10% (3)	19% (12)	0.106
• Anthropometrics				
BMI, kg/m^2	25 [6]	23 [4]	24 [5]	<0.001*
WC, cm	96 [21]	81 [15]	89 [18]	<0.001*
SCD, mm	16 [7]	11 [7]	15 [8]	<0.001*
• Liver disease etiology				
Viral (CHB, CHC)	35% (11)	-	-	-
MASLD	45% (14)	-	-	-
ALD	3% (1)	-	-	-
Coexistent CHB & ALD	10% (3)	-	-	-
Coexistent CHB & MASLD	6% (2)	-	-	-
• LSM in the supine position				
LS, kPa	13.1 [7]	4.6 [1]	7.8 [9]	<0.001*
IQR/median, %	24 [13]	26 [13]	25 [12]	0.368
Success rate§, %	100 [0]/100±0	100 [0]/97±6	100 [0]/99±4	0.005*
• LSM in the seated position				
LS, kPa	12.7 [7]	5.1 [2]	7.4 [8]	<0.001*
IQR/median, %	24 [13]	30 [23]	25 [18]	0.208
Success rate§, %	100 [7]/96±9	100 [0]/99±2	100 [0]/98±6	0.072
• LSM in the standing position				
LS, kPa	13.0 [7]	6.2 [2]	7.9 [7]	<0.001*
IQR/median, %	26 [20]	30 [19]	28 [18]	0.559
Success rate§, %	100 [0]/99±3	100 [0]/99±3	100 [0]/99±3	0.687

All data are median [IQR] or % (n), unless otherwise indicated.

ALD = alcoholic liver disease; BMI = body mass index; CHB = chronic hepatitis B; CHC = chronic hepatitis C; LS = liver stiffness; LSM = liver stiffness measurement; MASLD = metabolic dysfunction-associated steatotic liver disease; SCD = skin-liver capsule distance; WC = waist circumference.

[¶] Quantitative variables between groups were compared by Mann-Whitney U test; categorical variables were compared by Fisher's exact test.

[§] Data are presented as median [IQR] / mean ± standard deviation; * $p < 0.05$.

4.4.2 Inter-Posture Difference Comparison

Boxplots of LS vs. fibrosis stage stratified by posture are illustrated in **Figure 4-4**. A two-way mixed ANOVA identified a statistically significant interaction between 'posture' and 'LS group' on LS, $F(2,120) = 21.242$, $p < 0.001$, partial $\eta 2 = 0.26$. This implied that the effect of posture is dependent on the magnitude of LS itself. Therefore, two separate one-way repeated measures ANOVAs were run to examine simple main effects of 'posture' within each LS group. Of 31 controls with baseline LS < 8kPa, significant differences in LS existed among three posture conditions, $F(2,60) = 8.518$, $p < 0.001$, partial $\eta^2 = 0.22$. Post-hoc analyses with Bonferroni correction showed a statistically significant increase in LS from the supine to seated position (5.0 ± 1.0 vs. 5.7 ± 1.4 kPa; $p = 0.036$), and from the supine to standing position (5.0 ± 1.0 vs. 6.2 ± 1.7 kPa; $p = 0.002$), indicating that upright positioning generally causes the stiffening of healthy livers. However, LS did not significantly differ between these two upright positions (5.7 vs. 6.1 kPa, mean difference of 0.5 kPa; $p = 0.305$). Of note, we observed a greater magnitude of increase in LS in the standing position compared to the seated position (percentage change from supine: 24% vs. 14%).

In contrast, an opposite trend was noted in 31 patients with baseline LS >8kPa who were classified as having fibrosis, $F(2,60) = 13.837$, $p < 0.001$, partial $\eta^2 = 0.32$. There was a statistically significant decrease in LS from the supine to seated position (15.9 ± 7.3 vs. 13.8 ± 6.2 kPa; $p < 0.001$), as well as from the supine to standing position (15.9 ± 7.3 kPa vs. 13.9 ± 6.2 kPa; $p = 0.001$), but not between the seated and standing positions (13.8 vs. 13.9 kPa, mean difference of 0.03 kPa; $p = 1.0$). These post-hoc comparison results suggest liver softening in the upright postures among patients with fibrosis. The magnitude of decline in LS in the seated position was comparable to that in the standing position (percentage change from supine: 15% vs.

14%).

To determine the extent to which fibrosis can influence the response pattern of LS to postural changes, 31 patients were further divided into two fibrosis categories based on predefined cutoffs. Subgroup analyses were conducted according to the degree of liver fibrosis (i.e., no fibrosis vs. clinically significant fibrosis vs. cirrhosis). In cirrhotic patients with baseline LS > 13kPa, LS declined markedly as the posture transitioned from the supine to seated position (20.5 ± 7.6 vs. 17.7 ± 6.3 kPa, percentage decrease: 16%; p = 0.005) and to standing position (20.5 ± 7.6 vs. 17.3 ± 6.4 kPa, percentage decrease: 18%; p < 0.001), which coincide with the results in the LS > 8kPa group. Interestingly, LS remained fairly unchanged across all postures in patients with baseline LS of 8–13 kPa, indicative of less fibrosis (supine, 11.0 ± 1.2 kPa; seated, 9.7 ± 2.4 kPa; standing, 10.2 ± 3.4 kPa; p = 0.107).

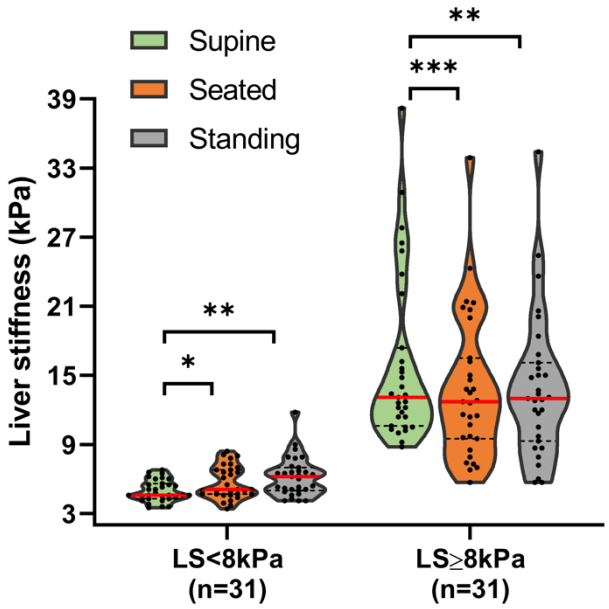

(A)

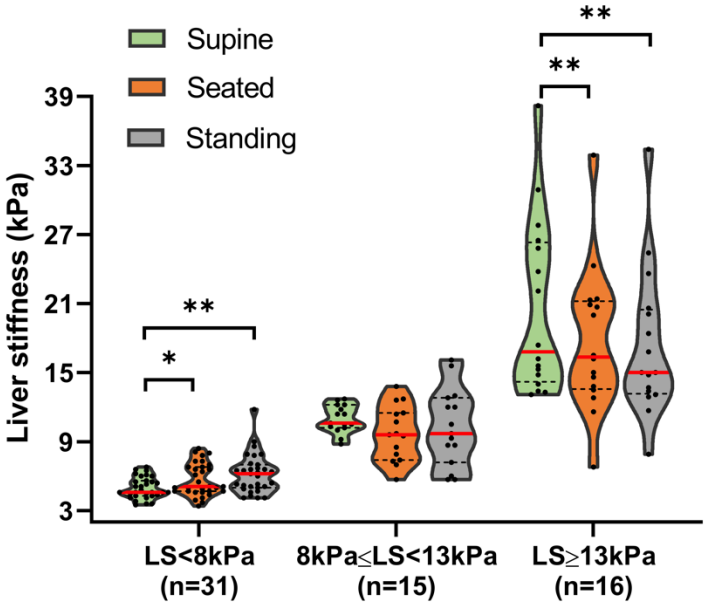

(B)

Figure 4-4. Effect of posture on LS between (A) two LS subgroups; (B) three LS subgroups (*$p \leq 0.05$; **$p \leq 0.01$; ***$p \leq 0.001$; $p > 0.05$ otherwise).

An intraindividual analysis was further conducted within these three subgroups. The results indicate that the posture-induced changes in LS led to discordance of at least one predefined stage between the supine and upright positions. Among the healthy controls, five out of 31 (16%) shifted from no fibrosis (<8kPa) to a higher category. Of 31 patients, four (13%) shifted from cirrhosis (≥13 kPa) to a lower category, while nine (29%) with fibrosis (8–13 kPa) shifted to an adjacent category, i.e., either no fibrosis or cirrhosis.

Figure 4-5 depicts the absolute magnitude of stiffness-change in response to both seated and standing postures among 62 subjects. The Spearman correlation analyses showed a non-significant relationship between the LS measured in the supine posture and the magnitude of stiffness-change for either the seated or standing condition (both $p > 0.05$). No statistically significant association between these two variables implies that the ability of LS to change in response to an upright posture does not vary with

fibrosis severity. Additionally, no statistically significant linear fit was observed between these two variables (both $p > 0.05$).

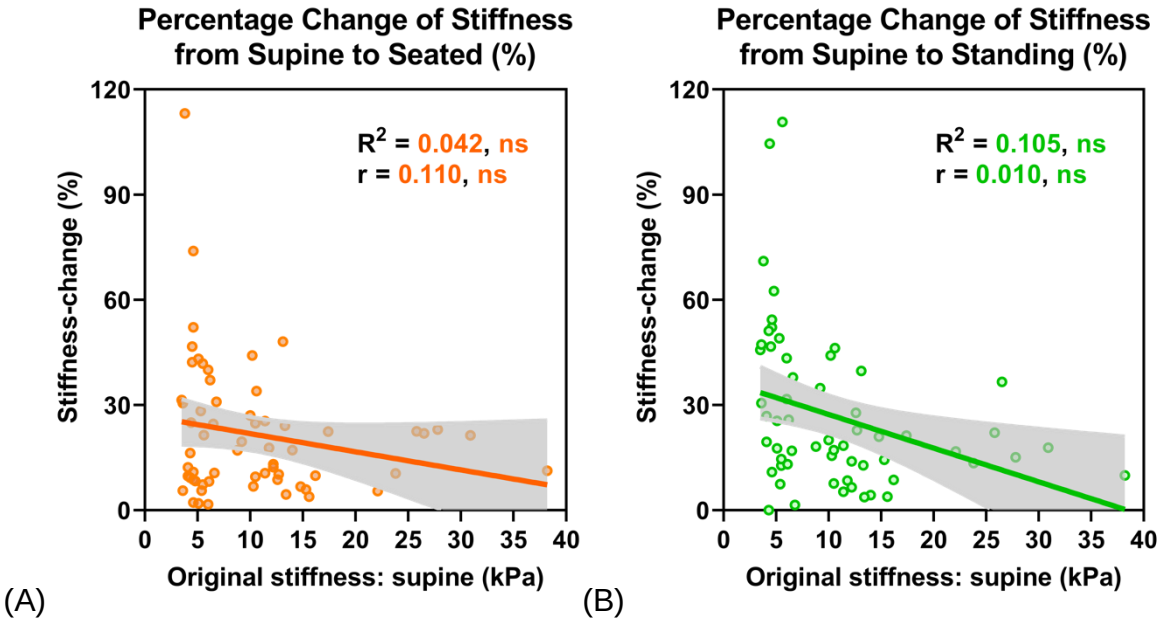

Figure 4-5. Relationship between LS measured in the supine posture (kPa) vs. magnitude of stiffness-change (%) when transitioning from the supine to (A) seated and (B) standing postures.

We also compared the feasibility and reliability of LSM among all posture conditions. **Figure 4-6** depicts the success rate and IQR/median of LSMs by posture. Although the use of the upright position (seated, 29 ± 15%; standing, 29 ± 12%) marginally increased the IQR/median compared to the supine position (25 ± 8%), the differences were not statistically significant, $F(2,111) = 2.233$, $p = 0.117$, partial $\eta^2 = 0.04$. Similarly, the incidence of successful LSMs did not significantly differ between different postures (supine, 98.6%; seated, 97.6%; standing, 99.1%), $\chi^2(2) = 2.710$, $p = 0.258$.

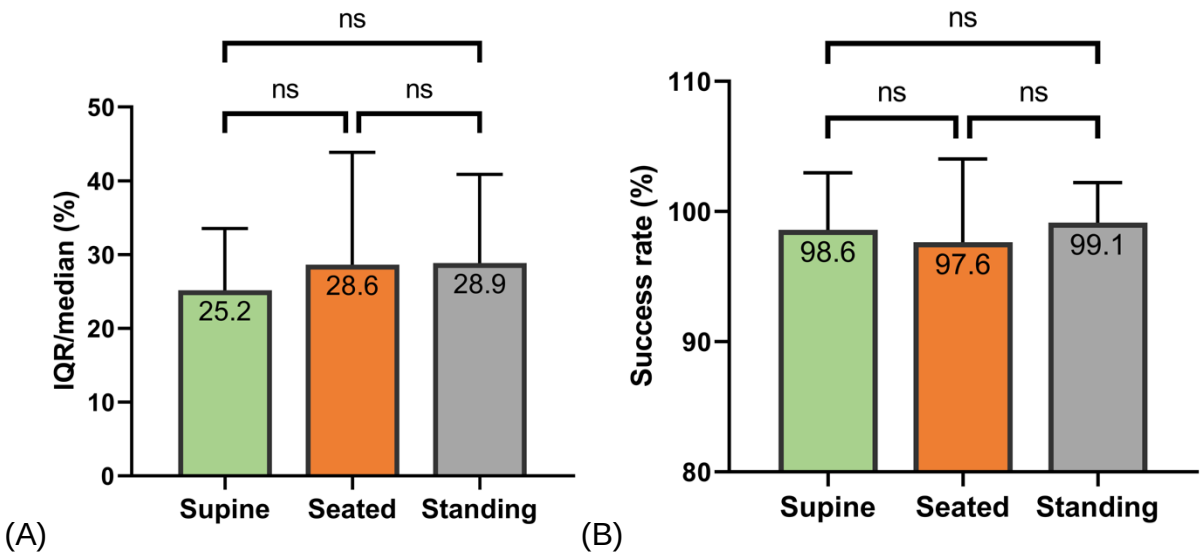

Figure 4-6. Effect of posture on the quality criteria of LSM. (A) IQR/median (%) of 10 LSMs; (B) Success rate (%) of 15 LSM attempts (ns: $p > 0.05$; $p \leq 0.05$ otherwise).

4.4.3 Inter-Rater Agreement

The percentage agreement for the two raters was 99.5%, based on their assessments of whether the 2790 elastograms, obtained from three postures of all 62 study participants, were classified as successful acquisitions. Cohen's kappa (κ) statistic was calculated to quantify the agreement between the novice and experienced raters' judgements, yielding an excellent level of inter-rater agreement (κ = 0.813, 95% CI: 0.717–0.909, $p < 0.005$).

4.4.4 Pairwise comparison of TE Techniques

As shown in **Figure 4-7**, the correlation strength of LS between conventional and B-mode guided TE varied by posture (r_s ranging from 0.79–0.94, all $p < 0.001$). The strongest correlation (r_s = 0.936, 95% CI: 0.894–0.961) and linearity (R^2 = 0.964) were observed in the pair of the supine conditions. On subsequent subgroup analysis, the correlation between techniques was more pronounced among liver disease patients (r_s = 0.867) than controls (r_s = 0.620).

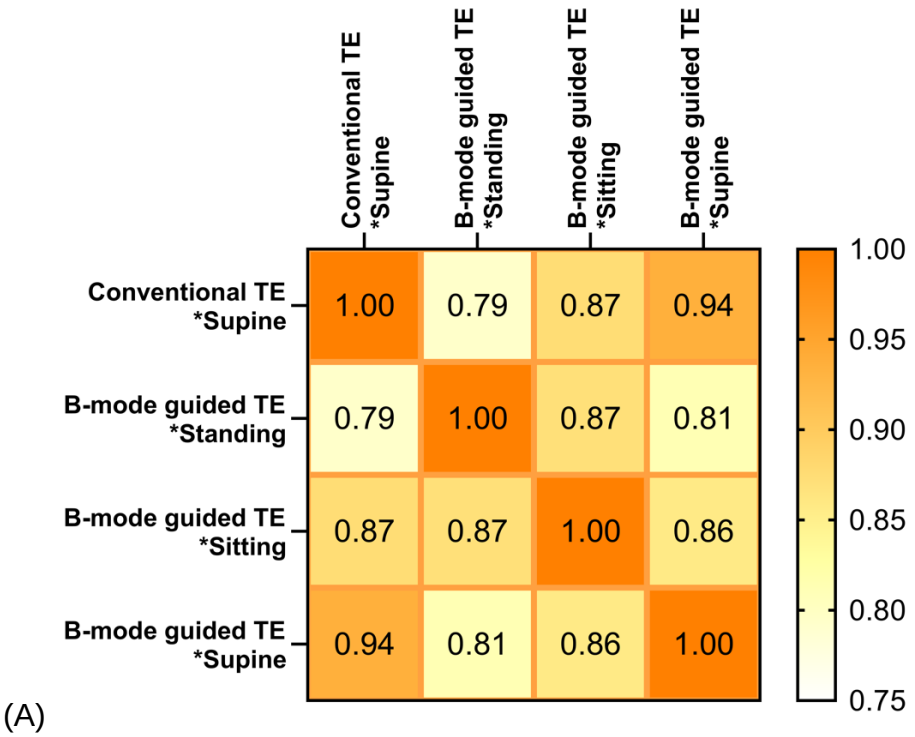

(A)

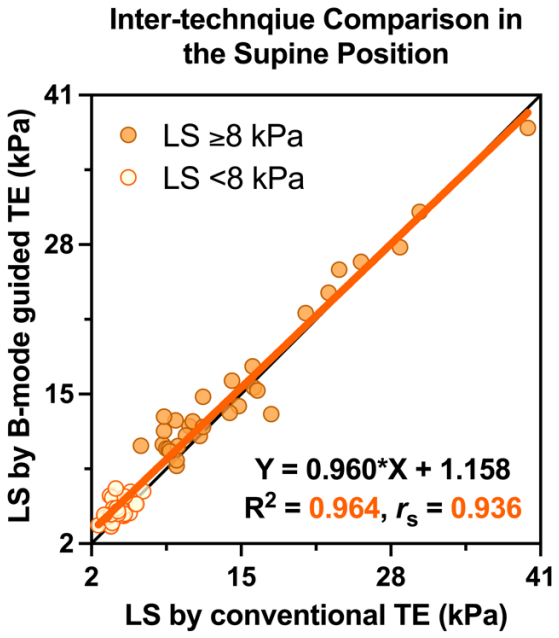

(B)

Figure 4-7. Relationship between LS measured by conventional vs. B-mode guided TE. (A) Spearman correlation matrix depicting LS comparison between TE techniques; (B) Scatterplot with Spearman correlation and simple linear regression analyses (orange and light-yellow circles indicate the patients with liver diseases and the controls, respectively).

4.5 Discussion

LS can be influenced by factors beyond fibrosis stage, with body posture potentially serving as a clinically relevant confounder. This study employed a two-group comparison design to compare the change in LS under different body positions (supine vs. seated vs. standing). Results indicate that the patient group of fibrotic or cirrhotic livers and the control group of healthy livers behaved very differently in response to an upright position. On the other hand, the feasibility and reliability of LSMs were not compromised upon postural changes. Our data have highlighted the fact that posture affected TE, which necessitates the standardization of patient positioning and advances the knowledge defining the physical parameter of LS.

Posture effect on LS. To the authors' knowledge, this is the first work to systematically report the effect of normal daily postures (i.e., supine, seated, standing) on LS in both healthy and diseased livers. Our data clearly demonstrate that, in comparison to the supine position, both seated and standing positions induced liver stiffening, resulting in increased LS among apparently healthy controls (i.e., baseline LS <8 kPa). Conversely, the two upright positions were associated with decreased LS in patients across a spectrum of fibrosis (i.e., baseline LS ≥8 kPa), implying a softening effect on the liver. Subgroup analysis revealed a marked decrease in LS during seating and standing in cirrhotic patients (i.e., baseline LS ≥13 kPa), whereas LS remained stable in patients with clinically significant fibrosis (i.e., baseline LS of 8–13 kPa). Current literature on how LS would respond to a postural change is scarce. We only found three other previous studies investigating the relationship between posture and LS [99, 189, 190]. Adolf et al. first reported the potential confounding effect of posture in a congress abstract, noting a significant increase in LS in healthy individuals when

seated or standing [99]. However, this study lacked ample statistical reporting, making the finding inconclusive. Another study based on point shear wave elastography (pSWE) further confirmed significantly higher LS in the standing position than in the supine position [190]. These prior results are consistent with our observations in the healthy livers. Nevertheless, little is known about the biomechanical response of fibrotic livers to postural changes. In a recent study, Suda et al. shed light on the differential effect of the supine vs. left lateral decubitus positions on LS [189]. Surprisingly, LS was found to be decreased by the left decubitus positioning in 17 cases with confirmed liver fibrosis. Although Suda's work used a different elastography technique, namely two-dimensional shear wave elastography (2D-SWE), and involved a side-lying position, the observed liver softening aligns with our finding regarding the response to an upright position.

Possible mechanism behind. The underlying mechanism explaining the posture dependency on LS are rather complex, and remains a matter for speculation. The prevailing theory to explain relevant confounding conditions is the sinusoidal pressure hypothesis (SPH) [98], in which the pressure of hepatic sinus, reflecting LS, is affected by various pressure compartments. In this context, we initially hypothesized that physical interaction between the lung and liver would contribute to LS as a consequence of external pressure. Computational modeling indicated the morphological changes of the liver from the supine to seated position, notably a cranio-caudal translation of 21.9 mm due to the gravity [191]. This shift resulted in less constraint applied on the liver during respiratory movement, thereby generally decreasing LS in the upright position. The impact of the lung–liver interaction was likely more pronounced in our cohort, as we performed end-inspiratory LSMs. Another influencing factor is hemodynamic changes in the liver, which provide internal pressure.

An upright posture has been shown, across CT, MRI and ultrasound studies, to differentially impact the hepatic hemodynamics depending on the presence of fibrosis [184, 186, 189]. In the healthy individuals, the IVC metrics such as the diameter [183], cross-sectional area [182] and flow velocity [182] decreased significantly from the supine to upright positions, leading to an outflow blockage with higher hydrostatic pressure [189, 190]. This possibly caused intrahepatic blood stasis, and stretched the distensible Glisson' capsule, which in turn increased LS. Conversely, the cirrhotic liver and IVC might be less deformed by an upright posture change [189, 191], which contributes to maintain stable venous drainage and resist dramatic changes in LS. Other factors like the uneven impact of gravity, intra-abdominal pressure differences, and delayed hemodynamic responses in cirrhosis might also play a role [99, 100, 189]. Additionally, the tendency toward no difference between LS measured in the seated and standing postures is likely attributable to their similar hemodynamic characteristics. In summary, external respiratory pressure may synergistically act with internal hepatic hemodynamics to produce the diverse responses of LS observed in our study.

Posture effect on measurement success and reliability criterion. Prior to our work, whether postural changes would influence the feasibility and reliability of LSM is yet a question in the fileld. Our data suggest that adopting upright postures did not compromise the success rate and IQR/median, compared with the supine posture. The incidences of LSM failure remained below 2.5% across all three postures, which align with the 3.1% failure rate previously reported for the supine LSM in the largest feasibility study of TE [75]. This evidence further supports either seated or standing postures as the backup measurement protocol, especially in cases of repeated LSM failure in the supine posture. On the other hand, we observed relatively large variability between LSMs, as demonstrated by IQR/median (supine, 25 ± 8%; seated, 29 ± 15%;

standing, 29 ± 12%). The inclusion of overweight individuals (35%) in our cohort, known as the main determinant of unreliable LSM [186], along with the use of a device with a small ultrasound beam width in this study [187], may account for this phenomenon.

Practical values of upright positioning. Our study also demonstrated the feasibility of utilizing upright positioning for TE in liver fibrosis assessment. From a practical perspective, this new attempt offers greater operational flexibility and has several advantages. Traditionally, TE is performed in the supine posture. However, not all acutely or critically ill patients can lie comfortably in this posture which also requires a bulky examination table. In this case, upright TE is of particular value for patients who cannot tolerate supine positioning, such as those with orthopnea, ankylosing spondylitis or other mobility constraints. Additionally, the literature widely recognized obesity as a predominant risk factor for the TE measurement failure, due to the obstruction of ultrasound and shear wave propagation by excessive subcutaneous tissues [75]. Our clinical observation indicated that upright TE may also facilitate assessing those morbidly obese individuals. This is likely because the standing position tends to reduce overlying abdominal wall thickness due to gravitational forces, thereby minimizing subcutaneous fat interference and improving intercostal access. Future studies are necessary to specifically compare the success rate of supine vs. upright TE in obese populations. We further propose that due to its ease of implementation, the non-lying position could facilitate TE in special settings such as outpatient consultations, home visits, mass screenings, particularly when a supine setup is not readily available.

Clinical relevance and implications. In the present study, we observed the

divergent biomechanical responses to postural changes, which have implications for clinical decision-making. In our view, the strategy of assessing LS in different body positions has the potential to aid in the differential diagnosis of abnormally elevated LS. Specifically, liver softening during seating or standing could serve as an indicator to confirm the presence of fibrotic accumulation, while liver stiffening possibly suggests no fibrosis. Future research should consider incorporating this novel indicator into a TE-based algorithm to enhance the identification of patients at risk of liver fibrosis. Larger studies are warranted to further validate its diagnostic performance and compare it with the accuracy of TE alone. Additionally, our findings may add insight to why LS has been shown to be higher with older age [192]. Evidence suggests that the average American spends the two-thirds of the day in either the seated or standing postures [193]. In this context, longstanding LS elevation resulting from prolonged periods of upright postures over a lifetime and subsequent activation of fibrogenesis pathways [97, 98] are postulated to play a role, although more data are required.

TE has gained increasing clinical attention and is now incorporated into HBV treatment guidelines [174]. Therefore, LS results need to be interpreted cautiously in the context, as it presents significant consequences for patient management. According to our intraindividual analysis, discordance of at least one fibrosis stage was observed in 18 subjects (29%) following a postural change. These resultant false positive or negative cases would become a source of misclassification. Moreover, to prevent unnecessary treatment prescriptions, clinical practitioners must be aware of the posture factor potentially interfering with LS independent of the actual stage. Current clinical guidelines establish LSM cutoff criteria based solely on a supine setup [56, 154, 175, 176]. Our study also emphasizes the need for standardizing patient positioning to ensure accurate TE assessment.

Strengths and limitations. The strengths of this study include the use of several strategies to control for extraneous variables. For example, this study involved a repeated measures design effectively controlling interindividual differences, and patients were carefully evaluated to exclude other known confounding factors influencing LS before inclusion in the experiment. We further acknowledge the crucial role of real-time B-mode guidance in locating the liver and select a consistent intra-hepatic measurement location across postures, which significantly contributed to eliminating liver heterogeneity as a source of bias. Otherwise, abdominal organ relocation following a posture change will pose a challenge for conventional TE without sufficient visual guidance [189, 191]. Second, efforts were made to maximize the validity of LS. They included the inter-technique comparison and elastogram quality assessment, as supported by the results of strong correlation between conventional vs. B-mode guided TE and excellent inter-rater agreement, respectively. Third, we sought to determine whether LSM would remain feasible and reliable in an upright position. Our data is a first-of-its-kind literature source for TE, and can inform the future uptake of this new positioning technique in clinical practice.

However, this study also has the following limitations. As a pilot proof-of-principle study, we included a relatively small cohort of 62 subjects. Although a *priori* calculation justified the adequacy of this sample size for the two-way mixed ANOVA, larger samples are preferable for additional subgroup analysis to increase greater statistical power. Furthermore, patients and control subjects were not well-matched according to BMI, which may complicate between-group comparisons. No participant was subjected to liver biopsy, which is the reference standard for staging fibrosis. While being justified by ethical considerations, the fact merits further research attention to assess the relative accuracy of LS obtained from different postures against histology

and to determine which posture best represents the actual fibrosis state. Another potential criticism is the lack of confirmatory hemodynamic data such as mean arterial pressure (MAP) or central venous pressure (CVP), which would allow for a better description of the direct causality between posture and LS. However, invasive hemodynamic monitoring is unethical for such research purposes in human subjects. In a future study, an animal model should be considered to reproduce the results and further verify the hypothesized mechanism behind posture-dependent changes in LS. Non-invasive tools for assessing MAP and CVP, such as Doppler ultrasound and cuff oscillometry, can greatly support such investigations. Additionally, we did not demonstrate the reversibility of LS between two posture sessions. It also remains unknown how long it takes for a change in LS to occur when transitioning from one posture to another. This data could inform the minimum duration of a rest period in the supine position required for measuring a stabilized LS. Such standardization efforts will be beneficial for everyday TE practice.

4.6 Summary

Chapter 4 investigated LS in response to postural changes from the supine to upright positions. This work provides the definitive evidence that performing TE in the non-lying positions is feasible, at least with a B-mode image guided TE device. LS depends directly upon body posture, and its response to the upright position varies according to fibrosis stage. Although not completely understood, the observed dependency of LS on posture is explained by the hypothesized mechanism combining external and internal pressure sources. Our findings further unravel a previously unrecognized role of transitioning between different postures in the confirmatory diagnosis of liver cirrhosis. Additionally, postural changes show no significant effect on both the success rate and reliability of LSMs when using a B-mode guided TE device. This has implications for clinical use of either seated or standing position as an alternative posture, especially in cases where obtaining LSMs proves challenging in the traditional supine position. However, caution should be exercised when interpreting LS obtained under different postures.

Chapter 5. Conclusions

5.1 Discussion and Chapter Summary

CLD is a major debilitating illness worldwide. Liver fibrosis is the common pathway for CLDs of various etiologies, culminating in cirrhosis, liver failure and liver cancer. Biopsy is the gold standard for diagnosing liver fibrosis. However, due to its invasiveness, sampling error and inter-pathologist variability, there has been a marked shift towards the development of non-invasive methods in the hepatology community. Among these, TE, recommended by the WHO, has become an established method for liver fibrosis characterization via LSM. Although considered the non-invasive standard of care and first-line diagnostic tool to assess liver fibrosis, TE has some pitfalls. From a technical perspective, one commonly reported limitation is the lack of a sufficient visual imaging guiding technique for sampling the liver of interest during TE. Additionally, conventional TE has limited clinical acceptance due to their bulky, immobile, and wired natures. Equipment size constraint has been a practical limitation in the widespread clinical adoption of this technique and the scale-up of liver screening programs. Another practical challenge is the lack of standardization [120], mainly due to the (1) rapid evolution of elastography techniques since TE; (2) inadequate validation and comparisons of technical performance with established techniques; and (3) complexity of liver stiffness itself as a physical parameter. A recent technical review article [39] indicated that a standardized examination procedure of liver elastography is a prerequisite for obtaining reliable and accurate results. In light of these obstacles, this thesis comprises a series of studies designed to bridge these gaps that impede the advancement of TE in hepatology. Considering the broader implications, the study vision focuses on enhancing the effectiveness of TE in terms of success rate,

examination and training efficiency, by resolving the existing barriers in both technical and implementation perspectives with an ultimate goal of benefiting countless liver disease sufferers through delivering an effective TE examination worldwide in the long run. Specifically, it introduces two distinct strategies, aimed at (a) mitigating the high rates of TE failure and unreliable results, and (b) streamlining the implementation of TE. As detailed in **Chapter 2**, the technical solution is the incorporation of POCUS and anatomic imaging guidance into the TE examination procedure. On the other hand, as presented in **Chapters 3 and 4**, the practical clinical solution is the establishment of TE examination standards.

Conventional TE requires wired connections, possesses a bulky size, and lacks adequate imaging guidance for precise liver localization. These technical barriers have precluded its efficient examination and point-of-care application. **In Chapter 2**, a methodological study was conducted to address these technical barriers that remain towards the cost-effective solution and point-of-care application of TE. In this connection, a newly developed TE system was introduced, which is palm-sized in dimension and incorporates real-time B-mode imaging guidance of liver anatomy. We report the design, phantom validation, and clinical evaluation of this system to perform simultaneous B-mode imaging and LSM. Specifically, the performance of this system was validated experimentally using tissue-equivalent reference phantoms (ground-truth: 1.45–75 kPa). Comparative studies against other liver elastography techniques, including conventional TE and 2D-SWE, were performed to evaluate its reliability and validity in adults with various chronic liver diseases. Besides, intra- and inter-operator reliability of LSM were established by an elastography expert and a novice. Additional research investigating the effect of vibration amplitude on TE was included. Results showed a good agreement between the Young's modulus reported by the phantom

manufacturer and this system (bias: 1.1–8.6%). Among 121 patients, liver stiffness measured by this system and conventional TE were highly correlated (r = 0.975) and strongly agreed with each other (mean difference: −0.77 kPa). Inter-correlation of this system with conventional TE and 2D-SWE was observed. Excellent-to-good operator reliability was demonstrated in 60 patients (ICCs: 0.824–0.913). Liver stiffness did not significantly differ between the 1-mm and 3-mm vibration amplitudes (p = 0.121). In conclusion, we demonstrated the feasibility of employing a fully integrated phased array probe for reliable and valid LSM, under the anatomic B-mode guidance. This system represents the first technical advancement toward point-of-care liver fibrosis assessment. Its small footprint, along with B-mode guidance capability, can improve examination efficiency and scale up screening for liver fibrosis.

Liver TE is typically performed via an intercostal approach. Although unreliable and failed results caused by ICS-associated factors, such as excessive subcutaneous fat, and a narrow ICS relative to the transducer size, and operator inexperience, are not uncommon, no guideline for ideal probe placement is currently available. In this connection, investigating the anatomical characteristics of the ICS is of great help to establish such a standard practice guideline. In **Chapter 3**, an observational study was conducted to identify an ideal measurement site and respiratory condition for single-element-specific TE by the morphological and biomechanical characterization of the ICSs, using 2D B-mode and elasticity imaging. An additional study was designed to determine an ideal measurement site for array-specific TE using 3D ultrasound imaging to characterize intercostal course. Intercostal ultrasound was performed pointwise at four specific sites in 59 patients to assess the width, stiffness, and SCD of the ICSs, both under end-inspiratory and end-expiratory conditions. In another cohort of 30 patients, 3D ultrasound measurements were taken of the width-change

and angle of the ICSs. Intersections between the 8th ICS and anterior axillary line, the 7th ICS and anterior axillary line, the 8th ICS and mid-axillary line, the 7th ICS and mid-axillary line, were defined as Sites 1 to 4, respectively. Results showed that the less angular and less irregular ICSs lie at Sites 3 and 4 and Sites 2 and 3, respectively. Greater intercostal width was found at Sites 2 and 3, and associated with male, SCD and BMI. Intercostal stiffness was lower at Sites 3 and 4, with height as the only determinant. Sites 2 and 3 exhibited a shorter SCD, indicating a thinner abdominal wall. The ICSs were significantly wider and stiffer at end-inspiration, in comparison with end-expiration. Additionally, the liver was more easily visualized at Sites 1 and 3. In conclusion, we recommend Site 3 for TE probe placement owing to its greater width, lower width-change, greater angle, lower stiffness, and smaller abdominal wall thickness. Performing TE at end-inspiration is preferred to minimize transducer-rib interferences. This study paves the way towards a standardized TE examination procedure. Protocol standardization for TE can aid in reducing invalid results, improving examination efficiency, and facilitating its use by non-specialists. This is also the first study to demonstrate the feasibility of utilizing 3D ultrasound imaging to study the ICSs, specifically to characterize their anatomical course. Our findings are applicable not only to conventional TE with a single-element transducer but also to TE based on array transducers.

Liver TE is typically performed with patients in the supine position. However, fibrosis degree is not the sole determinant of liver stiffness, necessitating the identification of relevant confounders. It remains unclear whether normal daily postures interfere with liver stiffness irrespective of fibrosis. In **Chapter 4**, a prospective two-group comparison study was conducted to investigate the relationship between posture and LSM. Sixty-two adults with liver stiffness ranging from 3.5 to 38.2

kPa participated and were assigned into two groups: patients with chronic liver disease and healthy controls. Both groups were assessed using TE under the supine, seated, and standing postures. A two-way mixed ANOVA was applied to assess the posture-dependence of LS and its variations between two groups. Results showed that posture differentially affected LS depending on the presence of liver fibrosis. In 31 healthy individuals, a transition from the supine to seated (p = 0.036) or standing (p = 0.002) positions increased LS, indicating liver stiffening. Conversely, in 31 patients with varying fibrosis stages, posture decreased LS from the supine to seated (p < 0.001) or standing (p = 0.001) positions. No significant difference in LS was observed between the seated and standing positions in both groups. Additionally, different postures did not elicit significant changes in the success rate (p = 0.117) and IQR/median value (p = 0.258), implying no impact on both measurement feasibility and reliability. In conclusion, we demonstrated the feasibility of utilizing upright postures as an alternative measurement protocol for TE. Daily physiological activity of postural changes suffices to alter LS. The observed postural dependency of liver stiffness emphasizes the need for standardizing body positioning for TE.

In summary, this thesis endeavours to achieve the technical improvement and procedural standardization of TE, which can provide new insights into addressing challenging cases and scaling up liver fibrosis assessment. Specifically, the key findings presented may advance TE technique in the long run, ultimately eliminating the failure and unreliable results, alleviating the training burden of TE practitioners, and streamlining the examination procedure in clinics. **Figure 5-1** schematically summarizes the background, key findings, and significance of the thesis work as a whole.

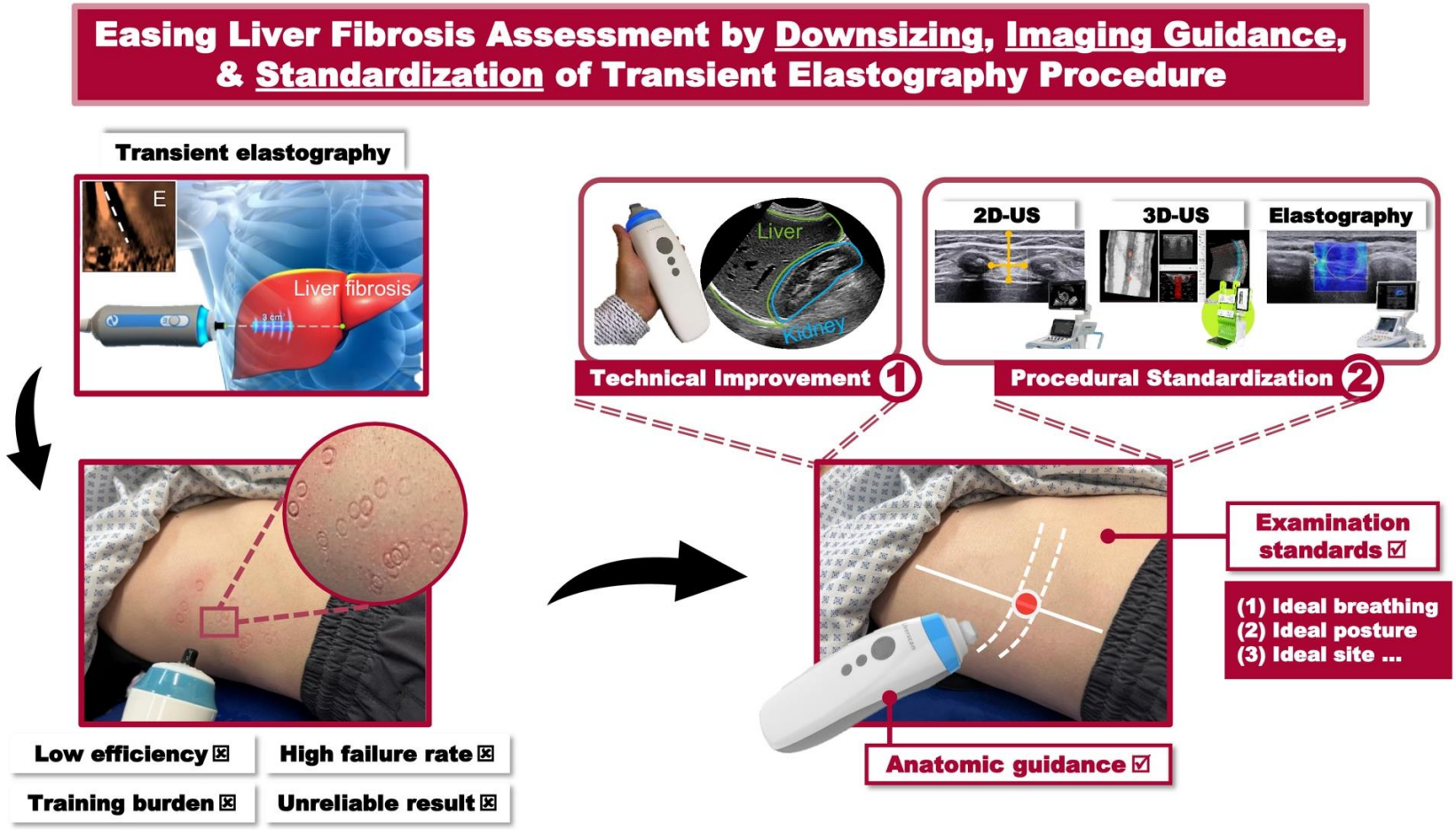

Figure 5-1. Graphical abstract of the thesis summarizing the research territory, clinical problems, methodologies, and main findings.

5.2 Novelty of the Studies

The thesis has made the following contributions to the field of ultrasound elastography assessment for liver fibrosis:

I. **Chapter 2** is the first to report on the engineering prototyping of TE in a fully integrated, wireless probe setting.

II. **Chapter 2** demonstrates the use of phased array transducers to allow for B-mode guided TE in real-time.

III. **Chapter 2** is the first to demonstrate the feasibility of real-time sector B-mode imaging as procedural guidance for TE.

IV. **Chapter 2** utilizes a head-to-head comparison design, supporting the feasibility, reliability, and validity of this newly introduced array-based TE as a liver elastography technique.

V. **Chapter 2** is the first to report the incorporation of POCUS into TE, representing a pioneering technical advancement toward point-of-care fibrosis assessment.

VI. **Chapters 3 and 4** fill a gap in the literature by providing evidence-based guidelines for a streamlined, standard practice of liver TE, including a specified measurement site, respiratory condition, and body positioning. A standardized measurement protocol was first established to improve the success and efficiency of the examination procedure.

VII. **Chapter 3** is the first work to investigate the relevance of intercostal anatomy in the context of liver elastography and to employ intercostal elastography of the ICS overlying the liver.

VIII. **Chapter 3** pioneers the use of 3D ultrasound for imaging the rib cage and associated ICS.

IX. **Chapter 4**, for the first time, compares the effects of supine versus upright (i.e., seated or standing) postures on liver stiffness as well as on the feasibility and reliability of TE.

X. **Chapter 4** unravels a previously unrecognized role of transitioning between different postures in confirming diagnoses of liver fibrosis versus its absence.

XI. **Chapter 4** highlights the potential of adopting readily available non-supine postures as alternatives for TE. Yet, liver stiffness results must be interpreted cautiously, as they are influenced by specific postural conditions.

5.3 Suggestions for Future Research

The limitations and proposed future directions of the three main studies are specified in each of the corresponding sections of **Chapter 2.5**, **Chapter 3.5** and **Chapter 4.5**. Building upon this thesis, future efforts will consolidate an evidence-based measurement protocol for TE to enhance diagnosis accuracy, measurement quality, and procedural efficiency. Herein, recommendations for additional research directions are summarized as follows.

5.3.1 Development of Multi-Dimensional TE for Liver Fibrosis Heterogeneity Assessment

Despite that hepatic fibrogenesis is often considered a diffuse state, spatial distribution can be inhomogeneous. Heterogeneity in liver fibrosis has long been a matter of speculation. In one MRE study [194], the heterogeneous stiffness distribution was analysed via 3D reconstruction of elastograms. The findings further revealed a discordance between and MRE-based and histological fibrosis staging. This clinical appearance can bias a diagnostic result, while relevant research is scarce. Currently, the method available for assessing this hypothesized condition is lacking. The gold standard of liver biopsy is invasive, making it unethical and unsuitable for sampling a liver specimen from different sites. While 2D-SWE provides a 2D stiffness map of the liver, it potentially contains misleading information due to the reverberation artifact. Lefebvre et al. [143] pointed out the underlying spatial heterogeneity of fibrosis possibly contributing to lesser diagnostic performance and higher unreliable rates. The 1D-TE lacks the capability to map the Young's modulus and it only reports a single value corresponding to the Young's modulus of a 40-mm liver tissue length. To further validate the assumption that liver fibrosis is not necessarily uniform, a system capable

of characterizing fibrotic tissue distribution over a larger liver region is required.

Future works should focus on developing a multi-dimensional TE for ultrasound assessment of heterogenous stiffening. The extension from existing 1D-TE to 2D-TE will be a direction for future research **(Figure 5-2)**. Owing to the 32-element array configuration that introduced in **Chapter 2**, simultaneous RF acquisition from multiple scan lines opens the possibility for LSM at multiple locations. By using two arrays of transducers arranged orthogonally, the exact location of intra-hepatic tissue under LSM can be precisely recorded on anatomic B-mode images. This facilitates the visualization of the spatial distribution of the Young's modulus throughout the liver that can better reflect the fibrosis state. In this regard, potential under-staging or over-staging of fibrosis severity can be alleviated. Such a modification signifies a TE advancement, because it transforms the single-value nature into a multi-dimensional measurement to improve examination efficiency and reduce sampling error. 3D-TE will be possible by steering the ultrasound beam towards different locations to conduct TE measurements, while the liver keeps moving with periodic breathing **(Figure 5-2)**.

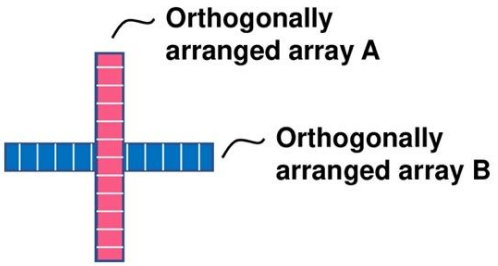

(A)

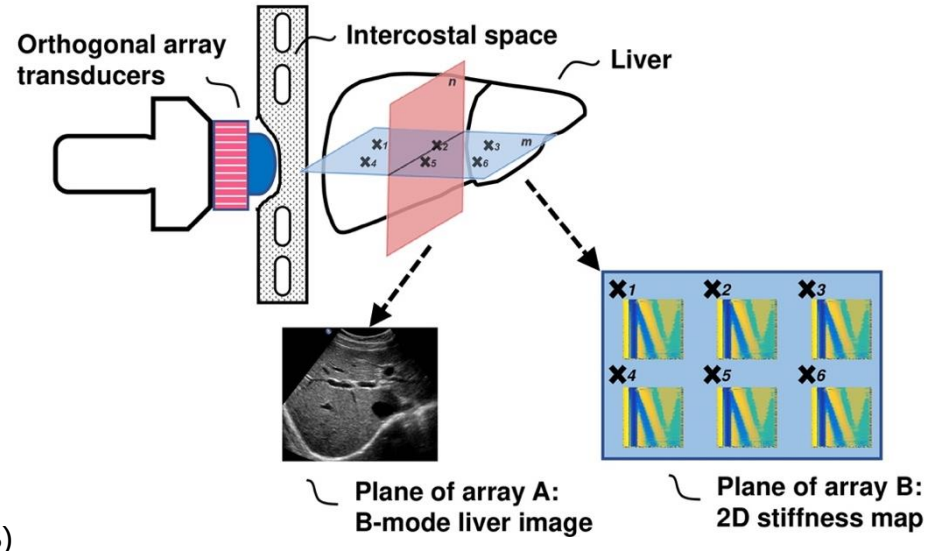

(B)

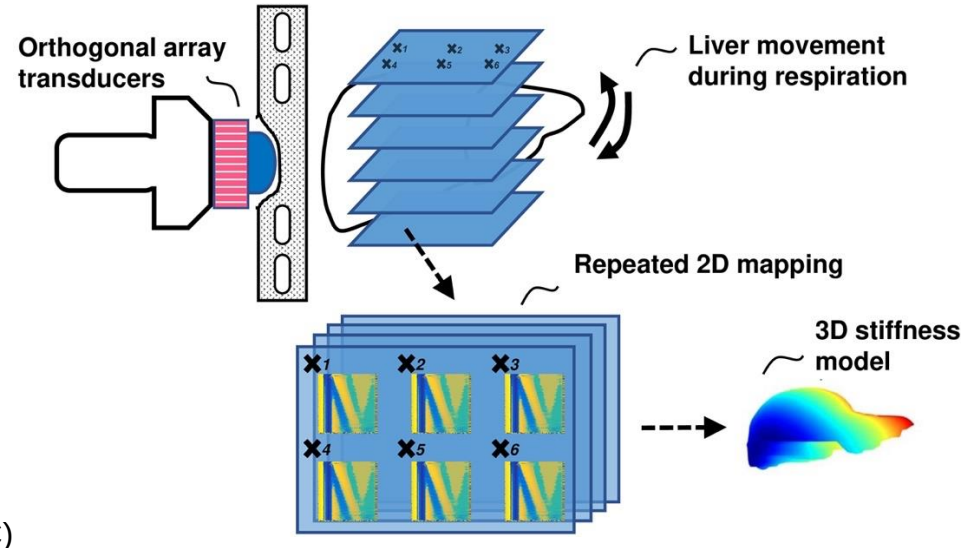

(C)

Figure 5-2. Schematic illustrations of future research on multi-dimensional TE development. (A) Orthogonal configuration design of multi-element array; (B) 2D-TE; (C) 3D-TE.

In a future performance analysis, this system will be validated against phantoms with multi-layered elasticity or with individual inclusions of varying elasticity values. A large-scale clinical trial will be also necessary to evaluate its reliability and validity. Furthermore, a measurement protocol needs to be newly established. By employing

this system, clinical practitioners may visualize the distribution patterns of liver fibrosis over a larger parenchymal region, which facilitate an accurate staging. Additionally, researchers may gain new insights into the onset mechanism of how fibrotic tissues affect the liver.

5.3.2 Stiffness Difference Between the Left and Right Lobe

Traditionally, TE is performed via the right intercostal approach to assess a specific portion of the right liver lobe only. However, studies using ARFI measurements in the left liver lobe elicited significantly higher stiffness values and showed more variability than those in the right lobe [53, 195, 196]. Measuring the stiffness of the smaller-sized left lobe is challenging with conventional TE, probably due to the lack of anatomical imaging guidance and interference from the nearby palpating heart. It remains unknown whether liver stiffness differs between the two lobes of the liver. Moreover, the feasibility of performing TE in the left lobe is yet to be proven. A potential difference in stiffness between two lobes likely causes the mis-diagnosed cases of liver fibrosis. Future research will be conducted to assess the inter-lobe difference, using the B-mode guided TE. This information will contribute to the establishment of a standardized TE examination procedure for selecting the intra-hepatic measurement location.

5.3.3 Effect of the Number of Measurements on TE Accuracy

Traditionally, TE is performed ten times to arrive at a median value representing the Young's modulus of the liver. This practice is essential for several reasons. Firstly, the liver stiffness may vary across different intra-hepatic locations due to the heterogeneity of hepatic fibrosis. Thus, multiple LSMs ensure that the final median result accurately reflects the liver as a whole. Secondly, conventional TE lacked real-

time image guidance during LSM, potentially increasing the likelihood of unreliable elastogram acquisitions. The use of the median calculation mitigates the impact of these measurement errors. While theoretically, increasing the number of repeated measurements could enhance the accuracy of the final result, it will reduce examination efficiency. Although this practice is well-established, little research has compared the diagnostic accuracy of taking fewer than ten measurements. Future developments of 2D- or 3D-TE have the potential to simultaneously perform multiple LSMs to map the distribution of liver stiffness. While streamlining the examination procedure of TE, this grouped measurement strategy warrants further investigation.

Future research should determine if a minimum of three to five individual or grouped measurements suffices to accurately assess liver fibrosis and compare the corresponding reliability criteria. The diagnostic performance of various measurement combinations and strategies will be evaluated by calculating the AUROC, using liver biopsy as the reference standard. These findings will refine the existing examination standard, which currently requires ten exact acquisitions, and develop a cost-effective measurement protocol to streamline the procedure of TE.

References

[1] A. M. Moon, A. G. Singal, and E. B. Tapper, "Contemporary Epidemiology of Chronic Liver Disease and Cirrhosis," (in eng), *Clin Gastroenterol Hepatol,* vol. 18, no. 12, pp. 2650-2666, Nov 2020, doi: 10.1016/j.cgh.2019.07.060.

[2] G. B. D. Disease, I. Injury, and C. Prevalence, "Global, regional, and national incidence, prevalence, and years lived with disability for 354 diseases and injuries for 195 countries and territories, 1990-2017: a systematic analysis for the Global Burden of Disease Study 2017," *LANCET,* vol. 392, no. 10159, pp. 1789-1858, 2018, doi: 10.1016/S0140-6736(18)32279-7.

[3] A. Pellicoro, P. Ramachandran, J. P. Iredale, and J. A. Fallowfield, "Liver fibrosis and repair: Immune regulation of wound healing in a solid organ," *Nature reviews. Immunology,* vol. 14, no. 3, pp. 181-194, 2014, doi: 10.1038/nri3623.

[4] P. Udompap, D. Kim, and W. R. Kim, "Current and Future Burden of Chronic Nonmalignant Liver Disease," (in eng), *Clin Gastroenterol Hepatol,* vol. 13, no. 12, pp. 2031-41, Nov 2015, doi: 10.1016/j.cgh.2015.08.015.

[5] S. K. Asrani, H. Devarbhavi, J. Eaton, and P. S. Kamath, "Burden of liver diseases in the world," *Journal of hepatology,* vol. 70, no. 1, pp. 151-171, 2019, doi: 10.1016/j.jhep.2018.09.014.

[6] B. C. Cowie and J. H. MacLachlan, "The global burden of liver disease attributable to hepatitis B, hepatitis C, and alcohol: increasing mortality, differing causes: 23," *Hepatology,* vol. 58, pp. 218A-219A, 2013.

[7] G. Garcia-Tsao, S. Friedman, J. Iredale, and M. Pinzani, "Now there are many (stages) where before there was one: In search of a pathophysiological

classification of cirrhosis," *Hepatology (Baltimore, Md.),* vol. 51, no. 4, pp. 1445-1449, 2010, doi: 10.1002/hep.23478.

[8] J. Choi, S. Han, N. Kim, and Y. S. Lim, "Increasing burden of liver cancer despite extensive use of antiviral agents in a hepatitis B virus-endemic population," *Hepatology (Baltimore, Md.),* vol. 66, no. 5, pp. 1454-1463, 2017, doi: 10.1002/hep.29321.

[9] P. Ginès *et al.*, "Screening for liver fibrosis in the general population: a call for action," (in eng), *Lancet Gastroenterol Hepatol,* vol. 1, no. 3, pp. 256-260, Nov 2016, doi: 10.1016/s2468-1253(16)30081-4.

[10] S. Liangpunsakul, P. Haber, and G. W. McCaughan, "Alcoholic Liver Disease in Asia, Europe, and North America," (in eng), *Gastroenterology,* vol. 150, no. 8, pp. 1786-97, Jun 2016, doi: 10.1053/j.gastro.2016.02.043.

[11] R. Bataller and D. A. Brenner, "Liver fibrosis," *The Journal of clinical investigation,* vol. 115, no. 2, pp. 209-218, 2005.

[12] P. P. Anthony, K. G. Ishak, N. C. Nayak, H. E. Poulsen, P. J. Scheuer, and L. H. Sobin, "The morphology of cirrhosis: definition, nomenclature, and classification," (in eng), *Bull World Health Organ,* vol. 55, no. 4, pp. 521-40, 1977.

[13] M. Berenguer *et al.*, "Severe recurrent hepatitis C after liver retransplantation for hepatitis C virus–related graft cirrhosis," *Liver transplantation,* vol. 9, no. 3, pp. 228-235, 2003, doi: 10.1053/jlts.2003.50029.

[14] R. Issa *et al.*, "Spontaneous recovery from micronodular cirrhosis: evidence for incomplete resolution associated with matrix cross-linking," (in eng), *Gastroenterology,* vol. 126, no. 7, pp. 1795-808, Jun 2004, doi: 10.1053/j.gastro.2004.03.009.

[15] M. J. Arthur, "Reversibility of liver fibrosis and cirrhosis following treatment for hepatitis C," (in eng), *Gastroenterology,* vol. 122, no. 5, pp. 1525-8, May 2002, doi: 10.1053/gast.2002.33367.

[16] T. Kisseleva and D. Brenner, "Molecular and cellular mechanisms of liver fibrosis and its regression," *Nature Reviews Gastroenterology & Hepatology,* vol. 18, no. 3, pp. 151-166, 2021.

[17] A. J. Czaja, "Hepatic inflammation and progressive liver fibrosis in chronic liver disease," (in eng), *World J Gastroenterol,* vol. 20, no. 10, pp. 2515-32, Mar 14 2014, doi: 10.3748/wjg.v20.i10.2515.

[18] D. Roulot *et al.*, "Transient elastography as a screening tool for liver fibrosis and cirrhosis in a community-based population aged over 45 years," *Gut,* vol. 60, no. 7, pp. 977-984, 2011, doi: 10.1136/gut.2010.221382.

[19] E. M. Koehler *et al.*, "Presence of diabetes mellitus and steatosis is associated with liver stiffness in a general population: The Rotterdam study," *Hepatology (Baltimore, Md.),* vol. 63, no. 1, pp. 138-147, 2016, doi: 10.1002/hep.27981.

[20] R. Harris, D. J. Harman, T. R. Card, G. P. Aithal, and I. N. Guha, "Prevalence of clinically significant liver disease within the general population, as defined by non-invasive markers of liver fibrosis: a systematic review," (in eng), *Lancet Gastroenterol Hepatol,* vol. 2, no. 4, pp. 288-297, Apr 2017, doi: 10.1016/s2468-1253(16)30205-9.

[21] P. Ginès *et al.*, "Population screening for liver fibrosis: Toward early diagnosis and intervention for chronic liver diseases," *Hepatology (Baltimore, Md.),* vol. 75, no. 1, pp. 219-228, 2022, doi: 10.1002/hep.32163.

[22] T. Poynard *et al.*, "Prevalence of liver fibrosis and risk factors in a general population using non-invasive biomarkers (FibroTest)," *BMC gastroenterology,* vol. 10, no. 1, pp. 40-40, 2010, doi: 10.1186/1471-230X-10-40.

[23] S. Petta *et al.*, "Prevalence and severity of nonalcoholic fatty liver disease by transient elastography: Genetic and metabolic risk factors in a general population," *Liver international,* vol. 38, no. 11, pp. 2060-2068, 2018, doi: 10.1111/liv.13743.

[24] K. W. M. Abeysekera *et al.*, "Prevalence of steatosis and fibrosis in young adults in the UK: a population-based study," (in eng), *Lancet Gastroenterol Hepatol,* vol. 5, no. 3, pp. 295-305, Mar 2020, doi: 10.1016/s2468-1253(19)30419-4.

[25] S. L. Friedman, "Hepatic Stellate Cells: Protean, Multifunctional, and Enigmatic Cells of the Liver," *Physiological reviews,* vol. 88, no. 1, pp. 125-172, 2008, doi: 10.1152/physrev.00013.2007.

[26] M. Pinzani, "Liver fibrosis: Fibrosis," *Springer seminars in immunopathology,* vol. 21, no. 4, pp. 475-490, 1999, doi: 10.1007/BF00870306.

[27] M. Pinzani and J. Macias-Barragan, "Update on the pathophysiology of liver fibrosis," (in eng), *Expert Rev Gastroenterol Hepatol,* vol. 4, no. 4, pp. 459-72, Aug 2010, doi: 10.1586/egh.10.47.

[28] E. Gäbele, D. A. Brenner, and R. A. Rippe, "Liver fibrosis: signals leading to the amplification of the fibrogenic hepatic stellate cell," *Frontiers in bioscience,* vol. 8, pp. d69-77, 2003, doi: 10.2741/887.

[29] C. Liu, X. Chen, L. Yang, T. Kisseleva, D. A. Brenner, and E. Seki, "Transcriptional Repression of the Transforming Growth Factor β (TGF-β) Pseudoreceptor BMP and Activin Membrane-bound Inhibitor (BAMBI) by Nuclear Factor κB (NF-κB) p50 Enhances TGF-β Signaling in Hepatic Stellate

Cells," *The Journal of biological chemistry,* vol. 289, no. 10, pp. 7082-7091, 2014, doi: 10.1074/jbc.M113.543769.

[30] N. M. W. de Alwis and C. P. Day, "Non-alcoholic fatty liver disease: The mist gradually clears," *Journal of hepatology,* vol. 48, no. 1, pp. S104-S112, 2008, doi: 10.1016/j.jhep.2008.01.009.

[31] B. Schnabl and D. A. Brenner, "Interactions Between the Intestinal Microbiome and Liver Diseases," *Gastroenterology,* vol. 146, no. 6, pp. 1513-1524, 2014.

[32] S. T. Magness, R. Bataller, Y. Liu, and D. A. Brenner, "A dual reporter gene transgenic mouse demonstrates heterogeneity in hepatic fibrogenic cell populations," *Hepatology (Baltimore, Md.),* vol. 40, no. 5, pp. 1151-1159, 2004, doi: 10.1002/hep.20427.

[33] N. Kinnman and C. Housset, "Peribiliary myofibroblasts in biliary type liver fibrosis," *Frontiers in bioscience,* vol. 7, no. 4, pp. d496-503, 2002, doi: 10.2741/a790.

[34] Z. D. Goodman, "Grading and staging systems for inflammation and fibrosis in chronic liver diseases," *Journal of hepatology,* vol. 47, no. 4, pp. 598-607, 2007, doi: 10.1016/j.jhep.2007.07.006.

[35] Z. M. Younossi *et al.*, "Pathologic criteria for nonalcoholic steatohepatitis: Interprotocol agreement and ability to predict liver-related mortality," *Hepatology (Baltimore, Md.),* vol. 53, no. 6, pp. 1874-1882, 2011, doi: 10.1002/hep.24268.

[36] S. Kose, G. Ersan, B. Tatar, P. Adar, and B. E. Sengel, "Evaluation of percutaneous liver biopsy complications in patients with chronic viral hepatitis," *The Eurasian journal of medicine,* vol. 47, no. 3, pp. 161-164, 2015, doi: 10.5152/eurasianjmed.2015.107.

[37] R. P. Myers, A. Fong, and A. A. M. Shaheen, "Utilization rates, complications and costs of percutaneous liver biopsy: a population-based study including 4275 biopsies," *Liver international,* vol. 28, no. 5, pp. 705-712, 2008, doi: 10.1111/j.1478-3231.2008.01691.x.

[38] P. Bedossa, D. Dargère, and V. Paradis, "Sampling variability of liver fibrosis in chronic hepatitis C," *Hepatology (Baltimore, Md.),* vol. 38, no. 6, pp. 1449-1457, 2003, doi: 10.1016/j.hep.2003.09.022.

[39] R. M. S. Sigrist, J. Liau, A. E. Kaffas, M. C. Chammas, and J. K. Willmann, "Ultrasound elastography: Review of techniques and clinical applications," *Theranostics,* vol. 7, no. 5, pp. 1303-1329, 2017, doi: 10.7150/thno.18650.

[40] G. Colloredo, M. Guido, A. Sonzogni, and G. Leandro, "Impact of liver biopsy size on histological evaluation of chronic viral hepatitis: the smaller the sample, the milder the disease," *Journal of hepatology,* vol. 39, no. 2, pp. 239-244, 2003, doi: 10.1016/S0168-8278(03)00191-0.

[41] M. Hagan, S. K. Asrani, and J. Talwalkar, "Non-invasive assessment of liver fibrosis and prognosis," (in eng), *Expert Rev Gastroenterol Hepatol,* vol. 9, no. 10, pp. 1251-60, 2015, doi: 10.1586/17474124.2015.1075391.

[42] A. G. Shah, A. Lydecker, K. Murray, B. N. Tetri, M. J. Contos, and A. J. Sanyal, "Comparison of noninvasive markers of fibrosis in patients with nonalcoholic fatty liver disease," (in eng), *Clin Gastroenterol Hepatol,* vol. 7, no. 10, pp. 1104-12, Oct 2009, doi: 10.1016/j.cgh.2009.05.033.

[43] P. Angulo *et al.*, "The NAFLD fibrosis score: A noninvasive system that identifies liver fibrosis in patients with NAFLD," *Hepatology (Baltimore, Md.),* vol. 45, no. 4, pp. 846-854, 2007, doi: 10.1002/hep.21496.

[44] T. Poynard *et al.*, "Applicability and precautions of use of liver injury biomarker FibroTest. A reappraisal at 7 years of age," *BMC gastroenterology,* vol. 11, no. 1, pp. 39-39, 2011, doi: 10.1186/1471-230X-11-39.

[45] P. Calès *et al.*, "Reproducibility of blood tests of liver fibrosis in clinical practice," *Clinical biochemistry,* vol. 41, no. 1, pp. 10-18, 2008, doi: 10.1016/j.clinbiochem.2007.08.009.

[46] D. C. Rockey and D. M. Bissell, "Noninvasive measures of liver fibrosis," *Hepatology (Baltimore, Md.),* vol. 43, no. S1, pp. S113-S120, 2006, doi: 10.1002/hep.21046.

[47] T. Gabbani *et al.*, "Metabolomic analysis with 1H-NMR for non-invasive diagnosis of hepatic fibrosis degree in patients with chronic hepatitis C," *Digestive and liver disease,* vol. 49, no. 12, pp. 1338-1344, 2017, doi: 10.1016/j.dld.2017.05.018.

[48] B. Taouli and D.-M. Koh, "Diffusion-weighted MR Imaging of the Liver," *Radiology,* vol. 254, no. 1, pp. 47-66, 2010, doi: 10.1148/radiol.09090021.

[49] R. Catania, A. Furlan, A. D. Smith, J. Behari, M. E. Tublin, and A. A. Borhani, "Diagnostic value of MRI-derived liver surface nodularity score for the non-invasive quantification of hepatic fibrosis in non-alcoholic fatty liver disease," *European radiology,* vol. 31, no. 1, pp. 256-263, 2021, doi: 10.1007/s00330-020-07114-y.

[50] A. A. Elkassem *et al.*, "Multiinstitutional Evaluation of the Liver Surface Nodularity Score on CT for Staging Liver Fibrosis and Predicting Liver-Related Events in Patients With Hepatitis C," *American journal of roentgenology (1976),* vol. 218, no. 5, pp. 833-845, 2022, doi: 10.2214/AJR.21.27062.

[51] T. Heye *et al.*, "MR relaxometry of the liver: significant elevation of T1 relaxation time in patients with liver cirrhosis," *European radiology,* vol. 22, no. 6, pp. 1224-1232, 2012, doi: 10.1007/s00330-012-2378-5.

[52] V. L. Yarnykh, E. V. Tartaglione, and G. N. Ioannou, "Fast macromolecular proton fraction mapping of the human liver in vivo for quantitative assessment of hepatic fibrosis: Macromolecular Proton Fraction Mapping in Hepatic Fibrosis," *NMR in biomedicine,* vol. 28, no. 12, pp. 1716-1725, 2015, doi: 10.1002/nbm.3437.

[53] C. F. Dietrich *et al.*, "EFSUMB guidelines and recommendations on the clinical use of liver ultrasound elastography, update 2017 (long version)," *Ultraschall in der Medizin-European Journal of Ultrasound,* vol. 38, no. 04, pp. e16-e47, 2017.

[54] L. Castera *et al.*, "EASL-ALEH Clinical Practice Guidelines: Non-invasive tests for evaluation of liver disease severity and prognosis," *Journal of hepatology,* vol. 63, no. 1, pp. 237-264, 2015, doi: 10.1016/j.jhep.2015.04.006.

[55] R. G. Barr *et al.*, "Elastography Assessment of Liver Fibrosis: Society of Radiologists in Ultrasound Consensus Conference Statement," *Ultrasound quarterly,* vol. 32, no. 2, pp. 94-107, 2016, doi: 10.1097/RUQ.0000000000000209.

[56] G. Shiha *et al.*, "Asian-Pacific Association for the Study of the Liver (APASL) consensus guidelines on invasive and non-invasive assessment of hepatic fibrosis: a 2016 update," *Hepatology international,* vol. 11, no. 1, pp. 1-30, 2017, doi: 10.1007/s12072-016-9760-3.

[57] C. Fang *et al.*, "Strain elastography for noninvasive assessment of liver fibrosis: A prospective study with histological comparison," *Ultrasound (Leeds, England),* vol. 27, no. 4, pp. 262-271, 2019, doi: 10.1177/1742271X19862836.

[58] K. Tajiri, K. Kawai, and T. Sugiyama, "Strain elastography for assessment of liver fibrosis and prognosis in patients with chronic liver diseases," *Journal of gastroenterology,* vol. 52, no. 6, pp. 724-733, 2017, doi: 10.1007/s00535-016-1277-y.

[59] A. Tang, G. Cloutier, N. M. Szeverenyi, and C. B. Sirlin, "Ultrasound elastography and MR elastography for assessing liver fibrosis: Part 1, principles and techniques," *American journal of roentgenology (1976),* vol. 205, no. 1, pp. 22-32, 2015, doi: 10.2214/AJR.15.14552.

[60] R. Muthupillai, D. J. Lomas, P. J. Rossman, J. F. Greenleaf, A. Manduca, and R. L. Ehman, "Magnetic Resonance Elastography by Direct Visualization of Propagating Acoustic Strain Waves," *Science (American Association for the Advancement of Science),* vol. 269, no. 5232, pp. 1854-1857, 1995, doi: 10.1126/science.7569924.

[61] S. K. Venkatesh, M. Yin, and R. L. Ehman, "Magnetic resonance elastography of liver: Technique, analysis, and clinical applications," *Journal of magnetic resonance imaging,* vol. 37, no. 3, pp. 544-555, 2013, doi: 10.1002/jmri.23731.

[62] M. Yin and S. K. Venkatesh, "Ultrasound or MR elastography of liver: which one shall I use?," *Abdominal radiology (New York),* vol. 43, no. 7, pp. 1546-1551, 2018, doi: 10.1007/s00261-017-1340-z.

[63] S. Singh *et al.*, "Magnetic resonance elastography for staging liver fibrosis in non-alcoholic fatty liver disease: a diagnostic accuracy systematic review and

individual participant data pooled analysis," *European radiology,* vol. 26, no. 5, pp. 1431-1440, 2016, doi: 10.1007/s00330-015-3949-z.

[64] S. Singh *et al.*, "Diagnostic performance of magnetic resonance elastography in staging liver fibrosis: a systematic review and meta-analysis of individual participant data," (in eng), *Clin Gastroenterol Hepatol,* vol. 13, no. 3, pp. 440-451.e6, Mar 2015, doi: 10.1016/j.cgh.2014.09.046.

[65] J. Chen *et al.*, "Diagnostic performance of MR elastography and vibration-controlled transient elastography in the detection of hepatic fibrosis in patients with severe to morbid obesity," *Radiology,* vol. 283, no. 2, pp. 418-428, 2017, doi: 10.1148/radiol.2016160685.

[66] C. Hsu *et al.*, "Magnetic Resonance vs Transient Elastography Analysis of Patients With Nonalcoholic Fatty Liver Disease: A Systematic Review and Pooled Analysis of Individual Participants," *Clinical Gastroenterology and Hepatology,* vol. 17, no. 4, pp. 630-637.e8, 2019.

[67] É. Bavu *et al.*, "Noninvasive In Vivo Liver Fibrosis Evaluation Using Supersonic Shear Imaging: A Clinical Study on 113 Hepatitis C Virus Patients," *Ultrasound in medicine & biology,* vol. 37, no. 9, pp. 1361-1373, 2011, doi: 10.1016/j.ultrasmedbio.2011.05.016.

[68] S. B. Paul *et al.*, "Assessment of liver fibrosis in chronic hepatitis: comparison of shear wave elastography and transient elastography," *Abdominal radiology (New York),* vol. 42, no. 12, pp. 2864-2873, 2017, doi: 10.1007/s00261-017-1213-5.

[69] G. Ferraioli, C. Tinelli, B. Dal Bello, M. Zicchetti, G. Filice, and C. Filice, "Accuracy of real-time shear wave elastography for assessing liver fibrosis in

chronic hepatitis C: A pilot study," *Hepatology (Baltimore, Md.),* vol. 56, no. 6, pp. 2125-2133, 2012, doi: 10.1002/hep.25936.

[70] K. Wang *et al.*, "Deep learning radiomics of shear wave elastography significantly improved diagnostic performance for assessing liver fibrosis in chronic hepatitis B: A prospective multicentre study," *Gut,* vol. 68, no. 4, pp. 729-741, 2019, doi: 10.1136/gutjnl-2018-316204.

[71] J. Trebicka *et al.*, "Two-dimensional shear wave elastography predicts survival in advanced chronic liver disease," *Gut,* vol. 71, no. 2, pp. 402-414, 2022, doi: 10.1136/gutjnl-2020-323419.

[72] L. Sandrin, S. Catheline, M. Tanter, X. Hennequin, and M. Fink, "Time-Resolved Pulsed Elastography with Ultrafast Ultrasonic Imaging," *Ultrasonic imaging,* vol. 21, no. 4, pp. 259-272, 1999, doi: 10.1177/016173469902100402.

[73] L. Sandrin, M. Tanter, J. L. Gennisson, S. Catheline, and M. Fink, "Shear elasticity probe for soft tissues with 1-D transient elastography," *IEEE transactions on ultrasonics, ferroelectrics, and frequency control,* vol. 49, no. 4, pp. 436-446, 2002, doi: 10.1109/58.996561.

[74] L. Sandrin *et al.*, "Transient elastography: a new noninvasive method for assessment of hepatic fibrosis," *Ultrasound in medicine & biology,* vol. 29, no. 12, pp. 1705-1713, 2003, doi: 10.1016/j.ultrasmedbio.2003.07.001.

[75] L. Castéra *et al.*, "Pitfalls of liver stiffness measurement: A 5-year prospective study of 13,369 examinations," *Hepatology (Baltimore, Md.),* vol. 51, no. 3, pp. 828-835, 2010, doi: 10.1002/hep.23425.

[76] J. Boursier *et al.*, "Determination of reliability criteria for liver stiffness evaluation by transient elastography," *Hepatology (Baltimore, Md.),* vol. 57, no. 3, pp. 1182-1191, 2013, doi: 10.1002/hep.25993.

[77] P. N. Newsome *et al.*, "FibroScan-AST (FAST) score for the non-invasive identification of patients with non-alcoholic steatohepatitis with significant activity and fibrosis: a prospective derivation and global validation study," *The lancet Gastroenterology & hepatology,* vol. 5, no. 4, pp. 362-373, 2020.

[78] P. J. Eddowes *et al.*, "Accuracy of FibroScan controlled attenuation parameter and liver stiffness measurement in assessing steatosis and fibrosis in patients with nonalcoholic fatty liver disease," *Gastroenterology,* vol. 156, no. 6, pp. 1717-1730, 2019.

[79] E. A. Tsochatzis, K. S. Gurusamy, S. Ntaoula, E. Cholongitas, B. R. Davidson, and A. K. Burroughs, "Elastography for the diagnosis of severity of fibrosis in chronic liver disease: A meta-analysis of diagnostic accuracy," *Journal of hepatology,* vol. 54, no. 4, pp. 650-659, 2011, doi: 10.1016/j.jhep.2010.07.033.

[80] J. Boursier *et al.*, "Reproducibility of liver stiffness measurement by ultrasonographic elastometry," (in eng), *Clin Gastroenterol Hepatol,* vol. 6, no. 11, pp. 1263-9, Nov 2008, doi: 10.1016/j.cgh.2008.07.006.

[81] K.-Q. Shi *et al.*, "Transient elastography: a meta-analysis of diagnostic accuracy in evaluation of portal hypertension in chronic liver disease," *Liver international,* vol. 33, no. 1, pp. 62-71, 2013, doi: 10.1111/liv.12003.

[82] B. K. Kim, J. Fung, M. F. Yuen, and S. U. Kim, "Clinical application of liver stiffness measurement using transient elastography in chronic liver disease from longitudinal perspectives," *World journal of gastroenterology : WJG,* vol. 19, no. 12, pp. 1890-1900, 2013, doi: 10.3748/wjg.v19.i12.1890.

[83] C. Corpechot *et al.*, "Noninvasive elastography-based assessment of liver fibrosis progression and prognosis in primary biliary cirrhosis," *Hepatology (Baltimore, Md.),* vol. 56, no. 1, pp. 198-208, 2012, doi: 10.1002/hep.25599.

[84] C. Corpechot *et al.*, "Baseline values and changes in liver stiffness measured by transient elastography are associated with severity of fibrosis and outcomes of patients with primary sclerosing cholangitis," (in eng), *Gastroenterology,* vol. 146, no. 4, pp. 970-9; quiz e15-6, Apr 2014, doi: 10.1053/j.gastro.2013.12.030.

[85] A. Tang, G. Cloutier, N. M. Szeverenyi, and C. B. Sirlin, "Ultrasound elastography and MR elastography for assessing liver fibrosis: Part 2, diagnostic performance, confounders, and future directions," *American journal of roentgenology (1976),* vol. 205, no. 1, pp. 33-40, 2015, doi: 10.2214/AJR.15.14553.

[86] K. Patel and G. Sebastiani, "Limitations of non-invasive tests for assessment of liver fibrosis," *JHEP reports,* vol. 2, no. 2, pp. 100067-100067, 2020, doi: 10.1016/j.jhepr.2020.100067.

[87] T. M. Mak, Y. P. Huang, and Y. P. Zheng, "Liver fibrosis assessment using transient elastography guided with real-time B-mode ultrasound imaging: a feasibility study," *Ultrasound Med Biol,* vol. 39, no. 6, pp. 956-66, Jun 2013, doi: 10.1016/j.ultrasmedbio.2013.01.009.

[88] K. Patel and G. Sebastiani, "Limitations of non-invasive tests for assessment of liver fibrosis," *JHEP Reports,* vol. 2, no. 2, p. 100067, 2020.

[89] G. Ferraioli *et al.*, "Liver Ultrasound Elastography: An Update to the World Federation for Ultrasound in Medicine and Biology Guidelines and Recommendations," *Ultrasound in medicine & biology,* vol. 44, no. 12, pp. 2419-2440, 2018, doi: 10.1016/j.ultrasmedbio.2018.07.008.

[90] J. X. Q. Pang *et al.*, "The Feasibility and Reliability of Transient Elastography Using Fibroscan ® : A Practice Audit of 2335 Examinations," *Canadian journal*

of gastroenterology & hepatology, vol. 28, no. 3, pp. 143-149, 2014, doi: 10.1155/2014/952684.

[91] R. P. Myers *et al.*, "Feasibility and diagnostic performance of the FibroScan XL probe for liver stiffness measurement in overweight and obese patients," *Hepatology,* vol. 55, no. 1, pp. 199-208, Jan 2012, doi: 10.1002/hep.24624.

[92] F. Pradhan, F. Ladak, J. Tracey, P. Crotty, and R. P. Myers, "Feasibility and reliability of the FibroScan S2 (pediatric) probe compared with the M probe for liver stiffness measurement in small adults with chronic liver disease," *Annals of hepatology,* vol. 12, no. 1, pp. 100-107, 2013, doi: 10.1016/s1665-2681(19)31391-2.

[93] S. Naveau *et al.*, "The Diagnostic Accuracy of Transient Elastography for the Diagnosis of Liver Fibrosis in Bariatric Surgery Candidates with Suspected NAFLD," *Obesity surgery,* vol. 24, no. 10, pp. 1693-1701, 2014, doi: 10.1007/s11695-014-1235-9.

[94] V. De Lédinghen, J. Vergniol, J. Foucher, F. El-Hajbi, W. Merrouche, and V. Rigalleau, "Feasibility of liver transient elastography with FibroScan® using a new probe for obese patients," *Liver international,* vol. 30, no. 7, pp. 1043-1048, 2010, doi: 10.1111/j.1478-3231.2010.02258.x.

[95] G. M. D. Ferraioli *et al.*, "WFUMB Guidelines and Recommendations for Clinical Use of Ultrasound Elastography: Part 3: Liver," *Ultrasound in medicine & biology,* vol. 41, no. 5, pp. 1161-1179, 2015, doi: 10.1016/j.ultrasmedbio.2015.03.007.

[96] J. Boursier *et al.*, "Learning curve and interobserver reproducibility evaluation of liver stiffness measurement by transient elastography," *European journal of*

gastroenterology & hepatology, vol. 20, no. 7, pp. 693-701, 2008, doi: 10.1097/MEG.0b013e3282f51992.

[97] S. Mueller and L. Sandrin, "Liver stiffness: a novel parameter for the diagnosis of liver disease," *Hepatic medicine: evidence and research,* vol. 2, pp. 49-67, 2010, doi: 10.2147/hmer.s7394.

[98] S. Mueller, "Does pressure cause liver cirrhosis? The sinusoidal pressure hypothesis," *World journal of gastroenterology : WJG,* vol. 22, no. 48, pp. 10482-10501, 2016, doi: 10.3748/wjg.v22.i48.10482.

[99] S. Adolf, G. Millonig, S. Friedrich, H. K. Seitz, and S. Mueller, "411 VALSALVA AND ORTHOSTATIC MANEUVERS INCREASE LIVER STIFFNESS (FIBROSCAN®) IN HEALTHY VOLUNTEERS," *Journal of hepatology,* vol. 52, pp. S168-S168, 2010, doi: 10.1016/S0168-8278(10)60413-8.

[100] I. Mederacke *et al.*, "Food intake increases liver stiffness in patients with chronic or resolved hepatitis C virus infection," *Liver international,* vol. 29, no. 10, pp. 1500-1506, 2009, doi: 10.1111/j.1478-3231.2009.02100.x.

[101] U. Arena *et al.*, "Liver stiffness is influenced by a standardized meal in patients with chronic hepatitis C virus at different stages of fibrotic evolution," *Hepatology (Baltimore, Md.),* vol. 58, no. 1, pp. 65-72, 2013, doi: 10.1002/hep.26343.

[102] A. Sagir, A. Erhardt, M. Schmitt, and D. Häussinger, "Transient elastography is unreliable for detection of cirrhosis in patients with acute liver damage," *Hepatology (Baltimore, Md.),* vol. 47, no. 2, pp. 592-595, 2008, doi: 10.1002/hep.22056.

[103] U. Arena *et al.*, "Acute viral hepatitis increases liver stiffness values measured by transient elastography," *Hepatology (Baltimore, Md.),* vol. 47, no. 2, pp. 380-384, 2008, doi: 10.1002/hep.22007.

[104] G. Millonig *et al.*, "Liver stiffness is directly influenced by central venous pressure," *Journal of hepatology,* vol. 52, no. 2, pp. 206-210, 2010, doi: 10.1016/j.jhep.2009.11.018.

[105] A. Colli *et al.*, "Decompensated Chronic Heart Failure: Increased Liver Stiffness Measured by Means of Transient Elastography," *Radiology,* vol. 257, no. 3, pp. 872-878, 2010, doi: 10.1148/radiol.10100013.

[106] G. Millonig *et al.*, "Extrahepatic cholestasis increases liver stiffness (FibroScan) irrespective of fibrosis," *Hepatology (Baltimore, Md.),* vol. 48, no. 5, pp. 1718-1723, 2008, doi: 10.1002/hep.22577.

[107] F. Piecha *et al.*, "Rapid change of liver stiffness after variceal ligation and TIPS implantation," *American Journal of Physiology-Gastrointestinal and Liver Physiology,* vol. 314, no. 2, pp. G179-G187, 2018, doi: 10.1152/ajpgi.00239.2017.

[108] F. Piecha, T. Peccerella, T. Bruckner, H.-K. Seitz, V. Rausch, and S. Mueller, "Arterial pressure suffices to increase liver stiffness," *American journal of physiology: Gastrointestinal and liver physiology,* vol. 311, no. 5, pp. G945-G953, 2016, doi: 10.1152/ajpgi.00399.2015.

[109] G. L. Wong *et al.*, "Association between anthropometric parameters and measurements of liver stiffness by transient elastography," (in eng), *Clin Gastroenterol Hepatol,* vol. 11, no. 3, pp. 295-302.e1-3, Mar 2013, doi: 10.1016/j.cgh.2012.09.025.

[110] S. Mueller *et al.*, "Increased liver stiffness in alcoholic liver disease:Differentiating fibrosis from steatohepatitis," *World journal of gastroenterology : WJG,* vol. 16, no. 8, pp. 966-972, 2010, doi: 10.3748/wjg.v16.i8.966.

[111] S. Petta *et al.*, "The severity of steatosis influences liver stiffness measurement in patients with nonalcoholic fatty liver disease," *Hepatology (Baltimore, Md.),* vol. 62, no. 4, pp. 1101-1110, 2015, doi: 10.1002/hep.27844.

[112] F. S. Macaluso *et al.*, "Steatosis affects the performance of liver stiffness measurement for fibrosis assessment in patients with genotype 1 chronic hepatitis C," *Journal of hepatology,* vol. 61, no. 3, pp. 523-529, 2014, doi: 10.1016/j.jhep.2014.04.045.

[113] J. Boursier *et al.*, "Precise evaluation of liver histology by computerized morphometry shows that steatosis influences liver stiffness measured by transient elastography in chronic hepatitis C," *Journal of gastroenterology,* vol. 49, no. 3, pp. 527-537, 2014, doi: 10.1007/s00535-013-0819-9.

[114] V. W. S. Wong *et al.*, "Diagnosis of fibrosis and cirrhosis using liver stiffness measurement in nonalcoholic fatty liver disease," *Hepatology (Baltimore, Md.),* vol. 51, no. 2, pp. 454-462, 2010, doi: 10.1002/hep.23312.

[115] A. E. Samir *et al.*, "Shear-Wave elastography for the estimation of liver fibrosis in chronic liver disease: Determining accuracy and ideal site for measurement," *Radiology,* vol. 274, no. 3, pp. 888-896, 2015, doi: 10.1148/radiol.14140839.

[116] J. Zeng *et al.*, "Comparison of 2-D Shear Wave Elastography and Transient Elastography for Assessing Liver Fibrosis in Chronic Hepatitis B," *Ultrasound in medicine & biology,* vol. 43, no. 8, pp. 1563-1570, 2017, doi: 10.1016/j.ultrasmedbio.2017.03.014.

[117] V. Y.-f. Leung *et al.*, "Quantitative elastography of liver fibrosis and spleen stiffness in chronic hepatitis B carriers: comparison of shear-wave elastography and transient elastography with liver biopsy correlation," *Radiology,* vol. 269, no. 3, pp. 910-918, 2013, doi: 10.1148/radiol.13130128.

[118] J. Lee, H.-J. Kang, J. H. Yoon, and J. M. Lee, "Ultrasound-guided transient elastography and two-dimensional shear wave elastography for assessment of liver fibrosis: emphasis on technical success and reliable measurements," *Ultrasonography (Seoul, Korea),* vol. 40, no. 2, pp. 217-227, 2021, doi: 10.14366/usg.20036.

[119] C. Cassinotto *et al.*, "Learning curve of liver stiffness measurement using a new hybrid machine composed of transient elastography interfaced with ultrasound," *European radiology,* vol. 30, no. 2, pp. 1088-1095, 2020, doi: 10.1007/s00330-019-06388-1.

[120] S. Mueller, *Liver elastography : clinical use and interpretation* (Liver elastography : clinical use & interpretation). Cham: Springer, 2020.

[121] M. L. Palmeri *et al.*, "Radiological Society of North America/Quantitative Imaging Biomarker Alliance Shear Wave Speed Bias Quantification in Elastic and Viscoelastic Phantoms," *Journal of ultrasound in medicine,* vol. 40, no. 3, pp. 569-581, 2021, doi: 10.1002/jum.15609.

[122] M. Palmeri, "RSNA/QIBA efforts to standardize shear wave speed as a biomarker for liver fibrosis staging," *Ultrasound in medicine & biology,* vol. 45, pp. S24-S24, 2019, doi: 10.1016/j.ultrasmedbio.2019.07.491.

[123] S. U. Kim *et al.*, "Variability in liver stiffness values from different intercostal spaces," *Liver international,* vol. 29, no. 5, pp. 760-766, 2009, doi: 10.1111/j.1478-3231.2009.02035.x.

[124] P. Marcellin and B. K. Kutala, "Liver diseases: A major, neglected global public health problem requiring urgent actions and large-scale screening," *Liver international,* vol. 38, no. S1, pp. 2-6, 2018, doi: 10.1111/liv.13682.

[125] G. Feng *et al.*, "Recompensation in cirrhosis: unravelling the evolving natural history of nonalcoholic fatty liver disease," *Nature reviews. Gastroenterology & hepatology,* 2023, doi: 10.1038/s41575-023-00846-4.

[126] W. H. Organization, *Guidelines for the Screening Care and Treatment of Persons with Chronic Hepatitis C Infection Updated Version April 2016: Guidelines*. World Health Organization, 2016.

[127] W. H. Organization, *Guidelines for the prevention care and treatment of persons with chronic hepatitis B infection: Mar-15*. World Health Organization, 2015.

[128] G. Ferraioli *et al.*, "WFUMB Guideline/Guidance on Liver Multiparametric Ultrasound: Part 1. Update to 2018 Guidelines on Liver Ultrasound Elastography," (in eng), *Ultrasound Med Biol,* vol. 50, no. 8, pp. 1071-1087, Aug 2024, doi: 10.1016/j.ultrasmedbio.2024.03.013.

[129] J. Li, A. Delamarre, V. W. Wong, and V. de Lédinghen, "Diagnosis and assessment of disease severity in patients with nonalcoholic fatty liver disease," (in eng), *United European Gastroenterol J,* vol. 12, no. 2, pp. 219-225, Mar 2024, doi: 10.1002/ueg2.12491.

[130] P. Ginès *et al.*, "Screening for liver fibrosis in the general population: a call for action," *The lancet Gastroenterology & hepatology,* vol. 1, no. 3, pp. 256-260, 2016.

[131] A. Sourianarayanane and A. J. McCullough, "Accuracy of ultrasonographic fatty liver index using point-of-care ultrasound in stratifying non-alcoholic fatty liver

disease patients," *European journal of gastroenterology & hepatology,* vol. 35, no. 6, pp. 654-661, 2023, doi: 10.1097/MEG.0000000000002544.

[132] D. G. Bonett, "Sample size requirements for estimating intraclass correlations with desired precision," *Statist. Med,* vol. 21, no. 9, pp. 1331-1335, 2002, doi: 10.1002/sim.1108.

[133] M. Dhyani, J. R. Grajo, A. K. Bhan, K. Corey, R. Chung, and A. E. Samir, "Validation of Shear Wave Elastography Cutoff Values on the Supersonic Aixplorer for Practical Clinical Use in Liver Fibrosis Staging," *Ultrasound in medicine & biology,* vol. 43, no. 6, pp. 1125-1133, 2017, doi: 10.1016/j.ultrasmedbio.2017.01.022.

[134] D. L. Raunig *et al.*, "Quantitative imaging biomarkers: A review of statistical methods for technical performance assessment," *Statistical methods in medical research,* vol. 24, no. 1, pp. 27-67, 2015, doi: 10.1177/0962280214537344.

[135] T. K. Koo and M. Y. Li, "A Guideline of Selecting and Reporting Intraclass Correlation Coefficients for Reliability Research," *JOURNAL OF CHIROPRACTIC MEDICINE,* vol. 15, no. 2, pp. 155-163, 2016, doi: 10.1016/j.jcm.2016.02.012.

[136] C.-Z. Wang *et al.*, "Influence of Measurement Depth on the Stiffness Assessment of Healthy Liver with Real-Time Shear Wave Elastography," *Ultrasound in medicine & biology,* vol. 40, no. 3, pp. 461-469, 2014, doi: 10.1016/j.ultrasmedbio.2013.10.021.

[137] A. Mulabecirovic, A. B. Mjelle, O. H. Gilja, M. Vesterhus, and R. F. Havre, "Repeatability of shear wave elastography in liver fibrosis phantoms-Evaluation of five different systems," *PloS one,* vol. 13, no. 1, pp. e0189671-e0189671, 2018, doi: 10.1371/journal.pone.0189671.

[138] O. Ljungquist, J. Olinder, J. Tverring, C. Kjölvmark, and G. Torisson, "Agreement and reliability of hepatic transient elastography in patients with chronic hepatitis C: A cross-sectional test–retest study," *Health science reports,* vol. 6, no. 4, pp. e1184-n/a, 2023, doi: 10.1002/hsr2.1184.

[139] K. Imajo *et al.*, "Direct Comparison of US and MR Elastography for Staging Liver Fibrosis in Patients With Nonalcoholic Fatty Liver Disease," *Clinical Gastroenterology and Hepatology,* vol. 20, no. 4, pp. 908-917.e11, 2022/04/01/ 2022, doi: https://doi.org/10.1016/j.cgh.2020.12.016.

[140] C. Fang, E. Konstantatou, O. Romanos, G. T. Yusuf, D. J. Quinlan, and P. S. Sidhu, "Reproducibility of 2-Dimensional Shear Wave Elastography Assessment of the Liver: A Direct Comparison With Point Shear Wave Elastography in Healthy Volunteers," *Journal of ultrasound in medicine,* vol. 36, no. 8, pp. 1563-1569, 2017, doi: 10.7863/ultra.16.07018.

[141] P. Linek, T. Wolny, D. Sikora, and A. Klepek, "Intrarater Reliability of Shear Wave Elastography for the Quantification of Lateral Abdominal Muscle Elasticity in Idiopathic Scoliosis Patients," *Journal of manipulative and physiological therapeutics,* vol. 43, no. 4, pp. 303-310, 2020, doi: 10.1016/j.jmpt.2018.11.034.

[142] I. Sporea, S. Bota, O. Gradinaru-Taşcău, R. Şirli, A. Popescu, and A. Jurchiş, "Which are the cut-off values of 2D-Shear Wave Elastography (2D-SWE) liver stiffness measurements predicting different stages of liver fibrosis, considering Transient Elastography (TE) as the reference method?," *European journal of radiology,* vol. 83, no. 3, pp. e118-e122, 2014, doi: 10.1016/j.ejrad.2013.12.011.

[143] T. Lefebvre *et al.*, "Prospective comparison of transient, point shear wave, and magnetic resonance elastography for staging liver fibrosis," *European radiology,* vol. 29, no. 12, pp. 6477-6488, 2019, doi: 10.1007/s00330-019-06331-4.

[144] V. de Lédinghen *et al.*, "Diagnosis of liver fibrosis and cirrhosis using liver stiffness measurement: Comparison between M and XL probe of FibroScan," *Journal of hepatology,* vol. 56, no. 4, pp. 833-839, 2012, doi: 10.1016/j.jhep.2011.10.017.

[145] D. J. Harman *et al.*, "Direct targeting of risk factors significantly increases the detection of liver cirrhosis in primary care: a cross-sectional diagnostic study utilising transient elastography," *BMJ open,* vol. 5, no. 4, pp. e007516-e007516, 2015, doi: 10.1136/bmjopen-2014-007516.

[146] L. Sandrin, D. Cassereau, and M. Fink, "The role of the coupling term in transient elastography," *The Journal of the Acoustical Society of America,* vol. 115, no. 1, pp. 73-83, 2004, doi: 10.1121/1.1635412.

[147] S. p. Audière, E. D. Angelini, L. Sandrin, and M. Charbit, "Maximum Likelihood Estimation of Shear Wave Speed in Transient Elastography," *IEEE transactions on medical imaging,* vol. 33, no. 6, pp. 1338-1349, 2014, doi: 10.1109/TMI.2014.2311374.

[148] J. Oudry, T. Lynch, J. Vappou, L. Sandrin, and V. Miette, "Comparison of four different techniques to evaluate the elastic properties of phantom in elastography: is there a gold standard?," *Physics in medicine & biology,* vol. 59, no. 19, pp. 5775-5793, 2014, doi: 10.1088/0031-9155/59/19/5775.

[149] R. Z. Azar *et al.*, "Real-time transient elastography on standard ultrasound using mechanically induced vibration: System design and initial results," 2011: IEEE, pp. 2388-2391, doi: 10.1109/ULTSYM.2011.0593.

[150] Y. Xu *et al.*, "Comparison of FibroTouch and FibroScan for staging fibrosis in chronic liver disease: Single-center prospective study," *Dig Liver Dis,* vol. 51, no. 9, pp. 1323-1329, Sep 2019, doi: 10.1016/j.dld.2019.02.009.

[151] Y. Z. Ng, L. L. Lai, S. W. Wong, S. Y. Mohamad, K. H. Chuah, and W. K. Chan, "Attenuation parameter and liver stiffness measurement using FibroTouch vs Fibroscan in patients with chronic liver disease," *PloS one,* vol. 16, no. 5, pp. e0250300-e0250300, 2021, doi: 10.1371/journal.pone.0250300.

[152] M. Ronot *et al.*, "Comparison of liver stiffness measurements by a 2D-shear wave technique and transient elastography: results from a European prospective multi-centre study," *European radiology,* vol. 31, no. 3, pp. 1578-1587, 2021, doi: 10.1007/s00330-020-07212-x.

[153] P. S. Dulai *et al.*, "Increased risk of mortality by fibrosis stage in nonalcoholic fatty liver disease: Systematic review and meta-analysis," *Hepatology (Baltimore, Md.),* vol. 65, no. 5, pp. 1557-1565, 2017, doi: 10.1002/hep.29085.

[154] F. Kanwal *et al.*, "Clinical Care Pathway for the Risk Stratification and Management of Patients With Nonalcoholic Fatty Liver Disease," *Gastroenterology (New York, N.Y. 1943),* vol. 161, no. 5, pp. 1657-1669, 2021, doi: 10.1053/j.gastro.2021.07.049.

[155] G. L. H. Wong *et al.*, "Factors associated with unreliable liver stiffness measurement and its failure with transient elastography in the Chinese population," *Journal of gastroenterology and hepatology,* vol. 26, no. 2, pp. 300-305, 2011, doi: 10.1111/j.1440-1746.2010.06510.x.

[156] F. Faul, E. Erdfelder, A.-G. Lang, and A. Buchner, "GPower 3: a flexible statistical power analysis program for the social, behavioral, and biomedical sciences," *Behavior research methods,* vol. 39, no. 2, pp. 175-191, 2007, doi: 10.3758/BF03193146.

[157] E. D. von Elm, D. G. P. Altman, M. P. Egger, S. J. P. Pocock, P. C. M. D. Gøtzsche, and J. P. P. Vandenbroucke, "The Strengthening the Reporting of Observational Studies in Epidemiology (STROBE) statement: guidelines for reporting observational studies," *The Lancet (British edition),* vol. 370, no. 9596, pp. 1453-1457, 2007, doi: 10.1016/S0140-6736(07)61602-X.

[158] R. Huang *et al.*, "Fibroscan improves the diagnosis sensitivity of liver fibrosis in patients with chronic hepatitis B," *Experimental and therapeutic medicine,* vol. 11, no. 5, pp. 1673-1677, 2016, doi: 10.3892/etm.2016.3135.

[159] P. Song *et al.*, "Performance of 2-Dimensional Ultrasound Shear Wave Elastography in Liver Fibrosis Detection Using Magnetic Resonance Elastography as the Reference Standard: A Pilot Study," *Journal of ultrasound in medicine,* vol. 35, no. 2, pp. 401-412, 2016, doi: 10.7863/ultra.15.03036.

[160] T. Deffieux *et al.*, "Investigating liver stiffness and viscosity for fibrosis, steatosis and activity staging using shear wave elastography," *Journal of hepatology,* vol. 62, no. 2, pp. 317-324, 2015, doi: 10.1016/j.jhep.2014.09.020.

[161] S. Audière, Y. Mofid, M. Charbit, E. Angelini, V. Miette, and L. Sandrin, "Fibroscan® practice improvement with a real-time assistance ultrasound tool: a premiminary study," in *2009 IEEE International Ultrasonics Symposium*, 2009: IEEE, pp. 1455-1458.

[162] M. Pałac and P. Linek, "Intra-Rater Reliability of Shear Wave Elastography for the Quantification of Respiratory Muscles in Adolescent Athletes," *Sensors (Basel, Switzerland),* vol. 22, no. 17, p. 6622, 2022, doi: 10.3390/s22176622.

[163] K. M. Diab, A. Shalabi, J. A. Sevastik, and P. Güntner, "A method for morphometric study of the intercostal muscles by high-resolution ultrasound," *European spine journal,* vol. 7, no. 3, pp. 224-228, 1998, doi: 10.1007/s005860050061.

[164] Y.-S. Kim, M. J. Park, H. Rhim, M. W. Lee, and H. K. Lim, "Sonographic analysis of the intercostal spaces for the application of high-intensity focused ultrasound therapy to the liver," *American journal of roentgenology (1976),* vol. 203, no. 1, pp. 201-208, 2014, doi: 10.2214/AJR.13.11744.

[165] T. Terboven *et al.*, "Chest wall thickness and depth to vital structures in paediatric patients - Implications for prehospital needle decompression of tension pneumothorax," *Scandinavian journal of trauma, resuscitation and emergency medicine,* vol. 27, no. 1, pp. 45-45, 2019, doi: 10.1186/s13049-019-0623-5.

[166] S. Tuinder *et al.*, "Anatomical evaluation of the internal mammary vessels based on magnetic resonance imaging (MRI)," *Journal of plastic, reconstructive & aesthetic surgery,* vol. 65, no. 10, pp. 1363-1367, 2012, doi: 10.1016/j.bjps.2012.04.035.

[167] A. Hisaund, R. Pietton, R. Vialle, W. Skalli, and C. Vergari, "Feasibility of Rib Kinematics and Intercostal-Space Biomechanical Characterization by Ultrasound in Adolescent Idiopathic Scoliosis," *Ultrasound in medicine & biology,* vol. 47, no. 7, pp. 1957-1963, 2021, doi: 10.1016/j.ultrasmedbio.2021.03.017.

[168] R. Pietton *et al.*, "Biomechanical Evaluation of Intercostal Muscles in Healthy Children and Adolescent Idiopathic Scoliosis: A Preliminary Study," *Ultrasound in medicine & biology,* vol. 47, no. 1, pp. 51-57, 2021, doi: 10.1016/j.ultrasmedbio.2020.09.011.

[169] K. Chino, T. Ohya, K. Katayama, and Y. Suzuki, "Diaphragmatic shear modulus at various submaximal inspiratory mouth pressure levels," *Respiratory physiology & neurobiology,* vol. 252-253, pp. 52-57, 2018, doi: 10.1016/j.resp.2018.03.009.

[170] R. Yoshida *et al.*, "Measurement of intercostal muscle thickness with ultrasound imaging during maximal breathing," *Journal of physical therapy science,* vol. 31, no. 4, pp. 340-343, 2019, doi: 10.1589/jpts.31.340.

[171] S. J. Cala, C. M. Kenyon, A. Lee, K. Watkin, P. T. Macklem, and D. F. Rochester, "Respiratory Ultrasonography of Human Parasternal Intercostal Muscle In Vivo," *Ultrasound in medicine & biology,* vol. 24, no. 3, pp. 313-326, 1998, doi: 10.1016/S0301-5629(97)00271-8.

[172] P. Wallbridge *et al.*, "Parasternal intercostal muscle ultrasound in chronic obstructive pulmonary disease correlates with spirometric severity," *Scientific reports,* vol. 8, no. 1, pp. 15274-9, 2018, doi: 10.1038/s41598-018-33666-7.

[173] D. C. Rockey, S. H. Caldwell, Z. D. Goodman, R. C. Nelson, and A. D. Smith, "Liver biopsy," *Hepatology (Baltimore, Md.),* vol. 49, no. 3, pp. 1017-1044, 2009, doi: 10.1002/hep.22742.

[174] Who, *Guidelines for the Prevention Care and Treatment of Persons with Chronic Hepatitis B Virus Infection: Mar-15*, 1 ed. Geneva: World Health Organization, 2015.

[175] J. A. Lee *et al.*, "Diagnostic accuracy of non-invasive tests for advanced fibrosis in patients with NAFLD: an individual patient data meta-analysis," *Gut,* vol. 71, no. 5, pp. 1006-1019, 2022, doi: 10.1136/gutjnl-2021-324243.

[176] M. Friedrich–Rust *et al.*, "Performance of Transient Elastography for the Staging of Liver Fibrosis: A Meta-Analysis," *Gastroenterology (New York, N.Y. 1943),* vol. 134, no. 4, pp. 960-974.e8, 2008, doi: 10.1053/j.gastro.2008.01.034.

[177] D. Roulot, S. Czernichow, H. Le Clésiau, J.-L. Costes, A.-C. Vergnaud, and M. Beaugrand, "Liver stiffness values in apparently healthy subjects: Influence of gender and metabolic syndrome," *Journal of hepatology,* vol. 48, no. 4, pp. 606-613, 2008, doi: 10.1016/j.jhep.2007.11.020.

[178] M. Papatheodoridi *et al.*, "Refining the Baveno VI elastography criteria for the definition of compensated advanced chronic liver disease," *Journal of hepatology,* vol. 74, no. 5, pp. 1109-1116, 2021, doi: 10.1016/j.jhep.2020.11.050.

[179] A. Lanzi, A. Gianstefani, M. G. Mirarchi, P. Pini, F. Conti, and L. Bolondi, "Liver AL amyloidosis as a possible cause of high liver stiffness values," *European journal of gastroenterology & hepatology,* vol. 22, no. 7, p. 895, 2010, doi: 10.1097/MEG.0b013e3283309d5b.

[180] S. Adolf *et al.*, "Systemic Mastocytosis: A Rare Case of Increased Liver Stiffness," *Case reports in hepatology,* vol. 2012, pp. 728172-6, 2012, doi: 10.1155/2012/728172.

[181] M. H. Yun *et al.*, "The effect of the respiratory cycle on liver stiffness values as measured by transient elastography," *Journal of viral hepatitis,* vol. 18, no. 9, pp. 631-636, 2011, doi: 10.1111/j.1365-2893.2010.01376.x.

[182] Y. Kadoya, T. Miyati, S. Kobayashi, N. Ohno, and T. Gabata, "Evaluation of gravity effect on inferior vena cava and abdominal aortic flow using multi-posture MRI," *Acta radiologica (1987),* vol. 62, no. 8, pp. 1122-1128, 2021, doi: 10.1177/0284185120950112.

[183] Y. Ishizaki *et al.*, "Measurement of inferior vena cava diameter for evaluation of venous return in subjects on day 10 of a bed-rest experiment," *Journal of applied physiology (1985),* vol. 96, no. 6, pp. 2179-2186, 2004, doi: 10.1152/japplphysiol.01097.2003.

[184] K. Ohnishi *et al.*, "Portal venous hemodynamics in chronic liver disease: effects of posture change and exercise," *Radiology,* vol. 155, no. 3, pp. 757-761, 1985, doi: 10.1148/radiology.155.3.3890004.

[185] T. Iwao *et al.*, "Upright posture blunts postprandial splanchnic hyperemia in patients with cirrhosis and portal hypertension," *Journal of gastroenterology,* vol. 34, no. 3, p. 359, 1999, doi: 10.1007/s005350050274.

[186] B. E. Van Beers, I. Leconte, R. Materne, A. M. Smith, J. Jamart, and Y. Horsmans, "Hepatic Perfusion Parameters in Chronic Liver Disease: Dynamic CT Measurements Correlated with Disease Severity," *American journal of roentgenology (1976),* vol. 176, no. 3, pp. 667-673, 2001, doi: 10.2214/ajr.176.3.1760667.

[187] Z.-H. Huang *et al.*, "Palm-Sized Wireless Transient Elastography System with Real-Time B-Mode Ultrasound Imaging Guidance: Toward Point-of-Care Liver Fibrosis Assessment," *Diagnostics (Basel),* vol. 14, no. 2, p. 189, 2024, doi: 10.3390/diagnostics14020189.

[188] J. R. Landis and G. G. Koch, "The Measurement of Observer Agreement for Categorical Data," *Biometrics,* vol. 33, no. 1, pp. 159-174, 1977, doi: 10.2307/2529310.

[189] T. Suda *et al.*, "Gravity assistance enables liver stiffness measurements to detect liver fibrosis under congestive circumstances," *World journal of hepatology,* vol. 14, no. 4, pp. 778-790, 2022, doi: 10.4254/wjh.v14.i4.778.

[190] R. S. Goertz, C. Egger, M. F. Neurath, and D. Strobel, "Impact of food intake, ultrasound transducer, breathing maneuvers and body position on acoustic radiation force impulse (ARFI) elastometry of the liver," (in eng), *Ultraschall Med,* vol. 33, no. 4, pp. 380-5, Aug 2012, doi: 10.1055/s-0032-1312816.

[191] A. R. Hayes, F. S. Gayzik, D. P. Moreno, R. S. Martin, and J. D. Stitzel, "Comparison of Organ Location, Morphology, and Rib Coverage of a Midsized Male in the Supine and Seated Positions," *Computational and mathematical methods in medicine,* vol. 2013, pp. 419821-12, 2013, doi: 10.1155/2013/419821.

[192] N. Salles, P. Dussarat, J. Foucher, S. Villars, and V. de Lédinghen, "Non-invasive evaluation of liver fibrosis by transient elastography and biochemical markers in elderly inpatients," *Gastroentérologie clinique et biologique,* vol. 33, no. 2, pp. 126-132, 2009, doi: 10.1016/j.gcb.2008.12.003.

[193] A. M. Harris, L. M. Lanningham-Foster, S. K. McCrady, and J. A. Levine, "Nonexercise movement in elderly compared with young people," *American journal of physiology: endocrinology and metabolism,* vol. 292, no. 4, pp. E1207-E1212, 2007, doi: 10.1152/ajpendo.00509.2006.

[194] N. Kawamura *et al.*, "Influence of liver stiffness heterogeneity on staging fibrosis in patients with nonalcoholic fatty liver disease," *Hepatology (Baltimore, Md.),* vol. 76, no. 1, pp. 186-195, 2022, doi: 10.1002/hep.32302.

[195] T. Karlas *et al.*, "Acoustic radiation force impulse imaging (ARFI) for non-invasive detection of liver fibrosis: examination standards and evaluation of interlobe differences in healthy subjects and chronic liver disease," (in eng), *Scand J Gastroenterol,* vol. 46, no. 12, pp. 1458-67, Dec 2011, doi: 10.3109/00365521.2011.610004.

[196] S. Horster, P. Mandel, R. Zachoval, and D. A. Clevert, "Comparing acoustic radiation force impulse imaging to transient elastography to assess liver stiffness in healthy volunteers with and without valsalva manoeuvre," *Clinical hemorheology and microcirculation,* vol. 46, no. 2-3, pp. 159-168, 2010, doi: 10.3233/CH-2010-1342.